sid.inpe.br/mtc-m21d/2021/08.20.22.27-TDI

EVALUATION OF WIND PRODUCTS FROM SATELLITES AND REANALYSIS USING IN SITU DATA SAMPLED IN THE BRANSFIELD STRAIT, ANTARCTIC

Leandro de Brito Lanes

Master's Dissertation of the Graduate Course in Remote Sensing, guided by Drs. Luciano Ponzi Pezzi, and Jonas Takeo Carvalho, approved in August 18, 2021.

URL of the original document:
<http://urlib.net/8JMKD3MGP3W34T/45A8A4B>

INPE
São José dos Campos
2021

PUBLISHED BY:

Instituto Nacional de Pesquisas Espaciais - INPE
Coordenação de Ensino, Pesquisa e Extensão (COEPE)
Divisão de Biblioteca (DIBIB)
CEP 12.227-010
São José dos Campos - SP - Brasil
Tel.:(012) 3208-6923/7348
E-mail: pubtc@inpe.br

sid.inpe.br/mtc-m21d/2021/08.20.22.27-TDI

EVALUATION OF WIND PRODUCTS FROM SATELLITES AND REANALYSIS USING IN SITU DATA SAMPLED IN THE BRANSFIELD STRAIT, ANTARCTIC

Leandro de Brito Lanes

Master's Dissertation of the Graduate Course in Remote Sensing, guided by Drs. Luciano Ponzi Pezzi, and Jonas Takeo Carvalho, approved in August 18, 2021.

URL of the original document:
<http://urlib.net/8JMKD3MGP3W34T/45A8A4B>

INPE
São José dos Campos
2021

Cataloging in Publication Data

Lanes, Leandro de Brito.

L248e Evaluation of wind products from satellites and reanalysis using in situ data sampled in the Bransfield Strait, Antarctic / Leandro de Brito Lanes. – São José dos Campos : INPE, 2021.

xxiv + 106 p. ; (sid.inpe.br/mtc-m21d/2021/08.20.22.27-TDI)

Dissertation (Master in Remote Sensing) – Instituto Nacional de Pesquisas Espaciais, São José dos Campos, 2021.

Guiding : Drs. Luciano Ponzi Pezzi, and Jonas Takeo Carvalho.

1. SAR. 2. ASCAT. 3. ERA5. 4. Wind field. 5. Regional wind analysis. I.Title.

CDU 528.8.044.2

MINISTÉRIO DA CIÊNCIA, TECNOLOGIA E INOVAÇÕES

INSTITUTO NACIONAL DE PESQUISAS ESPACIAIS

Serviço de Pós-Graduação - SEPGR

DEFESA FINAL DE DISSERTAÇÃO DE LEANDRO DE BRITO LANES
BANCA Nº 216/2021, REG 783799/2019

No dia 18 de agosto de 2021, as 09h30min, por teleconferência, o(a) aluno(a) mencionado(a) acima defendeu seu trabalho final (apresentação oral seguida de arguição) perante uma Banca Examinadora, cujos membros estão listados abaixo. O(A) aluno(a) foi APROVADO(A) pela Banca Examinadora, por unanimidade, em cumprimento ao requisito exigido para obtenção do Título de Mestre em Sensoriamento Remoto. O trabalho precisa da incorporação das correções sugeridas pela Banca Examinadora e revisão final pelo(s) orientador(es).

Título: "Evaluation of wind products from satellites and reanalysis using in situ data sampled in the Bransfield Strait, Antarctic"

Observações da banca: O aluno deve incorporar as sugestões indicadas pela banca e submeter o documento dentro do prazo de 60 dias, de acordo com o regimento da PGSER.

Membros da banca:

Dr. Marcelo Freitas Santini - Presidente - INPE
Dr. Luciano Ponzi Pezzi - Orientador - INPE
Dr. Jonas Takeo Carvalho - Orientador - INPE
Dr. Jorge Arigony-Neto - Membro Externo - Universidade Federal do Rio Grande - FURG / Instituto de Oceanografia - IO

Documento assinado eletronicamente por **Luciano Ponzi Pezzi**, **Pesquisador**, em 10/11/2021, às 16:59 (horário oficial de Brasília), com fundamento no § 3º do art. 4º do Decreto nº 10.543, de 13 de novembro de 2020.

Documento assinado eletronicamente por **Jorge Arigony neto (E)**, **Usuário Externo**, em 12/11/2021, às 14:31 (horário oficial de Brasília), com fundamento no § 3º do art. 4º do Decreto nº 10.543, de 13 de novembro de 2020.

Documento assinado eletronicamente por **Marcelo freitas Santini (E)**, **Usuário Externo**, em 12/11/2021, às 18:42 (horário oficial de Brasília), com fundamento no § 3º do art. 4º do Decreto nº 10.543, de 13 de novembro de 2020.

Documento assinado eletronicamente por **Jonas takeo carvalho (E)**, **Usuário Externo**, em 01/12/2021, às 13:23 (horário oficial de Brasília), com fundamento no § 3º do art. 4º do Decreto nº 10.543, de 13 de novembro de 2020.

A autenticidade deste documento pode ser conferida no site http://sei.mctic.gov.br/verifica.html, informando o código verificador **8444311** e o código CRC **28FB9BA6**.

Referência: Processo nº 01340.005323/2021-34 SEI nº 8444311

“Audaces fortuna iuvat”.

PÚBLIO VERGILIUS MARO

“You can’t have a better tomorrow if you are thinking about yesterday all the time”.

CHARLES F. KETTERING
in *“Prophet of Progress: Selections from the Speeches of Charles F. Kettering”, quote page 16*, 1961

“Life is not always a matter of holding good cards, but sometimes, playing a poor hand well”.

JACK LONDON

*To my mother **Leonete** and to my father **Norberto**, to my sister **Érika**, to my brother **Rodrigo** and to my nephew **Gustavo***

ACKNOWLEDGEMENTS

I thank God for the health and for the strength to always go forward in the challenging journey of the Master's program in remote sensing.

I am very grateful for all of those who contributed to the successful completion of this work. My most heartfelt appreciation goes to my guiders: Drs. Luciano Ponzi Pezzi and Jonas Takeo Carvalho, for believing in my potential, for the immeasurable support and patience when clarifying my doubts and difficulties. As well as the support provided and utmost trust of Drs. Marcelo Freitas Santini and Joey Jeff Voermans for having shared kindly the data obtained in Operation Antartica 38 that were crucial for the development of this dissertation.

I thank INPE for having admitted me in the Master's program in Remote Sensing and for rendering available its physical infrastructure and technical support. I must also address my gratitude to the professors of the Postgraduate Program in Remote Sensing for the knowledge and experience they shared, as well as the care with me and all another students in this learning process, mainly by the coordinator Dr. Ieda Del'Arco Sanches. I am also especially grateful to the library team at INPE for their dedication and competence in preparing tutorials about formatting rules, as well as in exhibiting lectures about the elaboration of dissertations and theses and in finding articles in several journals.

I thank the Brazilian Navy for the authorization granted to attend the master's program, the Navy Acoustic and Electronic Warfare Center (CGAEM) for having admitted me to the selection process for the Remote Sensing Program in the Navy at the master's level in remote sensing, and, especially, the role of CT Paulo Victor Gonçalves SAMPAIO in administrative clearances as Chief of Department of Technical Coordination and Training from CGAEM in relation to administrative issues related to the authorization and transfer ordinance to attend the master's program.

I must also address my gratitude to Navy Studies Coordination Center in São Paulo (CCEMSP) for logistical and administrative support throughout the master's program, especially through the directors of this Center: CMG(EN) Rogério PRADO Lima de Souza (2018-2020). As well as, for CMG(EN) HÉLIO Meira dos Santos, Chief of the Teaching Department, and the 1T(RM2-T) HELEN Campolino de Menezes CABRAL in charge of the Graduation Division.

In addition, I also thank the support provided by the crew of the Polar Ship Admiral Maximiano (H-41) and the crew of the Antarctic Station Commander Ferraz (EACF) for making the ATMOS-1 cruise possible.

I am grateful to the Ministry of Science, Technology and Innovation (MCTI) and the Brazilian Antarctic Program (PROANTAR) for financing the ATMOS Project (CNPq / PROANTAR 443013 / 2018-7). ATMOS is partially financed through the CNPq Scientific Productivity Scholarship (CNPq / 304858 / 2019-6). As well as, also are grateful to ESA, EUMETSAT and the Copernicus Marine Environment Monitoring Service for their open access policy and for providing the satellite scenes used in this work.

In addition, thank all members of the Laboratory of Ocean and Atmosphere Studies (LOA) from INPE for make possible buoy's deployment and mooring, and for share all data.

My sincere and deep thanks go to the team of friends from Navy, from classroom and from the Laboratory of Ocean and Atmosphere Studies (LOA) of INPE who encouraged and helped me in the daily life of the journey of the Master's program in remote sensing:

a) Navy mates: CC VICTOR Silva ARAÚJO and CC ANDRÉ dos Santos ROCHA;

b) Classroom mates: Ana Larissa Ribeiro de Freitas, Cândida Caroline Souza de Santana Leite, Diego Xavier Bezerra, Danielle Silva de Paula, Gabriel Oliveira Chagas, Raíssa Caroline dos Santos Teixeira and Sabrina Paes Leme Passos Corrêa;

c) LOA: MSc. Celina Cândida Ferreira Rodrigues, MSc. Eliana Bertol Rosa and MSc. Luciana Shigihara Lima.

Also, I am grateful to the members of my dissertation committee, who openly accepted to evaluate and discuss this study.

Finally, but not the least, I will always be grateful to my mother Leonete Cardoso de Brito, to my father José Norberto Vieira Lanes, to my sister Érika de Brito Lanes, to my brother Rodrigo de Brito Lanes, and to my nephew Gustavo Lanes Carrilho for their support and encouragement.

ABSTRACT

The lack of availability of a robust long-term high-quality database with regional sea surface wind field data is a demand in the studies of ocean-atmosphere interaction in the Bransfield Strait region at Antarctic Peninsula. It was explored the comparison of level 2 satellite scenes from Sentinel-1 and Advanced Scatterometer, in addition with reanalysis data against *in situ* measurements. These *in situ* measurements were made by buoys' deployment from "Antarctic Modeling Observation System" (ATMOS) project, near King George Island (Antarctica) in November 2019 on board the Polar Ship Admiral Maximiano of the Brazilian Navy. Time series were also presented in order to demonstrate the consistency of all analyzed data. Overall, the satellite-derived data set showed a reliable accuracy when compared with data set from wind sensor installed in the anchored buoy, while reanalysis data set overestimated the wind sensor's measurements. To execute an spatial analysis, it was necessary at least two sources of data. In due to expected errors (temporal separation, spatial separation, sampling variability, satellite sensor and algorithm) all sources should be studied with attention. The statistical error analysis showed availability and feasibility of satellite scenes and reanalysis data for comparison against *in situ* measurements according to defined matchup criteria (previously defined) applied between the data, and found BIAS and RMSE values that are outside the ASCAT mission requirements (0.5 and 2.0 m/s, respectively) as well as the RMSE value of Sentinel-1 (2.0 m/s). However, this work endorses that the satellite-derived data are accurate and reliable, if the user can disconsider the mission requirements and uses them with attention. Then, it is possible to employ these data in Numerical Weather Prediction models and also for other applications in the regional analyses enhancement. Finally, the present work demonstrated the superior performance of ERA5 in wind speed measurements, and the slightly superior performance of ASCAT for wind direction measurements when compared with meteorological buoy and wave buoy.

Keywords: SAR. ASCAT. ERA5. Wind field. Regional wind analysis. Antarctica.

AVALIAÇÃO DE PRODUTOS DE VENTO DE SATÉLITES E REANÁLISE USANDO DADOS IN SITU AMOSTRADOS NO ESTREITO DE BRANSFIELD, ANTÁRTICA.

RESUMO

A falta de disponibilidade de um banco de dados robusto de longo prazo e de alta qualidade com dados regionais de campos de vento na superfície do mar é uma demanda nos estudos de interação oceano-atmosfera na região do Estreito de Bransfield na Península Antártica. Foi explorada a comparação de cenas de satélite de nível 2 do Sentinel-1 e do escaterômetro avançado, em adição com dados de reanálise contra medições *in situ*. Essas medições *in situ* foram feitas por meio da implantação de bóias do projeto "Antarctic Modeling Observation System" (ATMOS), próximo à Ilha King George (Antártica), em novembro de 2019, a bordo do Navio Polar Almirante Maximiano da Marinha do Brasil. Também foram apresentadas séries temporais para demonstrar a consistência de todos os dados analisados. No geral, o conjunto de dados derivados do satélite mostrou uma precisão confiável quando comparado com o conjunto de dados do sensor de vento instalado na bóia ancorada, enquanto o conjunto de dados de reanálise superestimou as medições do sensor de vento. Para realizar uma análise espacial, foram necessárias pelo menos duas fontes de dados. Devido aos erros esperados (separação temporal, separação espacial, variabilidade de amostragem, sensor de satélite e algoritmo), todas as fontes devem ser estudadas com atenção. A análise de erro estatístico mostrou a disponibilidade e a viabilidade de cenas de satélite e dados de reanálise para comparação com medições *in situ* de acordo com os critérios de confronto (previamente definidos) aplicados entre os dados, e encontrou valores de BIAS e RMSE que estão fora dos requisitos de missão ASCAT (0,5 e 2,0 m/s, respectivamente), bem como o valor RMSE do Sentinel-1 (2,0 m/s). No entanto, este trabalho confirma que os dados derivados do satélite são precisos e confiáveis, se o usuário puder desconsiderar os requisitos da missão e usá-los com atenção. Assim, é possível empregar esses dados em modelos de Previsão Numérica de Tempo e também para outras aplicações no aprimoramento de análises regionais. Finalmente, o presente trabalho demonstrou o desempenho superior do ERA5 em medições de velocidade do vento, e o desempenho levemente superior do ASCAT para medições de direção do vento quando comparado com bóia meteorológica e bóia de ondas.

Palavras-chave: SAR. ASCAT. ERA5. Campo de vento. Análise regional de vento. Antártica.

LIST OF FIGURES

Page

LIST OF TABLES

LIST OF ABBREVIATIONS

AIS	–	Automatic Identification System
ASCAT	–	Advanced Scatterometer
ATMOS	–	Antarctic Modeling Observation System
C3S	–	Copernicus Climate Change Service
CCMP	–	Cross-Calibrated Multi-Platform
COARE	–	Coupled Ocean–Atmosphere Response Experiment
EACF	–	Brazilian Antarctic Station Commander Ferraz
ECMWF	–	European Centre for Medium-Range Weather Forecasts
ERA5	–	ECMWF Reanalysis 5th Generation
ERA-Interim	–	ECMWF Interim Re-Analysis
ESA	–	European Space Agency
EUMETSAT	–	European Organization for the Exploitation of Meteorological Satellites
EW	–	Extra-Wide Swath Mode
GMF	–	Geophysical Model Function
INPE	–	Brazilian National Institute for Space Research
ISAR	–	Inverse synthetic-aperture radar
ITU	–	International Telecommunications Union
IW	–	Interferometric Wide Swath Mode
LOA	–	Laboratory of Ocean and Atmosphere Studies
MAE	–	Mean Absolute Error
ME	–	Mean Error
MetOp	–	Meteorological Operational Satellite
NCDC	–	National Climate Data Center
NCEP-DOE	–	National Centers for Environmental Prediction–Department of Energy reanalysis
NDBC	–	National Data Buoy Center
NRCS	–	Normalized Radar Cross Section
OPERANTAR 38	–	Antarctic Operation 38
PROANTAR	–	Brazilian Antarctic Program
RCS	–	Radar Cross Section
RMSE	–	Root-Mean Square Error
S-AIS	–	Satellite-AIS
SAR	–	Synthetic Aperture Radar
SCAR	–	Scientific Committee on Antarctic Research
SLAR	–	Side-Looking Airborne Radar
SM	–	Stripmap Mode
SST	–	Sea Surface Temperature
STA	–	System of Treaty of Antarctica
VTS	–	Vessel Traffic Services
WMO	–	World Meteorological Organization
WV	–	Wave Mode
WVCs	–	Wind Vector Cells

CONTENTS

Page

1 INTRODUCTION

The lack of availability of a robust long-term high-quality database containing data of *in situ* measurements of regional sea wind field is a demand in the studies of ocean-atmosphere interaction in high-latitude as reported in previous studies (CURRY et al., 2004; BOURASSA et al., 2010; BOURASSA et al., 2013; LI et al., 2013; BOURASSA; HUGHES, 2018; BOURASSA et al., 2019). In the Bransfield Strait region at Antarctic Peninsula, although there are several research stations in land, for example the Brazilian Antarctic Station Commander Ferraz (EACF), there is not always an availability of buoys to obtain data *in situ* at the sea, nor the public availability of these data. The harshness of Antarctic marine environment transforms *in situ* measurements at the sea in a thing that is extremely rare to obtain. Thereby, the Antarctic Modeling Observation System (ATMOS) project was conceived as a response to the Brazilian Antarctic Program (PROANTAR) and aims to improve our understanding of sea ice–ocean–atmosphere–waves interactions and turbulent fluxes exchanges in their interface, at micro- and mesoscales in the Atlantic sector of the Southern Ocean as described by Voermans et al. (2021) and Pezzi et al. (2021), continuing the scientific research carried out in previous works (PEZZI et al., 2005; PEZZI et al., 2009; ACEVEDO et al., 2010; CAMARGO et al., 2013; HACKEROTT et al., 2018; SANTINI et al., 2020). For this reason, the demand for accurate data from satellites and from model reanalysis has become our research challenge, as well as for all members of team of Laboratory of Ocean and Atmosphere Studies (LOA) of Brazilian National Institute for Space Research (INPE). Therefore, the ATMOS project made buoys deployment to execute the observational activity during the Antarctic Operation 38 (OPERANTAR 38) on board of Polar Ship Admiral Maximiano from the Brazilian Navy, between 01-13 and 20-27 November 2019, near King George Island (Antarctica) as showed in Figure 3.1.

According to the Brazilian Navy (MB, 2021b), currently 29 countries are advisory members of the System of Treaty of Antarctica (STA), including Brazil, all of which have research stations in Antarctica, and among these countries, 14 have more than one research station in the region. This fact demonstrates the importance of maintaining a permanent research structure in Antarctica. Brazil is the seventh closest country to Antarctica, and due to its relative proximity, it is directly influenced by the natural phenomena that occur there, for example Antarctic Ozone Hole and Antarctic Oscillation (KIRCHHOFF et al., 1996; PINHEIRO et al., 2010; COMBES; MATANO, 2014; ALVES et al., 2017). Antarctica plays an essential role in global and regional natural systems, controlling atmospheric and

oceanic circulations, and influencing the climate and living conditions around the globe (WHITE; PETERSON, 1996; MAYEWSKI et al., 2009; CONVEY et al., 2009; THOMPSON et al., 2011; HANSOM; GORDON, 2014). Therefore, the study of the Antarctic region is fundamental for all countries, especially for Brazil. Considering these circumstances, in addition to strategic, geopolitical and economic motivations, Brazil adhered to the Treaty of Antarctica, in 1975, and started PROANTAR in 1982. Moreover, research development is an essential condition for the country to maintain its condition of Advisory Member of the Treaty of Antarctica, enabling the country to be a member of the Scientific Committee on Antarctic Research (SCAR), with the right to participate in major global scientific projects, developed in an international partnership in Antarctica.

With the advances in space technology, there is an increase in the number of wind-sensing satellites in orbit. However, the temporal resolution at a single location is still low, once altimeter sensors revisit a location within 5 to 20 days, while radiometer missions revisit approximately twice per day (YOUNG; DONELAN, 2018). Thus, the quality control of satellite-derived data over the ocean, in case of lack of well-done *in situ* measurements, is desirable because allow to get confidence of the accuracy for the purpose of model calibration and validation, and the assimilation of real-time data in operational forecasting models (GILHOUSEN, 1994; VENKATESAN et al., 2018; VOERMANS et al., 2021).

The data of European Centre for Medium-Range Weather Forecasts (ECMWF) Reanalysis 5th Generation (ERA5) reanalysis have their accuracy, especially over the ocean, enhanced due to data input from *in situ* measurements made by ships, buoys and satellite-derived wind speeds. Previous papers also assessed the performance of numerical atmospheric models against *in situ* observations from ships and buoys (LI et al., 2013; STOPA; CHEUNG, 2014; JONES et al., 2016; SCHMIDT et al., 2017; ZHANG et al., 2018; BELMONTE RIVAS; STOFFELEN, 2019; DONG et al., 2020; LANDWEHR et al., 2020). They showed that model biases present variability depending on the region and season. However, in some of those works it is described that over the last few decades occurred significant improvements in the precision and accuracy of these models as consequence of the increasing on observed data quality and volume.

For example, Li et al. (2013) evaluated the performance of two numerical weather prediction reanalyses (Department of Energy from the National Centers for Environmental Prediction (NCEP–DOE) and ECMWF Interim Re-Analysis (ERA-

Interim)), and two satellite-based (National Climate Data Center (NCDC) and cross-calibrated multiplatform (CCMP)) sea surface wind speeds in the Southern Ocean. Such products were validated against *in situ* measurements. In their analysis, it was verified that all four products overestimated the wind speed under weak wind conditions (<4 m/s). Additionally, their results demonstrated that different products tend to have a better agreement with the observations under moderate wind conditions and that all four products underestimated the wind speed under high wind conditions (>25 m/s), although the authors had mentioned that more observations were needed to further confirm this. Afterwards, Dong et al. (2020) evaluated ERA5 and another five more recently released reanalysis products using 30 manned stations and 26 automatic weather stations, and concluded that the representation of near-surface wind speeds in all six reanalysis products depends on seasonality, with low performance in winter, and high performance in summer.

Likewise, previous studies (RANA et al., 2019; JANG et al., 2019) also assessed the performance of Synthetic Aperture Radar (SAR) against *in situ* observations from ships and buoys as well as others (TOMITA; KUBOTA, 2011; ABDALLA; DE CHIARA, 2017; HUTCHINGS et al., 2020) studied the scatterometers. As SAR has a higher spatial resolution than scatterometers such that it can produce much better wind field data with a high spatial resolution. Thus, it is possible to analyze detailed wind fields with much higher spectral energy than those derived from winds obtained by scatterometers (KORSBAKKEN et al., 1998; FUREVIK; KORSBAKKEN, 2000; YANG et al., 2011). For example, Jang et al. (2019) verified in the coastal region around the Korean Peninsula that wind speeds derived from the SAR data also presented a tendency for water depth to be overestimated over shallow bathymetry and to be underestimated at high wind speeds (>10 m/s). Moreover, they reported that the wind speed errors are associated with the regional and specific characteristics of the coastal region around the Korean Peninsula, such as, the sand ridges over the shallow region influenced the sea surface roughness because of the interaction between the bathymetry and tidal current, which resulted in significantly overestimated wind speeds, according to the spatial distribution of the Sentinel-1A/B wind speeds presented in their study.

Lastly, in this work, we explored the differences between values found for the level 2 scenes from Sentinel-1 (which has a SAR in C-Band on board) , level 2 scenes from Advanced Scatterometer (ASCAT), and data from ERA5 Reanalysis against *in situ* measurements at Peninsula Antarctic. The measurement errors

between the observations (*in situ* and by satellite) and the predictions originated from state-of-the-art numerical atmospheric model were analyzed by statistical parameters for enhancing regional wind analyses. Keeping in mind this is a region with few continuous long-term records, it was suggested the remote sensing data and reanalysis data can be useful tool to overcome this lack of data.

1.1 Motivation

As reported by Bourassa et al. (2019), satellite vector wind products are essential for determining the large-scale ocean circulation and transport. The reason is that vector winds are also needed to estimate the ageostrophic (Ekman) component of ocean currents, and consequently are linked to coastal upwelling, primary productivity, cross shelf transport, ice transport, mixed layer evolution, and deepwater formation. Moreover, for reliable computations of air/sea heat fluxes (sensible and latent heatfluxes) as well as mass fluxes (e.g., CO_2 and H_2O), accurate wind speeds are required, resulting in importance of surface winds for budgeting energy, moisture and carbon, and for studies of ocean acidification and fishstocks. Thus, surface wind speed and direction were listed by World Meteorological Organization (WMO) in the group of essential climate variables which is composed of physical, chemical or biological variables or a group of linked variables that critically contributes to the characterization of Earth' s climate.

1.1.1 Validation activities by ESA and EUMETSAT

According to ESA (2020b), the checks related to Sentinel-1 is only applicable to Level-2 products. Where a level 2 geophysical validation encompasses a verification of the geophysical variables against independent external measures like buoys (Figure 1.1) or other Earth Observation data source. And, the ocean wind field validation assesses the radiometric calibration performance for all combinations of mode, swath and polarization. It also analyzed wind retrieval performance as a function of the mode, incidence angle (swath), polarization and wind conditions, as follow:

a) geophysical validation is undertaken globally against collocated buoys;

b) inter-comparison of wind measurements from the different Sentinel-1 modes; and

c) inter-comparison with global winds retrieved from scatterometers (e.g. ASCAT)

Figure 1.1 - CMEMS buoy-based in-situ wave coverage.

In-situ wave data, typically provided by buoys, are very helpful to validate satellite wave products but in many areas of open water such buoys are not available, because of the difficulty and costliness of installation and maintenance.

SOURCE: ESA (2020a).

Figure 1.2 - Locations of the moored buoys used in the comparisons with ASCAT.

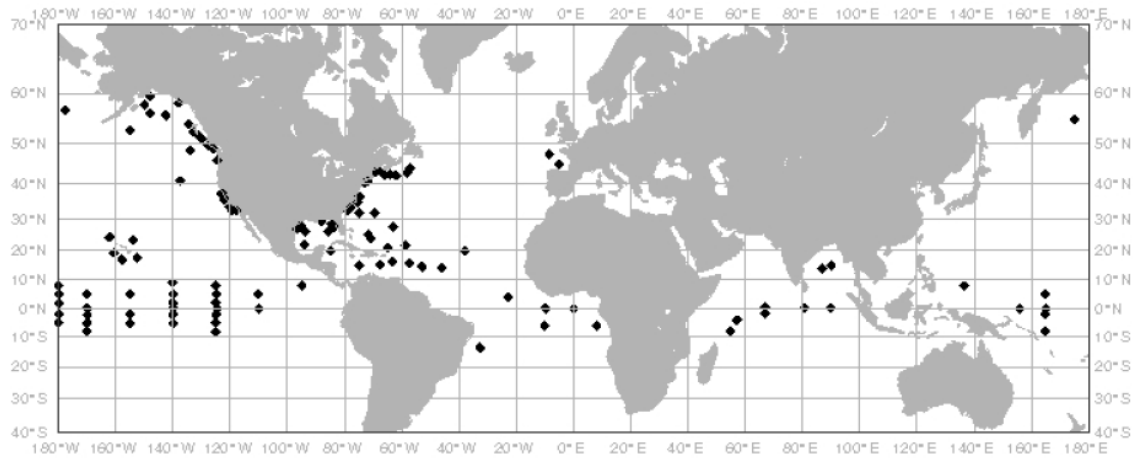

SOURCE: OSI SAF (2018b).

According to OSI SAF (2018b) and OSI SAF (2016), ASCAT's wind data are compared with in situ buoy wind measurements. The buoy winds are distributed through the Global Telecommunication System (GTS) and have been retrieved

from the ECMWF MARS archive. In addition, in OSI SAF (2018b) is reported that was used a set of 115 moored buoys spread over the oceans, most of them in the tropical oceans and near Europe and North America. The locations of the buoys used in the comparisons with ASCAT is showed in Figure 1.2. Note that there are practically no comparisons with buoys in the southern hemisphere, and that there are no comparisons with buoys in the Antarctic Peninsula region.

1.2 Objectives

The main objective of this research to master's dissertation was to determine the accuracy of satellite-derived (Sentinel-1 and ASCAT) wind field retrieved from the last level of processing and of reanalysis-derived wind field (ERA5) in the Bransfield Strait region at Antarctic Peninsula for enhancing regional analyses of wind and for overcoming this lack of data.

1.2.1 Specific objectives

In order to achieve such goal the following specific aims were elaborated:

a) To Evaluate of availability and feasibility of satellite scenes and reanalysis data for comparison against *in situ* measurements according to defined matchup criteria (detailed in Section 3.3);

b) To analysis spatially the statistical performance of Sentinel-1, ASCAT and ERA5 in Bransfield Strait region, taking each data source in pairs according to defined matchup criteria (detailed in Section 3.3);

c) To calculate the statistical performance of wind field measurements obtained by satellite and estimated by reanalysis against *in situ* measurements obtained in observational activities during the OPERANTAR 38 at Bransfield Strait region, using meteorological buoy (between 10 and 18 November, 2019) and wave buoy (from November 8, 2019 until March 1, 2020).

This study is organized as follows: Chapter 2 highlights some important previous knowledge about satellite remote sensing of the oceans. In the Chapter 3 it was described the methodology and a short overview of obtaining of *in situ* measurements and satellite-derived data. In Chapter 4 we presented our error analysis results. In Chapter 5 we showed and discussed our time series analysis. Finally, in Chapter 6 we present our conclusions, final remarks and future works.

2 BIBLIOGRAPHY REVIEW

2.1 Definition of remote sensing

In his book “Physical Principles of Remote Sensing”, Lorenzzetti (2015) teaches us that the definition of remote sensing can have different interpretations. According to Elachi and Zyl (2021) remote sensing is defined as the acquisition of information about some property of an object or phenomenon without physical contact with it. Moreover, it is exposed that information about a target would be obtained by detecting and measuring changes that the object imposes on the surrounding field, be it an electromagnetic, acoustic or potential field.

2.1.1 Applications of remote sensing

Remote Sensing Applications, as explained by Lorenzzetti (2015), can be divided into: environmental and military applications. In the military applications, the primary use is for detecting and classifying targets and in mapping terrain and facilities. Also, it can be used in tracking radar and in the guidance of intelligent weapons (RICHARDS et al., 2010). Its importance is highlighted in its use in search and rescue services within the world system of safeguard of human life at sea. For example, the ship surveillance (in open ocean or inland waters) is done in a collaborative method by the Automatic Identification System (AIS) which is a short-range monitoring system used on ships and Vessel Traffic Services (VTS) (MB, 2021a; WU et al., 2017; ARONSEN; LANDMARK, 2016). To detect AIS signatures, satellites can be also used, then the term Satellite-AIS (S-AIS) is used. On the other hand, within the environmental applications, we have:

a) *Atmospheric monitoring:* temperature, precipitation, cloud distribution and types, wind speed, gas concentration, such as water vapor, carbon dioxide, ozone, etc.

b) *Monitoring of land surface:* geology, geography, agronomy, limnology, forests, land cover and occupation, etc.

c) *Ocean monitoring:* offshore engineering design, testing of numerical models, studies of air–sea fluxes, sea surface temperature (SST), surface topography (ocean currents and tides), ocean color (pollution, sediments, chlorophyll concentration, primary productivity, etc.) and surface roughness (surface winds, waves, oil pollution, oceanic fronts, etc.).

d) *Monitoring the Earth's cryosphere:* ice and snow deposited in the polar regions, ice shelves and icebergs.

2.2 Microwave sensors

According to Ulaby and Long (2014), microwave remote sensing instruments can be divided into two broad classes: *passive*, known as radiometers, and *active*, known as radars. However, radars differ from radiometers because they include a transmitter as well. Passive and Active sensors have been used on aircraft and spacecraft to study the Earth as well as other planets, and can be subdivided into subclasses based on their general operating characteristics and functions as showed in Figure 2.1.

Figure 2.1 - Major classes of microwave remote sensors.

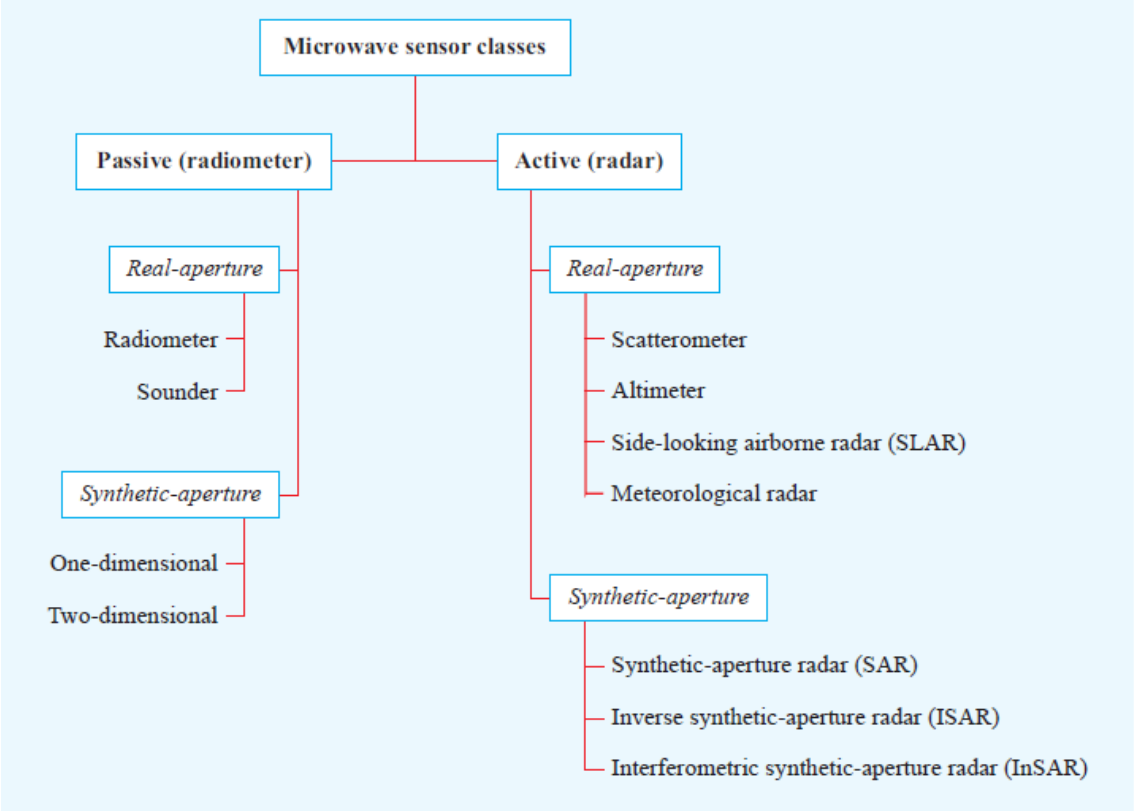

SOURCE: Ulaby and Long (2014).

Although Ulaby and Long (2014) show us that active microwave sensors can be grouped into five general classes: *synthetic-aperture radar* (SAR) systems, *side-looking airborne radar* (SLAR), *scatterometers*, *altimeters*, and *meteorological radars*. This work is focused in SAR (Sentinel-1) and scatterometers (ASCAT) due to reasons of data availability, and some characteristics are discussed in Section 2.3. In addition, as suggested by the name, SAR employs synthetic-aperture antenna-processing techniques, whereas the other sensor systems typically use real-aperture antennas. In his book, Richards et al. (2010) reported the use of *inverse synthetic-aperture radar* (ISAR) in military applications, for example, to provide images of threat targets to train pattern-recognition-based target identification systems by *radar cross section* measurement of indoor targets (missiles, artillery rounds and scale models of threat vehicles and aircraft) and outdoor targets (full-sized targets such as tanks and aircraft). While, the use of ISAR for groundbased sensing of extra-terrestrial bodies is mentioned by Ulaby and Long (2014).

Moreover, radar systems that are used for remote sensing can also be divided into two broad categories: *imaging radars* (SAR and SLAR), and *nonimaging radars* such as scatterometers, altimeters, and meteorological radars. Several remote sensing applications employ an imaging radar, but specialized applications, such as measuring winds at sea, use scatterometers. On the other hand, spaceborne scatterometers can be used to generate low-resolution imagery even though classified as a nonimaging sensor (ELACHI; ZYL, 2021; EMERY; CAMPS, 2017; WOODHOUSE, 2017; LORENZZETTI, 2015; ULABY; LONG, 2014).

In addition, radars operate in the range of 3 MHz to 300 GHz, though the large majority operate between about 300 MHz and 35 GHz as described by Richards et al. (2010). The Table 2.1 shows the International Telecommunications Union (ITU) frequencies authorized for radar use alongside the radar bands, and Figure 2.2 shows the different types of electromagnetic waves as a function of frequency, from electromagnetic telegraphy to gamma rays.

Table 2.1 - Radio-frequency and radar bands.

Band	Frequency Range	ITU Radar Frequency Range
High frequency (HF)	3–30 MHz	

(To be continued)

Table 2.1 - Conclusion.

Band	Frequency Range	ITU Radar Frequency Range
Very high frequency (VHF)	30–300 MHz	138–144 MHz 216–225 MHz
P (Ultra high frequency - UHF)	300 MHz–1 GHz	420–450 MHz 890–942 MHz
L	1–2 GHz	1.215–1.400 GHz
S	2–4 GHz	2.3–2.5 GHz 2.7–3.7 GHz
C	4–8 GHz	5.250–5.925 GHz
X	8–12 GHz	8.500–10.680 GHz
Ku (“under” K-band)	12–18 GHz	13.4–14.0 GHz 15.7–17.7 GHz
K	18–27 GHz	24.05–24.25 GHz 24.65–24.75 GHz
Ka (“above” K-band)	27–40 GHz	33.4–36.0 GHz
V	40–75 GHz	59.0–64.0 GHz
W	75–110 GHz	76.0–81.0 GHz 92.0–100.0 GHz
mm	110–300 GHz	126.0–142.0 GHz 144.0–149.0 GHz 231.0–235.0 GHz 238.0–248.0 GHz

Source: Adapted from Richards et al. (2010).

Figure 2.2 - Electromagnetic wave types.

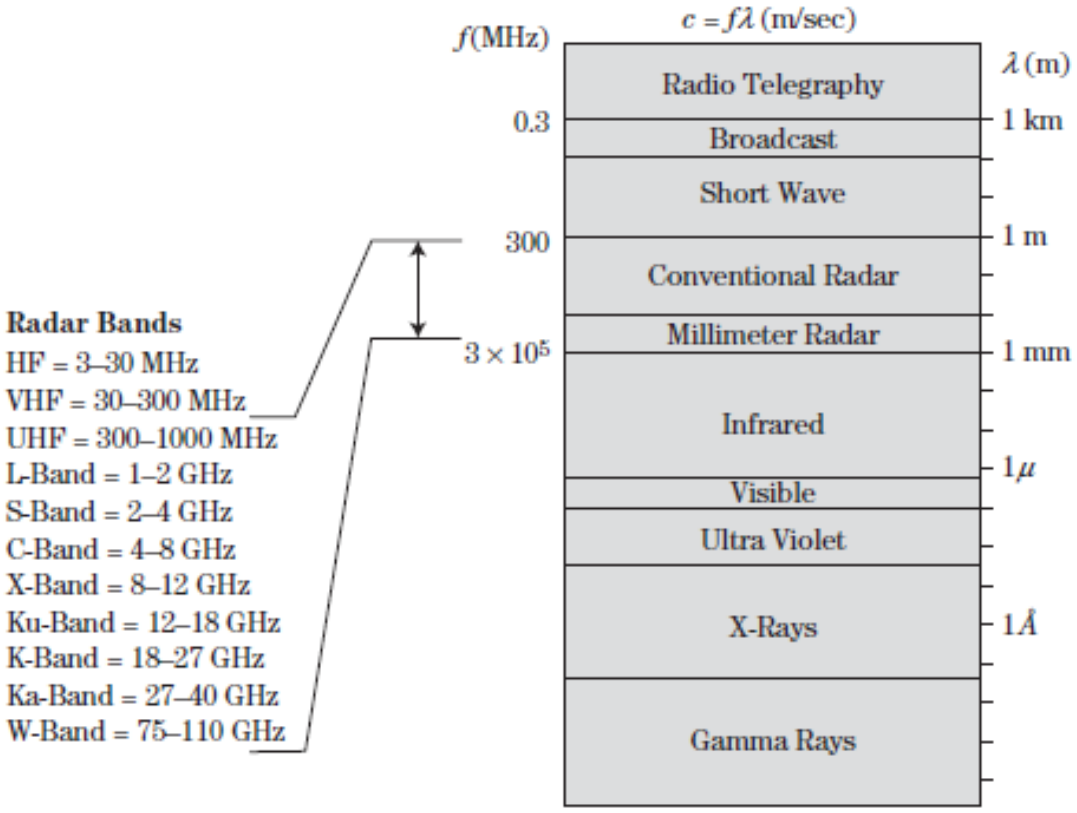

SOURCE: Richards et al. (2010).

2.2.1 Brief approach about the wave polarization

According to Richards et al. (2010) an electromagnetic wave is the self-propagating transport of energy (voltage and current) through space, without this energy being attached or directed via some external structure such as a transmission line or waveguide. James Clerk Maxwell showed in the 1860s that a time-changing electric field, $\vec{E}$ (V/m), is the source for the magnetic field, $\vec{H}$ (A/m), and, in turn, a time-changing $\vec{H}$ is the source for $\vec{E}$. As explained by Ulaby and Long (2014), this wave is said to be *transverse electromagnetic* in due to the fact of the electric and magnetic fields are perpendicular to each other, and both are perpendicular to the direction ($\vec{k}$) of wave propagation (Figure 2.3). The propagation vector $\vec{k}$ points in the direction of travel of the wave and has a scalar magnitude related to the reciprocal of wavelength, $k = 2\pi/\lambda$ (KNOTT et al., 2004). The po-

larization of a uniform plane wave describes the locus traced by the tip of the $\vec{E}$ vector (in the plane orthogonal to the direction of propagation) at a given point in space as a function of time. Thus, in the most general case, the locus of the tip of $\vec{E}$ is an ellipse, and the wave is said to be *elliptically polarized*. However, under certain conditions, the ellipse may degenerate into a circle or a straight line, in which case the polarization state is called *circular* or *linear*, respectively (ULABY; LONG, 2014).

Figure 2.3 - Wave nature of an electromagnetic field.

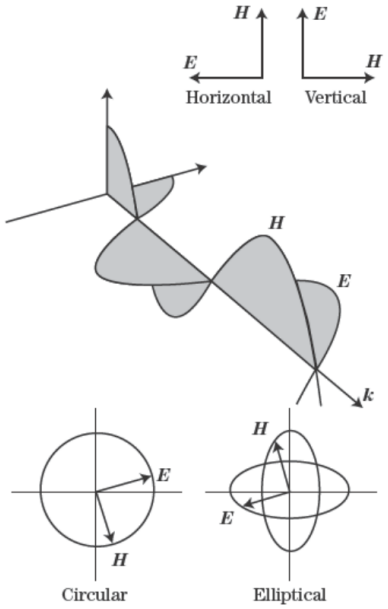

SOURCE: Knott et al. (2004).

In addition, Richards et al. (2010) explain that linear polarization is specified typically as relative to one's surroundings, and that in the real world with the earth as a reference, horizontal or vertical are usually chosen as linear polarization directions (Figure 2.4). While, in the computational world with spherical coordinates, polarization is specified in the azimuth, ϕ, and polar, θ, directions. On the other hand, circular polarization is specified as left or right circular rotation of $\vec{E}$. In remote sensing, the polarization with $\vec{E}$ perpendicular to the plane of incidence is also called horizontal polarization, because $\vec{E}$ is parallel to Earth's surface, and that with $\vec{E}$ parallel to the plane of incidence is called vertical polarization, because in this case it is the magnetic field that is parallel to Earth's surface (ULABY; LONG, 2014).

Figure 2.4 - Typical linear polarizations for experimental and analytical work.

(a) Experimental

(b) Analytical Spherical Coordinate System

SOURCE: Knott et al. (2004).

The most common, but not exclusive, method is to use linear horizontal and linear vertical polarizations, as described by Woodhouse (2017). For transmitters, these two linear states, could, in principle be used to generate any polarization state simply by controlling the relative amplitude and phase of the two waves. The converse is true for receivers: as long as we measure the phase difference as well as the amplitude in both linear polarizations, we can determine the complete polarization state of a wave. Thereby, four polarization combinations are normally used (ULABY; LONG, 2014):

a) HH – electromagnetic radiation is transmitted and received in horizontal polarization;

b) VV – electromagnetic radiation is transmitted and received in vertical polarization;

c) HV – electromagnetic radiation is transmitted in horizontal polarization and received in vertical polarization; and

d) VH – electromagnetic radiation is transmitted in vertical polarization and received in horizontal polarization.

Finally, the polarization information is needed to describe how an electromagnetic wave is both transmitted and received. The polarization of the outgoing electromagnetic wave is defined by the physical characteristics of the transmitting antenna. While, the amount of signal actually received from an incoming

electromagnetic wave of a given polarization is is defined by the receiving antenna polarization characteristic. Thus, *radar cross section* (defined in Subsection 2.2.2) becomes a function of both transmitter polarization and receiver polarization. In addition, some target reflection properties such as edges and surface waves are a function of the polarization of the incident wave relative to target geometry (RICHARDS et al., 2010).

2.2.2 The radar reflectivity

The ratio of the power scattered back to the radar receiver (P_{RX}) over the incident radar power density (P_{TX}) per unit of solid angle on the target as if the radiation were isotropic is defined as the *radar cross section* (RCS) of a target (ULABY; LONG, 2014). Mathematically, it is defined as 4π times the ratio of the power per unit solid angle scattered in a specified direction to the power per unit area in a plane wave incident on the scatterer from a specified direction. More precisely, it is the limit of that ratio as the distance from the scatterer to the point where the scattered power is measured approaches infinity (RICHARDS et al., 2010), and it is expressed by Equation 2.1:

$$\sigma_{RCS} = \lim_{r \to \infty} 4\pi \cdot r_0^2 \cdot \frac{P_{RX}}{P_{TX}} \tag{2.1}$$

where r_0 represents the distance between the radar and the target. In this equation, the limit states that the RCS is measured in the far-field. The RCS of a target is a function of several attributes of the target, of the radar observing the target, and the radar-target geometry (ULABY; LONG, 2014; RICHARDS et al., 2010), such as:

a) target geometry and material composition;

b) position of transmitter relative to target;

c) position of receiver relative to target;

d) frequency or wavelength;

e) transmitter polarization; and

f) receiver polarization.

The RCS describes the power efficiency of the scattering mechanism of a given target, but fails to describe homogeneous areas without clear boundaries. For these cases, the RCS can be averaged over the surface or volume where the scatterer extends. The average RCS per unit of resolution cell is denoted as *sigma naught*, *backscatter coefficient*, or *normalized radar cross section* (NRCS), and it can be expressed as:

$$\sigma^0 = \frac{\langle \sigma_{RCS} \rangle_{cell}}{A_{cell}} \tag{2.2}$$

where A_{cell} is the area of the resolution cell on the ground, and $\langle \cdot \rangle$ indicates spatial averaging over a multiplicity of observations. This equation is valid for imaged surfaces and can be consistently extended to the case of volumes by swapping the area in the denominator with a volume. However, a constant area on the ground might project differently on the geometry of the image depending on the local topography of the scene, which results in a terrain-dependent modulation of the scattering coefficient σ^0.

2.2.3 Brief approach about the radar range equation

Fundamentally, according to Ulaby and Long (2014), a radar can determine (1) direction (by the pointing of the antenna), (2) distance (by measuring the time of flight of the signal to and from the target), (3) speed (by measuring the Doppler shift of the echo), and (4) radar scattering cross section (by comparison of the energy of the echo return to that of the transmitted signal). On the other hand, Richards et al. (2010) understand that the three fundamental functions of radar systems are (1) to search for and find (detect) targets, (2) to track detected targets, and in some cases (3) to develop an image of the target. The idealized power budget of the radar link (transmitter-target-receiver) is usually known as the *radar equation* (Equation 2.3). A sketch of the radar operation is shown in Figure 2.5.

$$P_r = \frac{P_t G_t G_r \lambda^2 \sigma}{(4\pi)^3 R^4} \tag{2.3}$$

Where, P_t is the peak transmitted power in watts. G_t is the gain of the transmit antenna. G_r is the gain of the receive antenna. λ is the carrier wavelength in meters. σ is the mean RCS of the target in square meters. R is the range from the radar to the target in meters.

As the power received $P_r = Q_r \cdot A_e$, where A_e is effective area of antenna, and re-

ceive antenna gain is $G_r = 4\pi\eta_a A/\lambda^2 = 4\pi A_e/\lambda^2$, and η_a is the antenna efficiency whose value is between 0 and 1, we can do some substitutions, and thus obtain the Equation 2.3.

2.3 Satellite remote sensing of the oceans

In their paper, Young et al. (2017) affirm that the oceanographic satellites have now been in operation for more than 30 years, providing an almost continuous record of wind speed and wave height with global coverage. During this period, the global measurements of wind speed and/or wave height was obtained by four main instruments: altimeters, radiometers, scatterometers, and synthetic aperture radars. Moreover, the authors still report that more than 20 different satellite missions have employed these systems which are described in this section as follow.

2.3.1 Radar altimeters

The Radar altimeters has a footprint between 5 and 10 km in diameter. They can estimate the significant wave height (H_S) and wind speed (U_{10}), using the

Figure 2.5 - Power density (Q_r) back at the radar receive antenna.

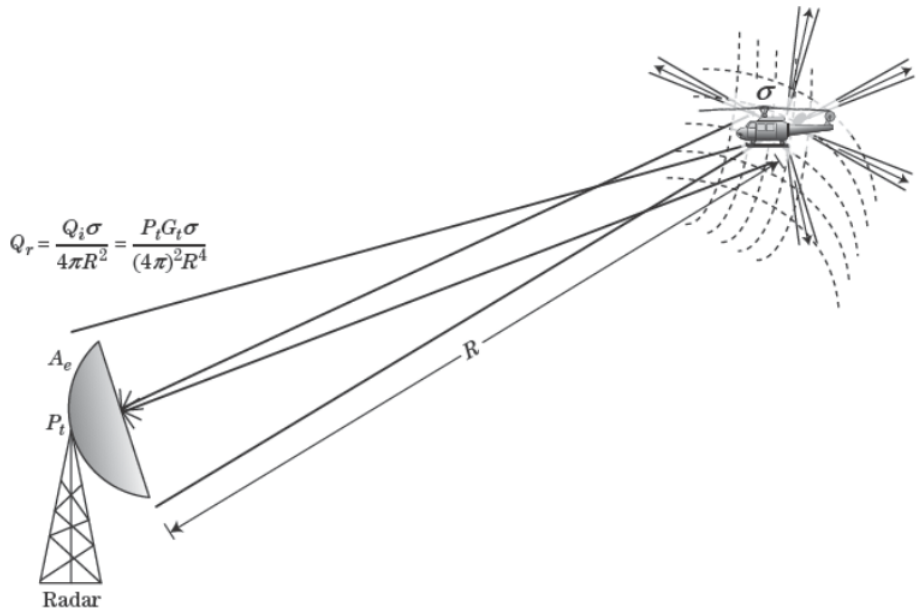

SOURCE: Richards et al. (2010).

shape and intensity of the returned radar signal from this footprint (YOUNG et al., 2017; ZIEGER et al., 2009; WOODHOUSE, 2017; QUEFFEULOU, 2004; CHELTON et al., 2001). The NRCS σ^0 measures the power of the return pulse and is used to estimate the wind speed, while the slope of the leading edge of the return pulse is employed to estimate significant wave height (EMERY; CAMPS, 2017; WOODHOUSE, 2017; HOLTHUIJSEN, 2007; CHELTON et al., 2001). However, some storm events may be undersampled or missed completely due to the low spatial/temporal resolution, despite such instruments have global coverage (YOUNG et al., 2017; ZIEGER et al., 2014).

2.3.2 Microwave radiometers

The emissivity and reflection properties of the ocean are related to the brightness temperature of the sea surface that is measured by the radiometers (ULABY; LONG, 2014). As cited by Young et al. (2017), Meissner and Wentz (2012), these in turn are a function of the roughness of the water surface, and thus, is also related with the wind stress, which in turn is related to the wind speed. When they are compared to altimeters, the radiometers provide much greater spatial and temporal resolution. Nevertheless, radiometers cannot provide reliable wind speed data in regions with heavy rain as reported by Meissner and Wentz (2009).

2.3.3 Scatterometers

This was one of the two sensors chosen to perform the comparisons in this work. A scatterometer is a microwave radar that emits electromagnetic pulses at a determined frequency and polarization to the Earth's surface. According to Ulaby and Long (2014), scatterometers are unique among satellite remote sensors in their ability to determine wind speed and direction over water. As cited by Young et al. (2017) scatterometers measure σ^0 from a range of different azimuth angles, thus also allowing the wind direction to be determined. To measure σ^0, the scatterometer transmits a pulse of electromagnetic wave in radio-frequency and measures the backscattered energy from this pulse as compared with the transmitted signal. Using the radar equation, it is possible to compute the (σ^0) of the ocean's surface. As explained by Ulaby and Long (2014), this estimate is then converted into the near-surface wind speed using a geophysical model function, which relates the backscatter intensity to the wind stress. Even then, another wind source (for example, external wind or atmospheric pressure measurements) is usually necessary to resolve a 180° ambiguity.

2.3.4 Synthetic Aperture Radar

This was the another sensor chosen to perform the comparisons in this work. As explained by Ulaby and Long (2014), when a synthetic-aperture radar is operating, it operates by "synthesizing" a long antenna aperture to produce finer resolution in the along-track direction.Therefore, the resolution of the radar is much greater than would be expected given the physical size of the radar antenna. As reported by Young et al. (2017) the SAR is the only instrument with the potential to measure the full directional wave spectrum and, as a minimum, the integral properties of the significant wave height, the mean/peak wave period, and the mean wave direction. Howerver, the relatively low spatial/temporal resolution has limited its application, despite its significant potential.

2.4 Brief approach about C-band Geophysical Model Function – CMOD5.N

The development of the CMOD family has its origin as a requirement of a geophysical model function for the C-band AMI scatterometer on-board ERS-1 that was launched by ESA. The geophysical model function (GMF) CMOD5.N calculates an empirical relation between C-band backscatter measured by the spaceborn ERS-2 and ASCAT scatterometers, and equivalent neutral ocean vector wind at 10-meter height (neutral surface wind) as function of scatterometer's incidence angle. Further information and technical details are covered in Hersbach (2008). All CMOD models provide an empirical functional relation in which the dependency of normalized backscatter σ^0 on wind speed v, wind direction χ, and incidence angle θ is described in Equation 2.4:

$$\sigma^0 = CMOD(c, v, \phi, \theta) = B0(c_0, v, \theta)[1 + B1(c_1, v, \theta)\cos(\phi) + B2(c_2, v, \theta)\cos(2\phi)]^p \tag{2.4}$$

Where, according to Hersbach (2008), $\phi = \chi - \alpha$ is the angle between wind direction and scatterometer azimuth look angle (both measured from the North), coefficients c_i (which are subsets from a larger set c) shape the terms Bi, and p is a parameter. The dependency on wind direction is described by only two harmonics. The dominant term $B0$ sets the speed scale for a given measurement. The upwind-crosswind asymmetry $B2$ allows for the determination of wind direction, while $B1$ attributes to resolve a remaining 180° ambiguity in wind direction.

2.5 Sentinel-1 specifications and key Features

The two Sentinel-1 satellites have a lifetime of 7 years (with consumables for 12 years) and fly in a near polar, sun-synchronized (dawn-dusk) orbit with an altitude of 693 km. Both Sentinel-1A and Sentinel-1B satellites share the same orbital plane with a phase difference of 180°. Each satellite has a 12-day cycle and 175 orbits per cycle, and is carrying an imaging C-band SAR instrument (5.405 GHz), and with the two satellites of the constellation operational, the cycle repetition is 6 days. The all-weather imaging capability of the C-SAR instrument allows to obtain measurement data at high and medium resolutions for land, coastal zones and ice observations in cloudy regions and during night, coupled with radar interferometry capability for detection of small (mm or sub-mm level) ground movements, with the appropriate frequencies and operating modes (ESA, 2019a).

2.5.1 Acquisition modes

There is four exclusive observation modes for Sentinel-1: Stripmap Mode (SM), Interferometric Wide Swath Mode (IW), Extra-Wide Swath Mode (EW) e Wave Mode (WV). The modes SM, IW and EW can operate in single polarization mode (HH or VV) or dual polarization (HH-HV, VV-VH), while WV operates in single polarization mode only. Information about acquisition modes and their respective applications was summarized in Table 2.2, Table 2.3 and Figure 2.6.

Table 2.2 - Mapping of Applications to Sentinel-1 Modes.

Application	**Mode**			
	SM	**IW**	**EW**	**WV**
Arctic and sea-ice		X	X	
Open ocean ship surveillance		X	X	
Oil pollution monitoring		X	X	
Marine winds		X	X	X
Forestry		X		
Agriculture		X		
Urban deformation mapping		X		
Flood monitoring	X	X		
Earthquake analysis	X	X		
Landslide and volcano monitoring	X	X		

SOURCE: ESA (2019f).

Table 2.3 - Performance parameters of the C-SAR instrument in the various operational modes.

Operational (mode)	Polarization	Swath width	Single Look Resolution (range x azimuth) and Access Angles
Stripmap (SM)	HH-HV or VV-VH	80 km	5 m x 5 m 20°–45°
Interferometric Wide Swath (IW)	HH-HV or VV-VH	250 km	5 m x 20 m 25°
Extra Wide Swath (EW)	HH-HV or VV-VH	400 km	25 m x 40 m 20°
Wave mode (WM)	HH (23°) or VV (36.5°)	20 km x 20 km (vignettes at 100 km intervals)	5 m x 5 m 23°and 36.5°

SOURCE: ESA (2019a).

Figure 2.6 - Acquisition modes of Sentinel-1.

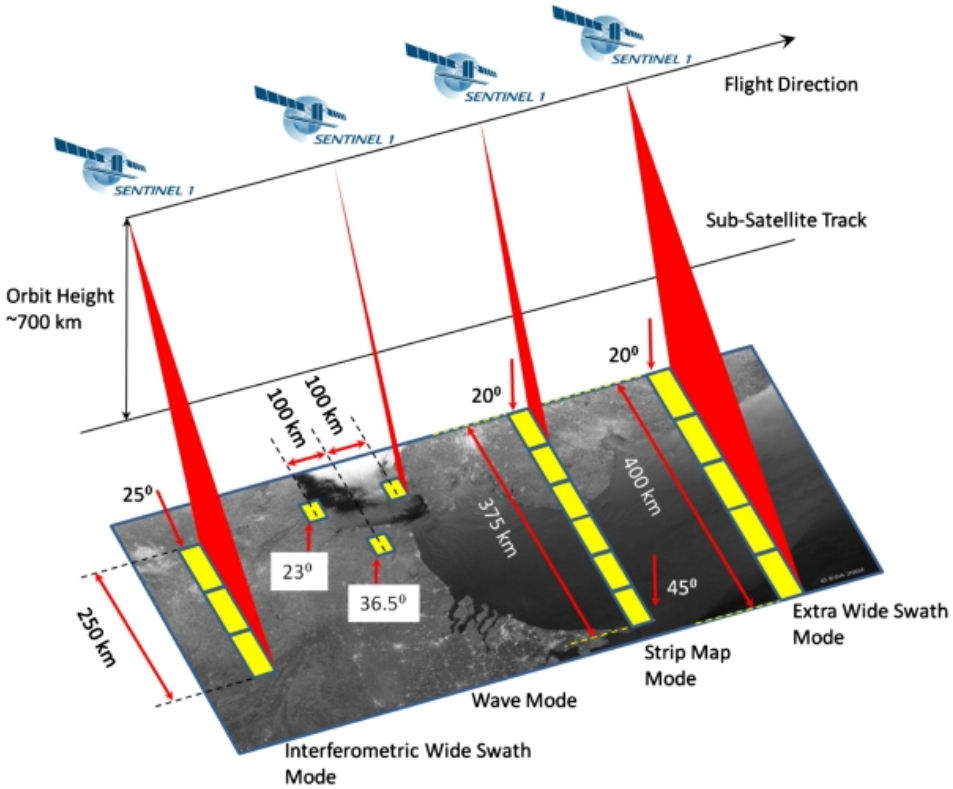

SOURCE: ESA (2019e).

2.5.2 Coverage and products

The following two maps (Figure 2.7 and Figure 2.8) describe the overall Sentinel-1 constellation observation scenario, in terms of SAR mode, polarization, observation geometry, revisit, and coverage frequency, as of May 2019 (ESA, 2019d). Wave mode, operated continuously by default in open oceans, is not shown on these maps. Data products are available in single polarisation (VV or HH) for Wave mode and dual polarisation (VV+VH or HH+HV) or single polarisation (HH or VV) for SM, IW and EW modes (ESA, 2019c). The level 2 ocean wind field has spatial resolution 1 km x 1km for SM, IW or EW modes, accuracy better than 2.0 m/s for wind speed and better than 30° for wind direction (ESA, 2019b). The products are distributed as shown in Figure 2.9.

Figure 2.7 - Revist and coverage of Sentinel-1.

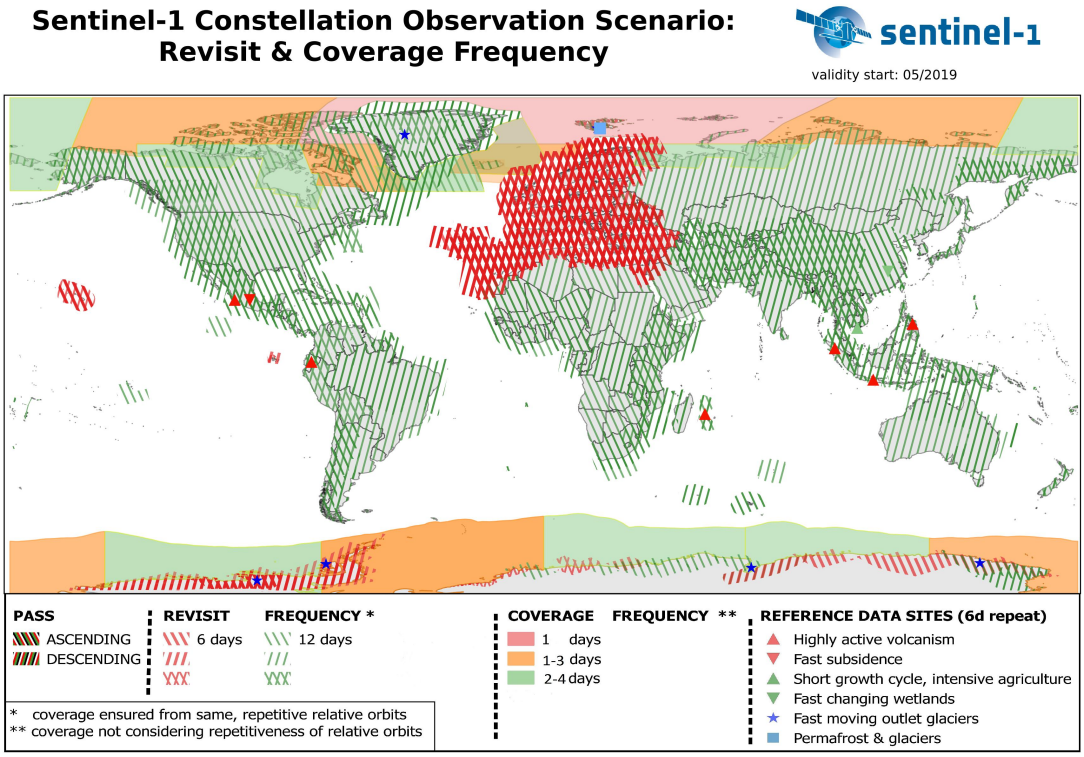

SOURCE: ESA (2019d).

Figure 2.8 - Coverage of acquisition modes and polarization of Sentinel-1.

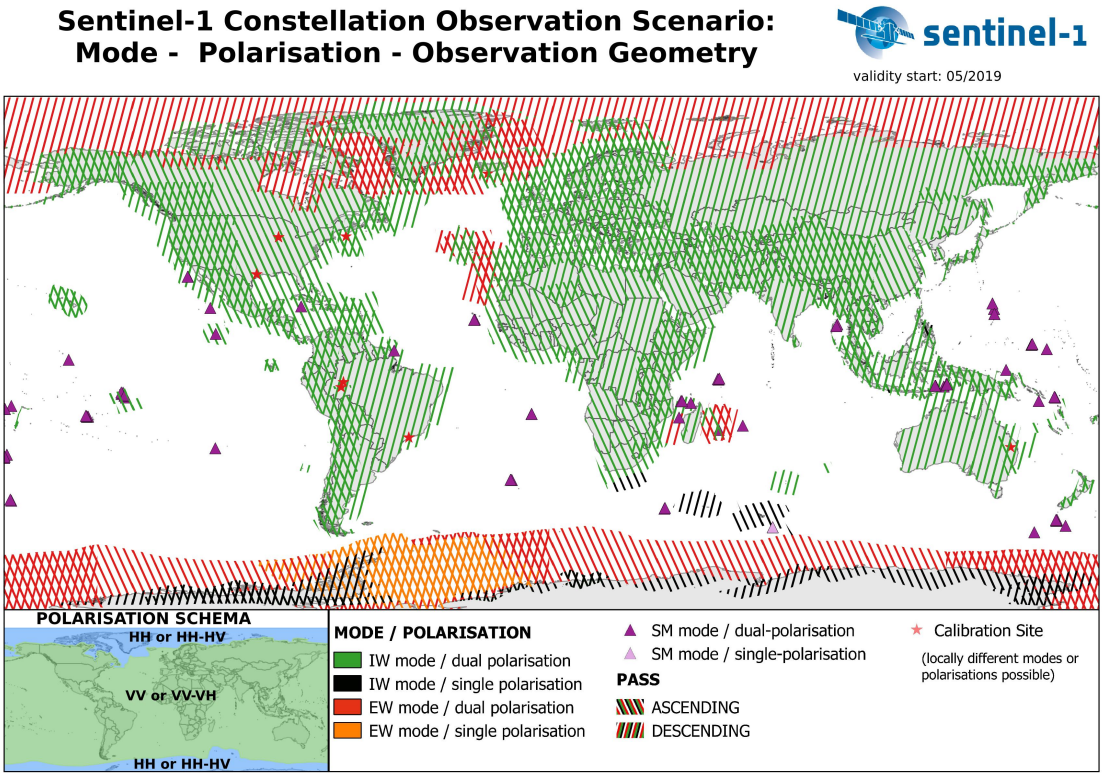

SOURCE: ESA (2019d).

Figure 2.9 - Graphical representation of Sentinel-1 core products.

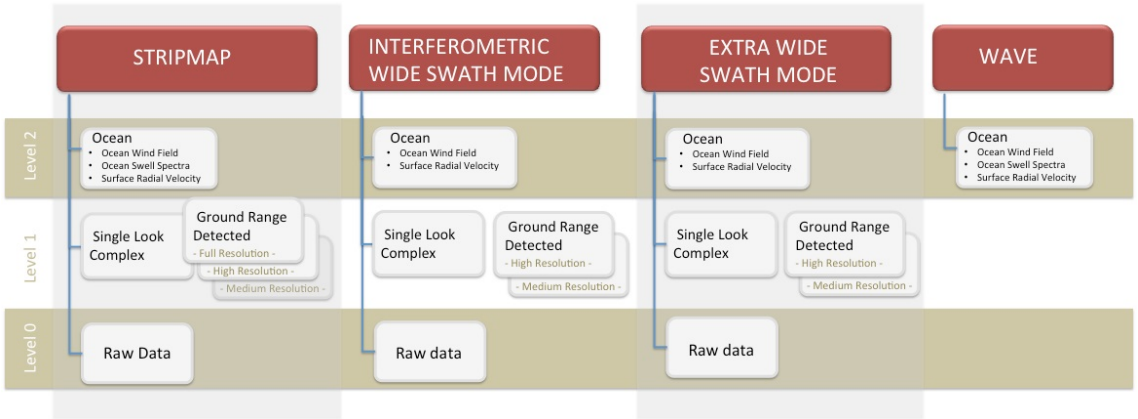

SOURCE: ESA (2019c).

2.6 ASCAT specifications and key features

According to OSI SAF (2019), the ASCAT is one of the instruments carried on-board the Meteorological Operational (MetOp) polar satellites launched by ESA and operated by the EUMETSAT. Metop-A was the first in a series of three satellites and was launched on 19 October 2006. Metop-B was launched on 17 September 2012 and Metop-C was launched on 7 November 2018.

As described in OSI SAF (2019) and in EUMETSAT (2017), ASCAT is a real aperture radar using vertically polarized antennas. Two sets of three antennas are used to generate radar beams looking 45° forward, sideways,and 45° backwards with respect to the satellites flight direction, on both sides of the satellite ground track. These beams illuminate approximately 550 km-wide swaths (separated by about 700 km, showed in Figure 2.10).

Figure 2.10 - ASCAT wind scatterometer geometry.

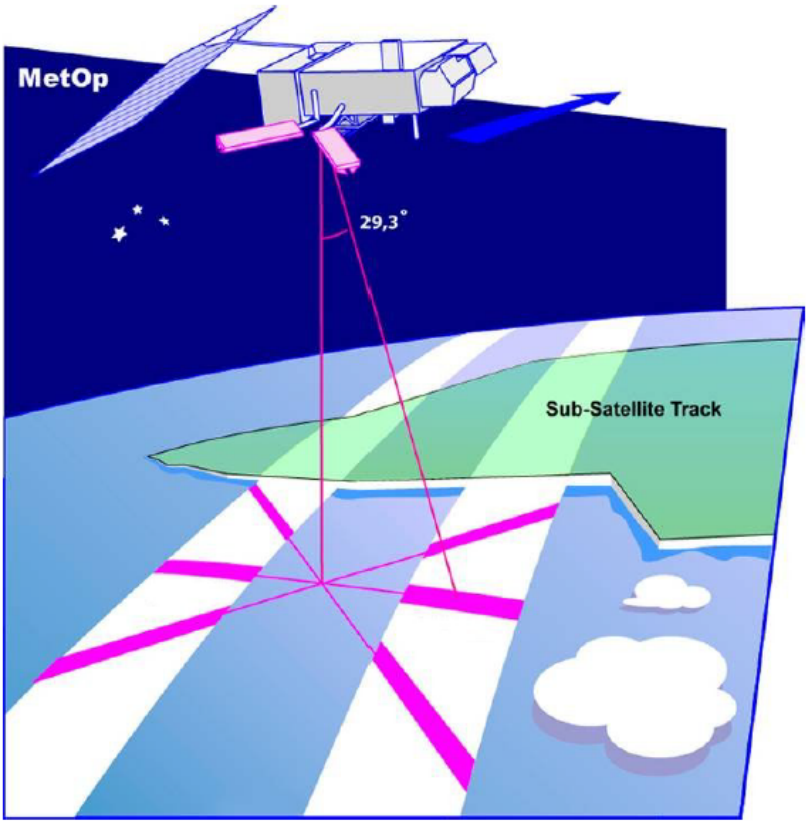

SOURCE: OSI SAF (2019).

While the satellite moves along its orbit, and each provide measurements of radar backscatter from the sea surface on a 25 km or 12.5 km grid. According to OSI SAF (2019) each swath is divided into 21 or 41 cells, and then named as Wind Vector Cells (WVCs). This brings the effective swath width to 525 km (21x25) or 512.5 km (41x12.5) for the 25-km and 12.5-km products, respectively. For the left and right swaths together, this results in 42 WVCs per row for 25-km and 82 WVCs per row for 12.5-km products. For each WVC, it was obtained three independent backscatter measurements using the three different viewing directions and separated by a short time delay. As reported in OSI SAF (2018a), the backscatter depends on the sea surface roughness as a function of the wind speed and direction at the ocean surface, and it is possible to calculate the surface wind speed and direction by using these data within a mathematical model. It was also reported in OSI SAF (2019) and in EUMETSAT (2017) that the instrument operates at a frequency of 5.255 GHz (C-band), which makes it rather insensitive to rain.

According to EUMETSAT (2017), the ASCAT instrument may operate in three different modes: *Measurement, Calibration* and *Test*. However, the only mode that generates science data for the users is Measurement mode. In addition, as reported in OSI SAF (2019), OSI SAF (2018a) and OSI SAF (2018b), the current geophysical model function (GMF) being used is CMOD7, where the GMF relates the normalized radar cross-section to the ocean surface wind speed and direction. The wind products are distributed in two resolutions: a 50-km resolution product with 25-km cell spacing and a 25-km resolution coastal product with 12.5-km cell spacing (OSI SAF, 2019).

3 DATA SET AND METHODS

The comparison methods used in this work are described below, and follow the approach adopted by Queffeulou et al. (2005), Young et al. (2017), Ribal and Young (2019). The present dataset is, however, restricted only to include Bransfield Strait, in Peninsula Antarctica. All satellite (Sentinel-1 and ASCAT) data are in the last level of processing (level 2). The data set of Sentinel-1 is controlled by European Space Agency (ESA) and can be accessed freely in web site https://scihub.copernicus.eu/. The ASCAT's data set is controlled by European Organization for the Exploitation of Meteorological Satellites (EUMETSAT) and also has a free and open access in web site https://eoportal.eumetsat.int/. Moreover, this work used the ERA5 reanalysis data set that is also freely distributed in web site of Copernicus Climate Change Service (C3S) (https://cds.climate.copernicus.eu/cdsapp#!/search?type=dataset). The ERA5 reanalysis provides hourly estimates of a large number of atmospheric, land and oceanic climate variables. While the *in situ* measurements were made consistently by an anchored meteorological buoy and by a wave buoy installed in the region, on the occasion of OPERANTAR 38 that was executed by Polar Ship Admiral Maximiano of the Brazilian Navy as also described in Voermans et al. (2021).

3.1 *In situ* measurements

The wave buoy used *in situ* measurements was V2 Spotter from Sofar Ocean Technologies. This buoy gives real-time observations of the wave spectrum and estimates of wind speed and direction. The wave parameters are calculated through 3-dimensional wave motion, with the methodology described by Lygre and Krogstad (1986). From the directional moment of the waves and with the spectrum of the wave energy variance, the two-dimensional spectrum is obtained. Thus, from the two-dimensional spectrum, the statistical parameters of the waves are extracted, such as: (1) significant height (H_s), (2) mean period and direction, and (3) period and peak direction.

As the spectrum observed by the buoy has great accuracy, it is possible to estimate the wind from Phillips theory (PHILLIPS, 1985), which demonstrates that the energy of the spectrum depends on the coefficient C, which depends on the friction speed of the wind. And this mathematical relationship is given by:

$$E(f) = C.f^{-4} \tag{3.1}$$

where E is the spectral energy (or simply spectrum), f is the frequency, and C is the wind-dependent constant. The spectrum and wind transformation algorithms were tested by previous works, and some of these results can be seen in Thomson et al. (2013) and Pearman et al. (2014).

Since this buoy estimate the wind from the waves, in the case of fast changing of winds, these estimates may lag the calculation conditions somewhat, since it takes some time for the wave field to adjust. In addition, according to the manufacturer, if this buoy is deployed near the shore, and the wind is blowing from shore, the limited fetch could result in an underestimate of the wind speed estimate (direction is fine). Therefore, all these conditions were considered in the comparisons. The wind speed estimated by wave buoy was compared to meteorological buoy's direct observations from a close-by (under 40 m). The area of Buoy deployment's study is presented in Figure 3.1.

Figure 3.1 - Buoy deployment executed by ATMOS project in the observational activity.

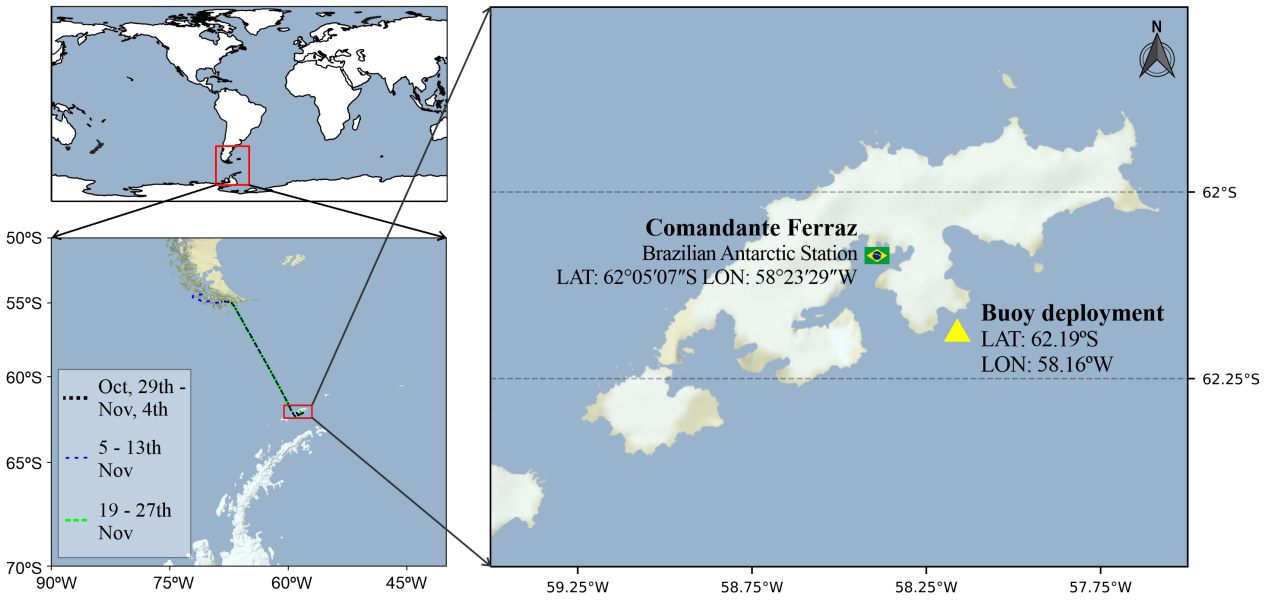

Buoy deployment executed by ATMOS project in the observational activity during the Antarctic Operation 38 (OPERANTAR 38) on board of Polar Ship Admiral Maximiano from the Brazilian Navy, between 01-13 and 20-27 November 2019, near King George Island (Antarctica).

SOURCE: Author's production.

Figure 3.2 - Planning of the buoy mooring system.

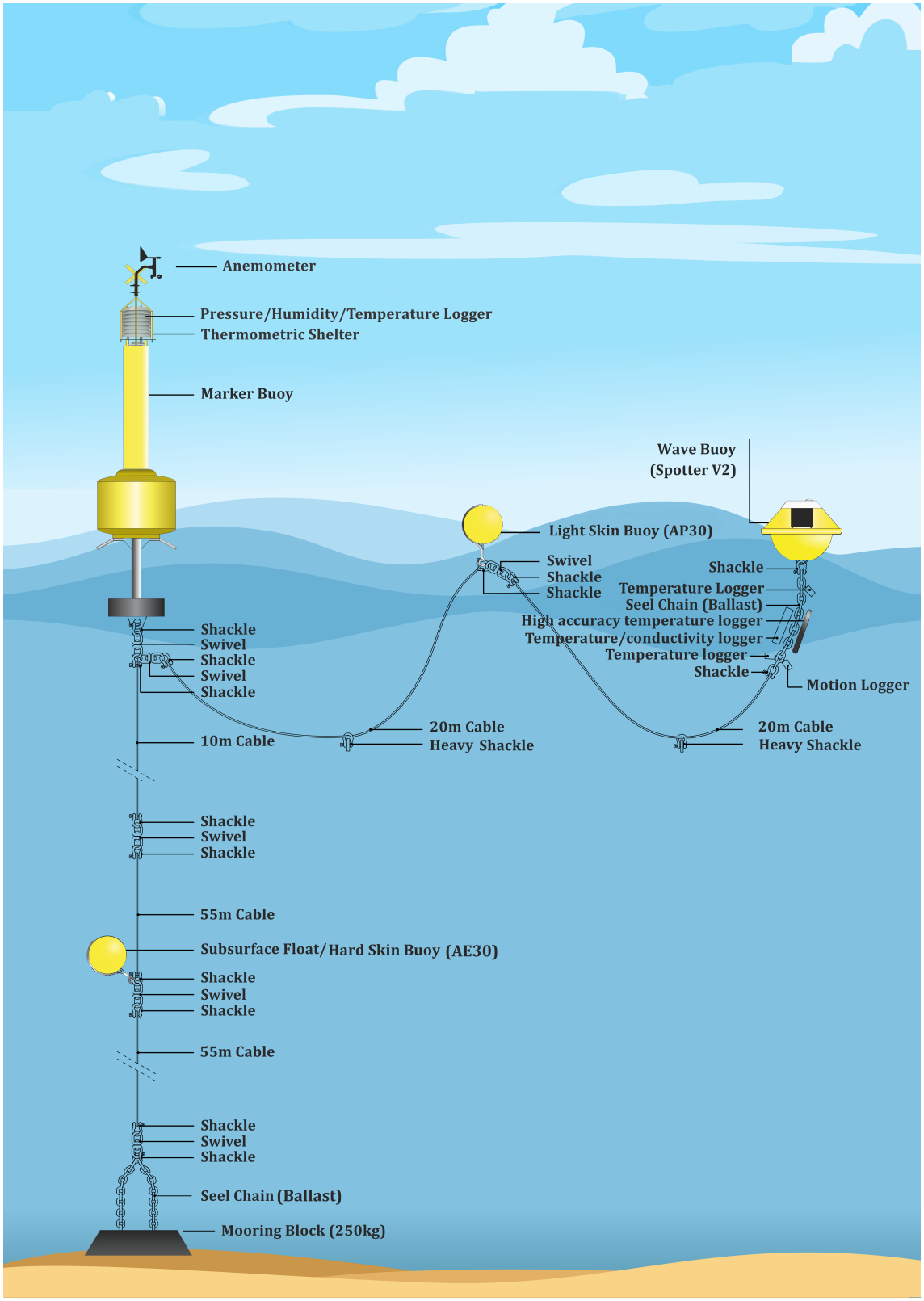

SOURCE: Author's production.

Thus, to avoid a low quality of the data observed *in situ* and according to the local bathymetry, a buoy mooring system was installed and fixed, as described in Figure 3.2, at mooring point where latitude is 62.19°S and longitude is 58.16°W. Moreover, all deployment followed best practices that were guided by on-board staff of the Brazilian Navy, by the "Guide to Moored Buoys and Other Ocean Data Acquisition Systems" written by Meindl (1996) and published by WMO, and by previous paper "Best Practices for the Ocean Moored Observatories" (VENKATESAN et al., 2018). The *in situ* measurements made by meteorological buoy occurred for the period between 10 and 18 November, 2019 at 10-minute intervals for a height of 2.5 meters, and then converted to a height of 10 meters. While the measurements of wave buoy were made between November 8, 2019 and March 1, 2020 at 2-hour intervals. The quality control of data set of the wave buoy follow the approach adopted by Voermans et al. (2021). The final positioning of buoys can be seen in Figure 3.3.

Figure 3.3 - The final positioning of buoys.

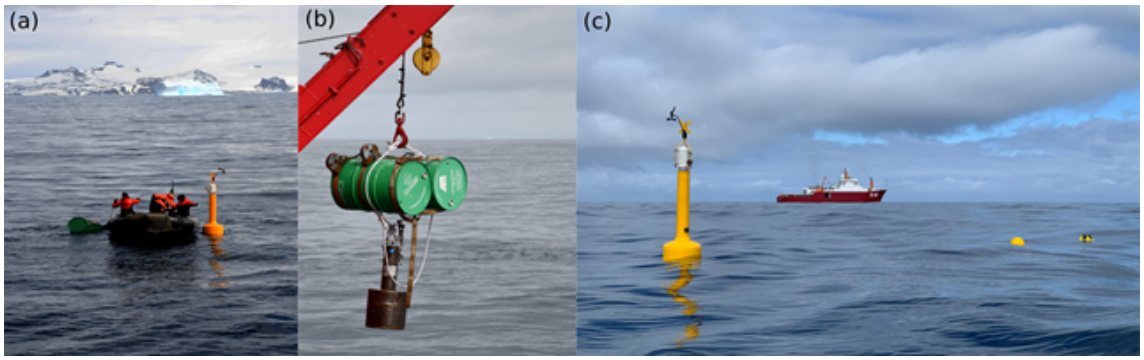

(a) the tow of the 2 buoys and the mooring block to the launch site. (b) mechanism to give buoyancy to the mooring block. (c) final configuration of the anchoring system showing the marker buoy with the coupled meteo-oceanographic sensors (on the left), the ship at the bottom, sturdy float (in the center) and wave float (on the right, showing the solar panels).

SOURCE: Adapted from LOA/INPE (2021) and Voermans et al. (2021).

3.2 The accuracies and limitations of observation methods and measurements for quality control

The wind sensor installed on the meteorological buoy is one "Pro-D Anemometer" which is connected to one "LeWL WindLogger", both from Logic En-

ergy. The Pro-D Anemometer has measuring range of 1-67m/s, an accuracy expected 2% (guarantee ±5%) and a resolution of 0.1m/s (wind run). Due to logistic problems and electric failure, it was only possible to register wind speed for the period between 10-18 November, 2019. More specifications about wind sensor can be found respectively in https://www.windlogger.com/collections/sensors/products/pro-d-anemometer and https://www.windlogger.com/products/lewl-wind-logger-1.

In this study, wind speed and direction were measured at 2.5 m above mean sea level. However, wind speed and direction is typically measured at 4–5 m above mean sea level and has an accuracy of ±1 m/s and ±10°, respectively. Although this seems large, this is standard and the same for National Data Buoy Center (NDBC) buoys to which satellite derived wind speed data is often calibrated (QUEFFEULOU, 2003; TOMITA; KUBOTA, 2011; YOUNG et al., 2017; RIBAL; YOUNG, 2019; RAGHUKUMAR et al., 2019; VOERMANS et al., 2020). Then, it was adopted the same approach of Voermans et al. (2020), where the measured wind speed was extrapolated to the standard height of 10 m using the power law $U_{10}/U_a = (10/z_a)^{0.11}$ (HSU et al., 1994), where U_a is the wind speed measured by the anemometer at height z_a.

As before explained, according to the manufacturer of the wave buoy, the distance from the shore is a limitation to estimate wind speed. Because, the accuracy of proxy measurements of wind depends on fetch, wave steepness, wave age, directional alignment between wind and dominant waves, and temporal variability of the wind. A detailed explanation of estimating wind speed and direction using wave spectra including analysis of variability between sites and influence of buoy size can be found in Voermans et al. (2020) and Raghukumar et al. (2019). For more detailed information about the wave buoy specifications, see the manufacturer's website (https://www.sofarocean.com/products/spotter).

In previous studies (GRIECO et al., 2020; HUTCHINGS et al., 2020; WEI et al., 2020; SREELAKSHMI; BHASKARAN, 2020; KILPATRICK et al., 2019; LINDSLEY et al., 2016; OWEN; LONG, 2009) about satellite-derived wind fields is showed there is a land contamination effect that can degrade the accuracy of wind field retrieval in ocean near-coastal zone. According to Owen and Long (2009), this happens because the radar backscatter from land is much brighter than that from calm ocean water, there is significant contamination of the backscatter measurements, termed σ°, near the coast due to antenna side lobes. On the other hand, near coast-

lines, quality control omits pixels contaminated by land that cause fundamentally different scattering than ocean waves (HASAGER et al., 2020).

3.3 ERA5 reanalysis data, sattelite-derived data and quality control

The scenes of Sentinel-1 and ASCAT processed in level 2 with wind data were organized by comparison the buoys measurements with each satellite passes, respectively. The buoy observations and satellite passes were considered a "matchup" if they satisfied the following criteria:

a) Satellite track was within a radius of 50 km of the buoys and the over-pass occurred within 30 minutes of the buoys recording data. These matchup criteria have been widely used in previous studies (ZIEGER et al., 2009; QUEFFEULOU, 2004; GOWER, 1996; MONALDO, 1988; DOBSON et al., 1987).

b) A minimum of five points were required in the altimeter pass within the circle with a radius of 50 km with the center in the buoy position (RIBAL; YOUNG, 2019; YOUNG et al., 2017).

The same criteria of distance and the minimum of five points were required and also applied for ERA5 Reanalysis. A linear regression analysis is then performed between the meteorological buoy against ERA5 and satellite-derived products matchup data (U_{10} values). Although the meteorological buoy data are considered "true values" for the purposes of this work, such data could only be recorded for approximately 8 days, due to an electrical breakdown caused by the harsh marine environment. Thus, after that period the reference data was replaced by the data of the wave buoy.

In addition, in order to execute the spatial analysis, it was necessary to change the meteorological buoy data are considered "true values". Such data was replaced by Sentinel-1 or ASCAT wind data to be considered "true values" (observed), depending on the type of comparison between the sources of data, such as:

a) Sentinel-1 (observed) *versus* ASCAT (predicted);

b) Sentinel-1 (observed) *versus* ERA5 (predicted); and

c) ASCAT (observed) *versus* ERA5 (predicted).

However, for each point of Sentinel-1 or ASCAT (when reproducing "observed data") with valid wind vector, it was required the five nearest points of ASCAT or ERA5 (when reproducing "predicted data") within a radius of 50 km with the center in the selected point of data set that was reproduced as observed data. Simultaneously, the time interval of 30 minutes between the data sets also was required. Thus, the statistical parameters, explained in Section 3.4, was calculated considering the "true" wind vector located in this "observed" point against the another five "predicted" wind vectors located in each one in these 5 nearest points.

Taking into account the mission requirements of Sentinel-1 (RMSE = 2.0) and ASCAT (BIAS = 0.5, RMSE = 2.0), and due to the Sentinel-1's resolution of 1km x 1km compared to the ASCAT of 12.5km and the ERA5 of 0.25°, approximately 28km. The values measured by Sentinel-1 was considered as "ground truth" with standard height of 10 m (U_{10}). The final manual selection was made considering the following criteria:

a) a *good* plot has the RMSE better than 2.0 m/s, a BIAS close to ±0.5 m/s, and only 20% of valid wind vectors with individual RMSE worse than 2.0 m/s when compared to the 5 plus points upcoming.

b) a plot is considered *bad* when "area of overlap" between Sentinel-1 *versus* ASCAT (RMSE or BIAS) is very small (look at the degraded graph of day November 19th, 2019 plotted in Figure A.6 for BIAS and RMSE in the confrontation Sentinel-1 *versus* ASCAT due to lack of overlap), and/or does not fit all the above criteria, simultaneously.

3.4 Statistical analysis

Algorithms in Python programming language were used to verify the performance of the satellite-derived data and ERA5 in comparison with the *in situ* measurements, the values of four statistical parameters are studied: Bias, Mean Absolute Error (MAE), Root-Mean Square Error (RMSE), and Pearson's Correlation Coefficient (ρ), where the suffixes e, m and n mean estimated, measured and number of observations, respectively (RIBAL; YOUNG, 2019; WALTHER; MOORE, 2005).

In this work, the bias measure called mean error (ME) was called simply by "BIAS". It is the mean of all differences between the estimated values and the true value, and indicates whether the estimator consistently under- or overestimates the total population (WALTHER; MOORE, 2005). The BIAS calculation is given by

the Equation 3.2:

$$BIAS = \frac{1}{n}\sum_{i=1}^{n}(e_i - m_i) \tag{3.2}$$

For RMSE, the lower the RMSE value obtained for the satellite data, the closer it will be to the in situ measurements. But, it tends to be dominated by outlying estimates far away from the true value, because it is calculated using squared differences (WALTHER; MOORE, 2005). The RMSE calculation is given by the Equation 3.3:

$$RMSE = \sqrt{\frac{1}{n}\sum_{i=1}^{n}(e_i - m_i)^2} \tag{3.3}$$

The outlying estimates is a potential problem. Thus, to avoid it, one may take the absolute value of the difference between the estimated values and the true values as a measure of accuracy, and then take the mean (WALTHER; MOORE, 2005). This resultant value is called mean absolute error (MAE) which calculation is given by the Equation 3.4:

$$MAE = \frac{1}{n}\sum_{i=1}^{n}|e_i - m_i| \tag{3.4}$$

The Pearson's correlation coefficient (RIBAL; YOUNG, 2019; WILKS, 2019; PECK; DEVORE, 2011; COHEN et al., 2009) indicates the magnitude and direction of the linear relationship between two variables. Their values are in the range between -1 and 1, where -1 indicates perfect inverse linear correlation, +1 corresponds to perfect direct linear correlation and 0 represents no linear correlation. It is calculated by the Equation 3.5:

$$\rho = \frac{cov(e, m)}{\sqrt{cov(e)\, cov(m)}} \tag{3.5}$$

4 RESULTS

4.1 Spatial analysis of statistical error between SENTINEL-1, ASCAT AND ERA5

In this chapter we present the spatial analysis of statistical error plotted in a map with focus in the Bransfield Strait. The study area is located between the 60°S and 65°S parallel and between the 55° and 65°W meridians, due to the availability of Sentinel-1 and ASCAT data in the vicinity of the EACF and buoy locations near Admiralty Bay (Figure 3.1). In addition, it is region studied by ESA, and an important access to scientific research bases, where research ships from the Brazilian Navy and other Navies need meteo-oceanographic information for decision-making and navigation safety.

The analysis was made considering the month of November, 2019. For this period, 33 Sentinel-1 level 2 scenes and 278 ASCAT level 2 scenes were found initially. Then, the plot of the individual wind field of each data source (Sentinel-1, ASCAT and ERA5) was done, with total of three graphs. And, for each statistical parameter (BIAS, RMSE and MAE) it was necessary to plot three more graphs (3+3+3, for example: “BIAS SENTINEL-1 x ASCAT”; “BIAS SENTINEL-1 x ERA5”; “BIAS ASCAT x ERA5”). Therefore, for each day there are a total of 12 graphics. Then, afterwards, it was necessary to make a confrontation, mostly performed by several algorithms, and the final selection stage was done manually in order to search for the “best scenes” and the “worst scenes”.

Several confrontations were made. First, an automated matchup was made for a maximum time difference of 30 minutes between scenes, where 15 Sentinel-1 scenes and 15 ASCAT scenes were selected. Second, the execution of a specific algorithm for the spatial plotting of each respective statistical parameter taking the data sources two by two (the complete spatial plotting of monthly cycle for a single statistical parameter between two data sources takes approximately 1 hour and 30 minutes). Third, the separation of the spatial plots by the criterion of five closest points within a radius of 50 km, where six plots were eliminated, and only nine plots remained. Finally, for each of these nine ASCAT scenes, there was a manual selection of spatial plots of statistical parameters for each point with valid wind vector.

The reason for choice of Sentinel-1 data as "ground truth" was the resolution of 1 km x 1 km compared to the ASCAT of 12.5 km and the ERA5 of 0.25°, approx-

imately 28 km (see Section 3.3). To illustrate the calculation of statistical parameters and their respective spatial plotting as "good plotting" or "bad plotting", two days are taken as examples and were presented nine graphics (three graphics about MAE are not presented) in Section 4.1.1 and Section 4.1.2 too. While another nine days are shown in Appendix A. . The definitions of "good plotting" or "bad plotting" were detailed in Section 3.3

4.1.1 Example of "good plotting"

Figure 4.1 - Sentinel-1 wind field plotting in level 2 - 2019-11-28.

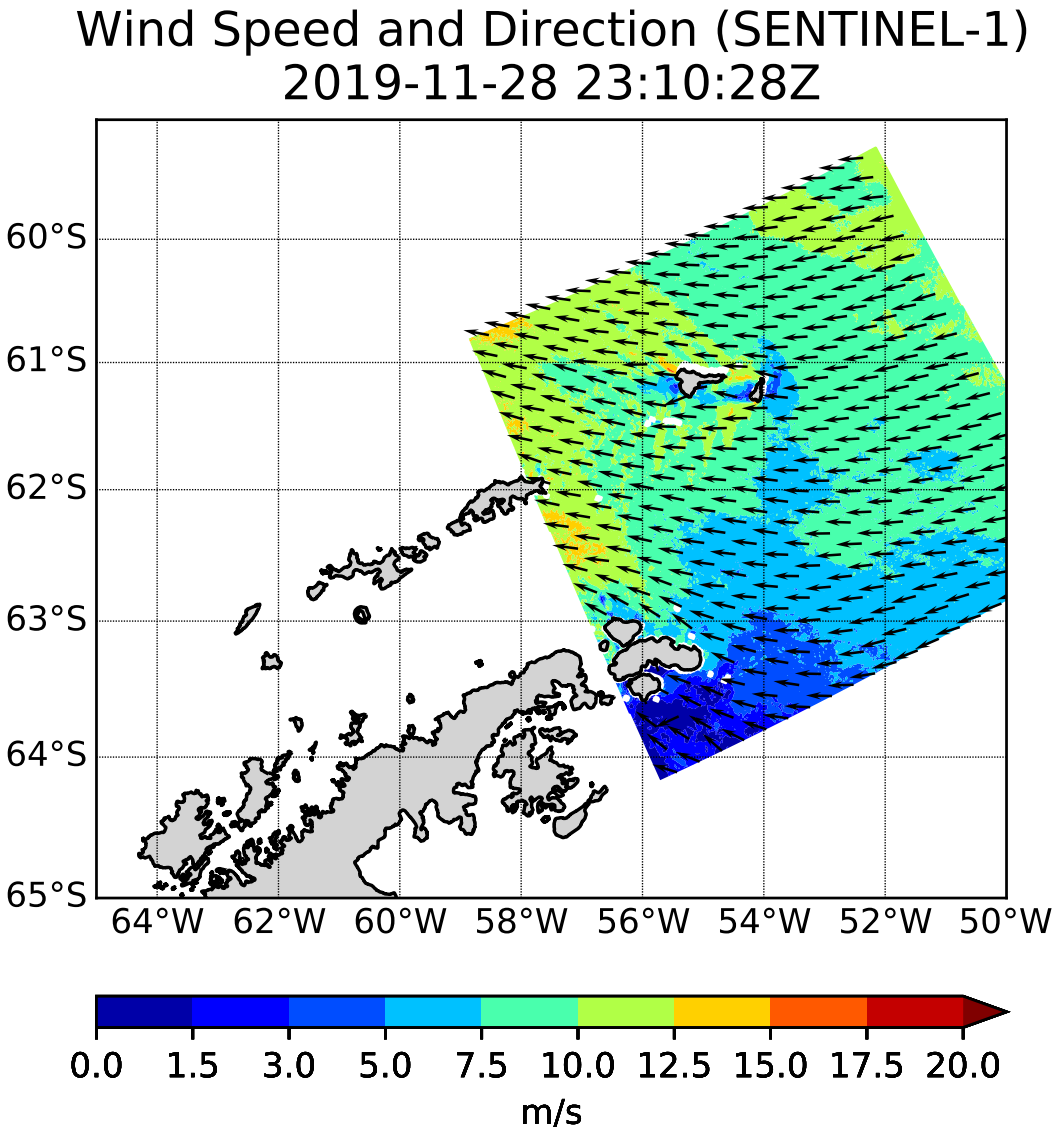

SOURCE: Author's production.

Figure 4.2 - ASCAT wind field plotting in level 2 - 2019-11-28.

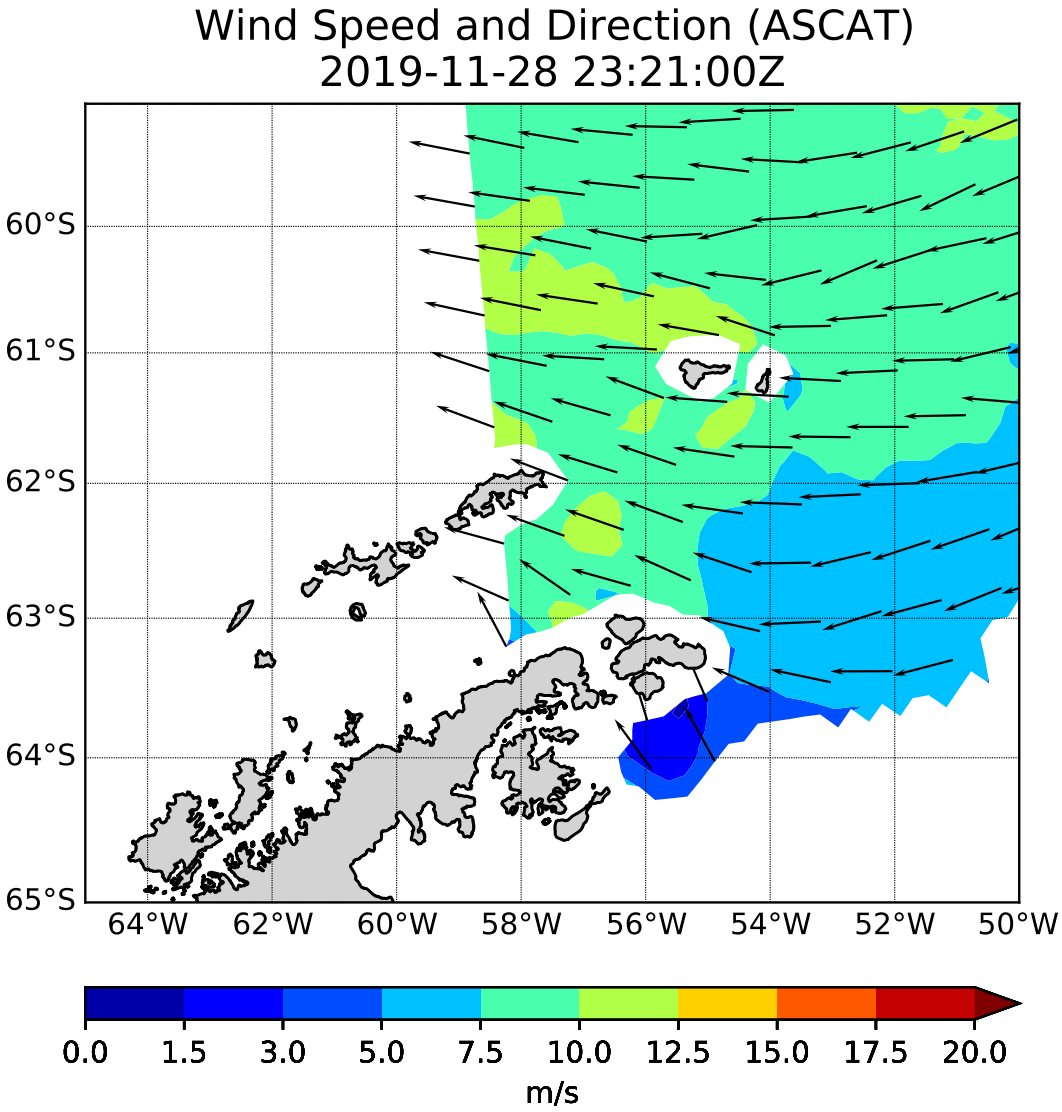

SOURCE: Author's production.

Figure 4.3 - ERA5 wind field plotting - 2019-11-28.

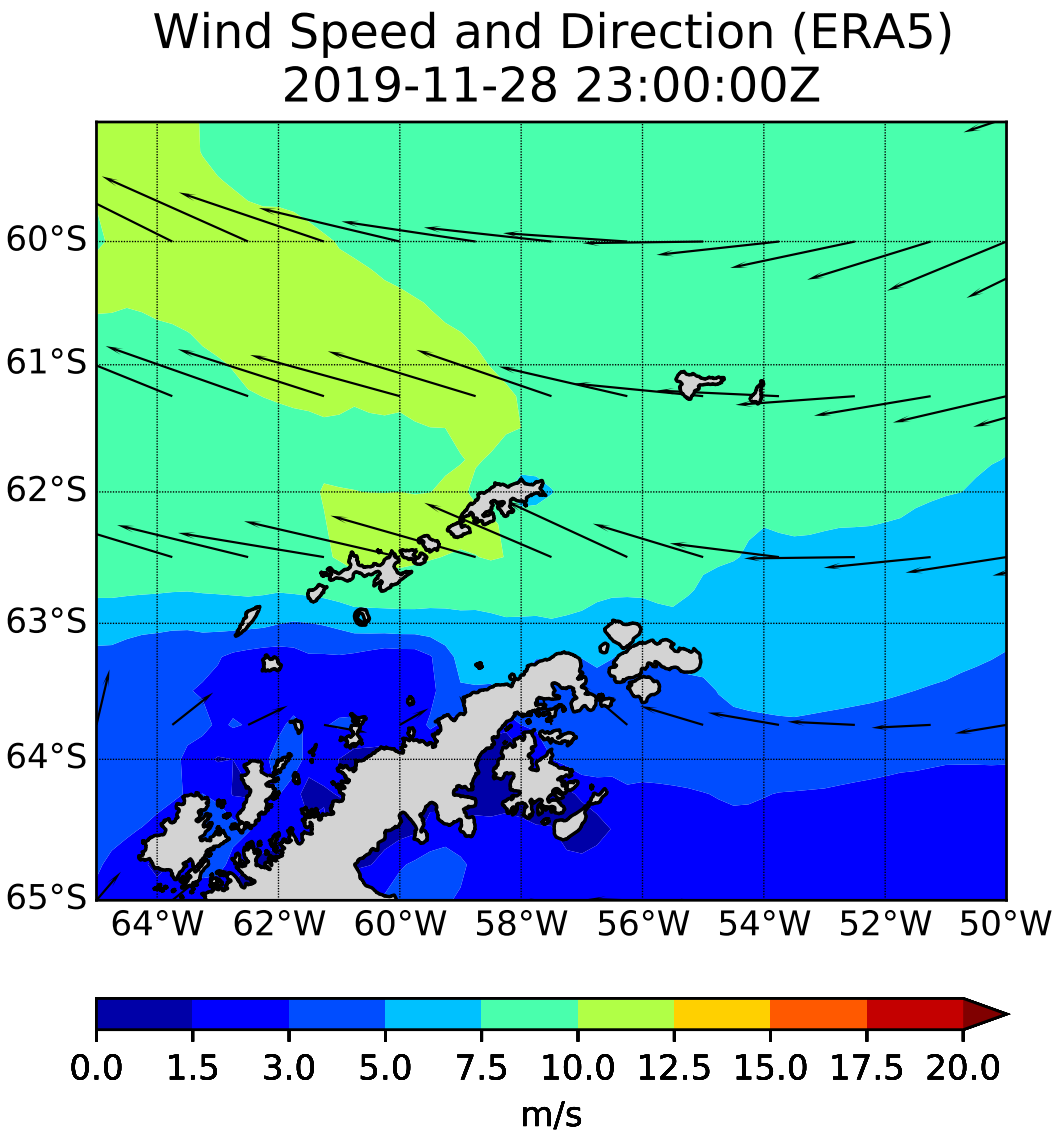

SOURCE: Author's production.

Figure 4.4 - RMSE Sentinel-1 *versus* ASCAT wind field plotting in level 2 - 2019-11-28.

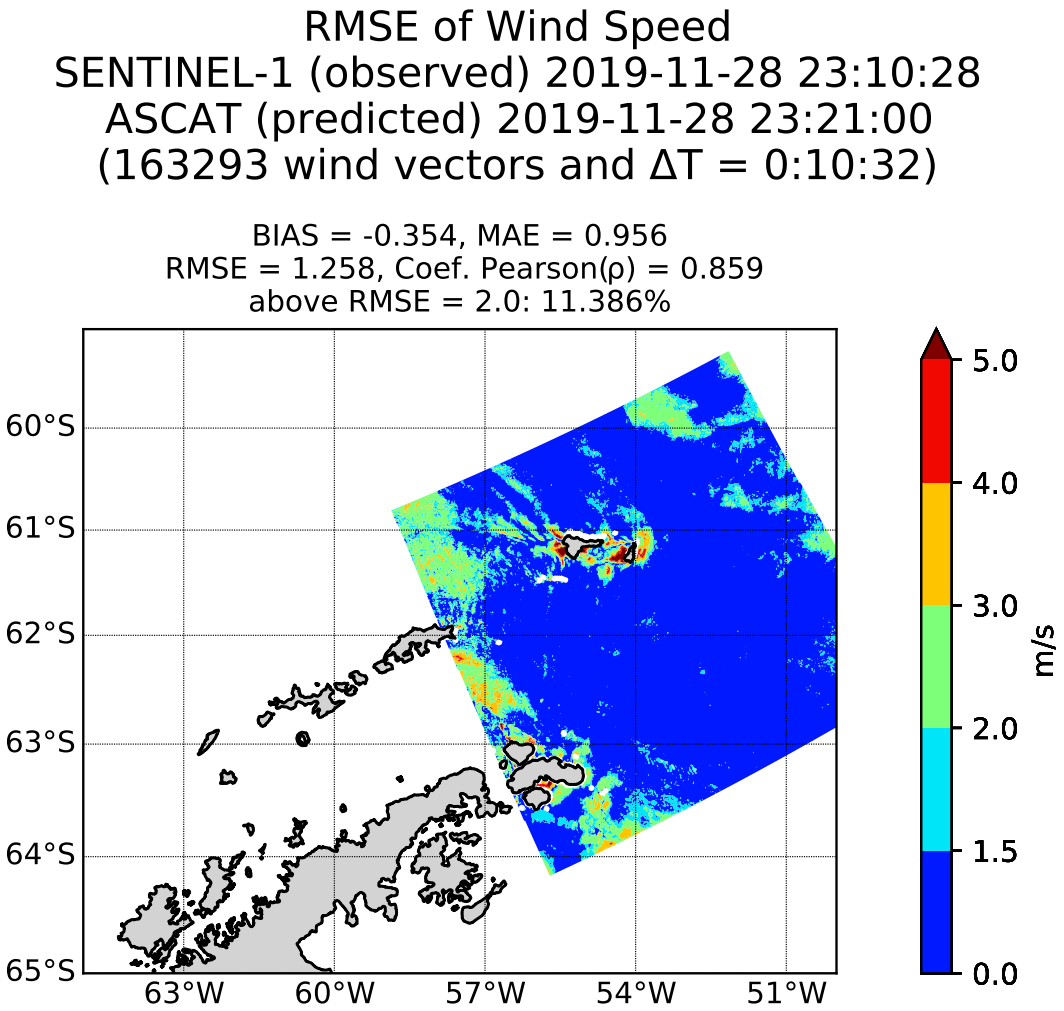

SOURCE: Author's production.

Figure 4.5 - RMSE Sentinel-1 *versus* ERA5 wind field plotting - 2019-11-28.

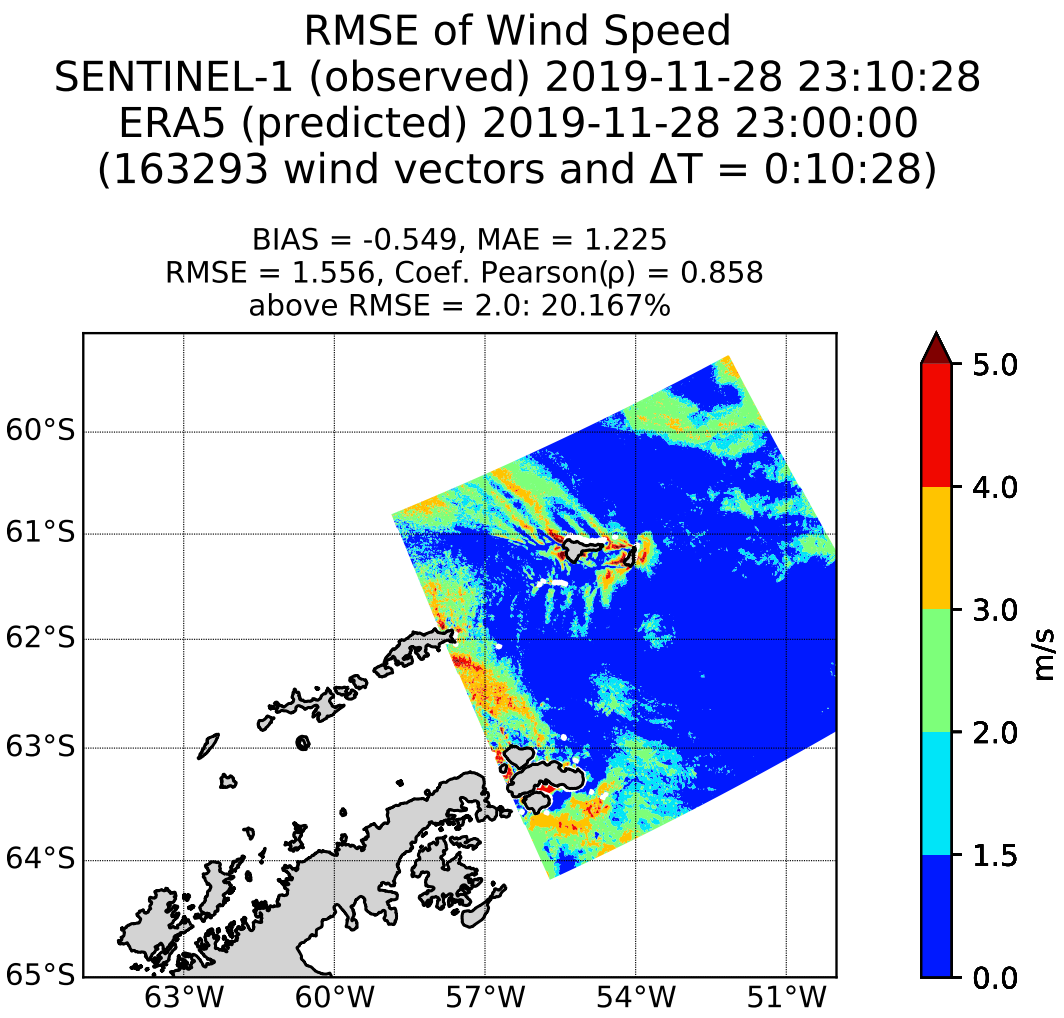

SOURCE: Author's production.

Figure 4.6 - RMSE ASCAT *versus* ERA5 wind field plotting - 2019-11-28.

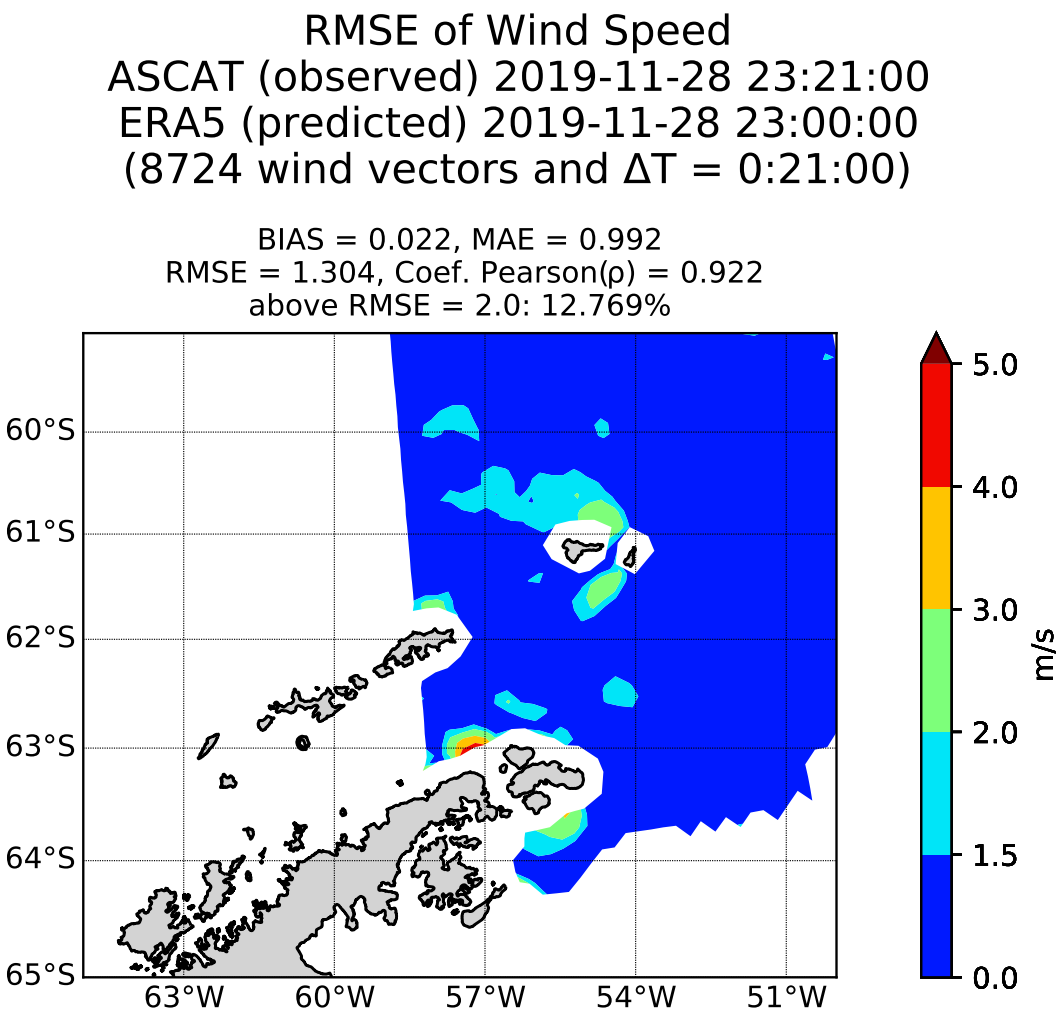

SOURCE: Author's production.

Figure 4.7 - BIAS Sentinel-1 *versus* ASCAT wind field plotting in level 2 - 2019-11-28.

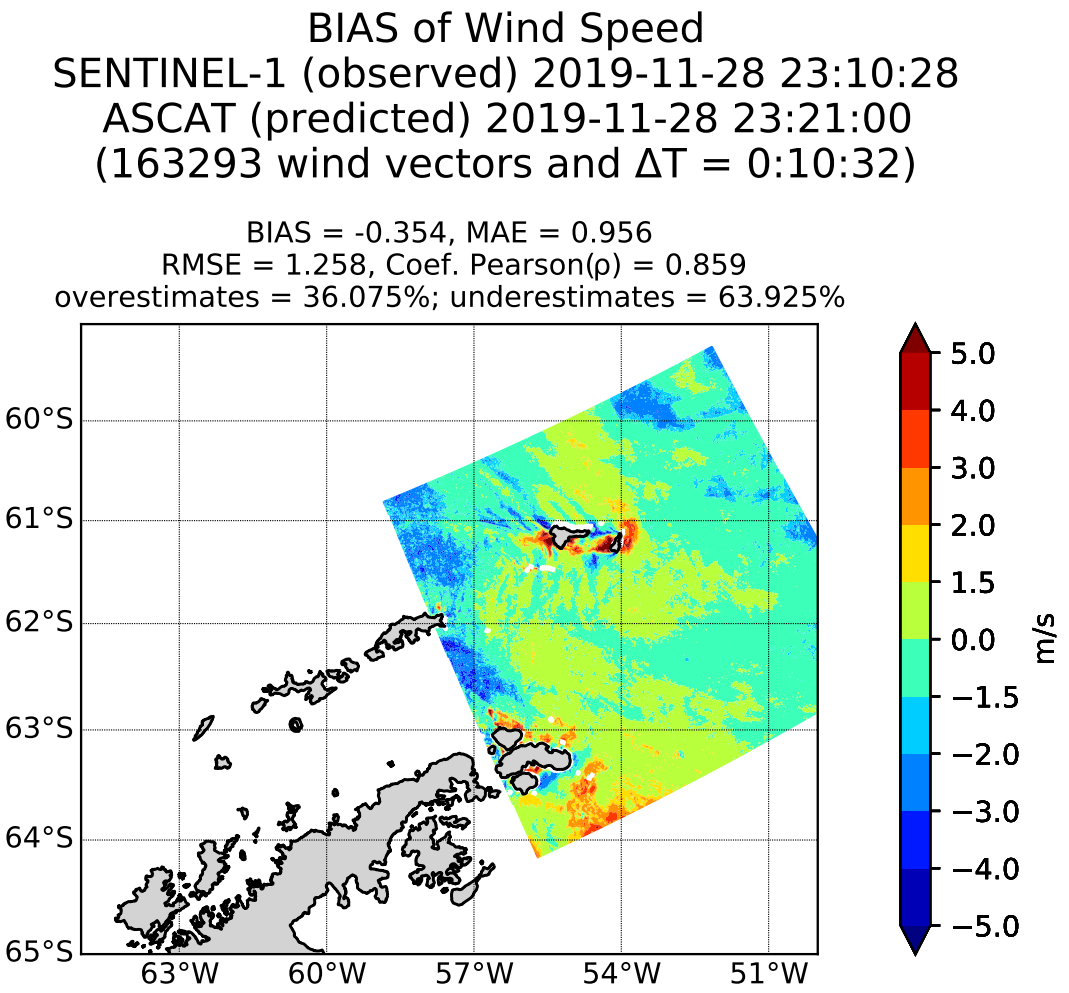

SOURCE: Author's production.

Figure 4.8 - BIAS Sentinel-1 *versus* ERA5 wind field plotting - 2019-11-28.

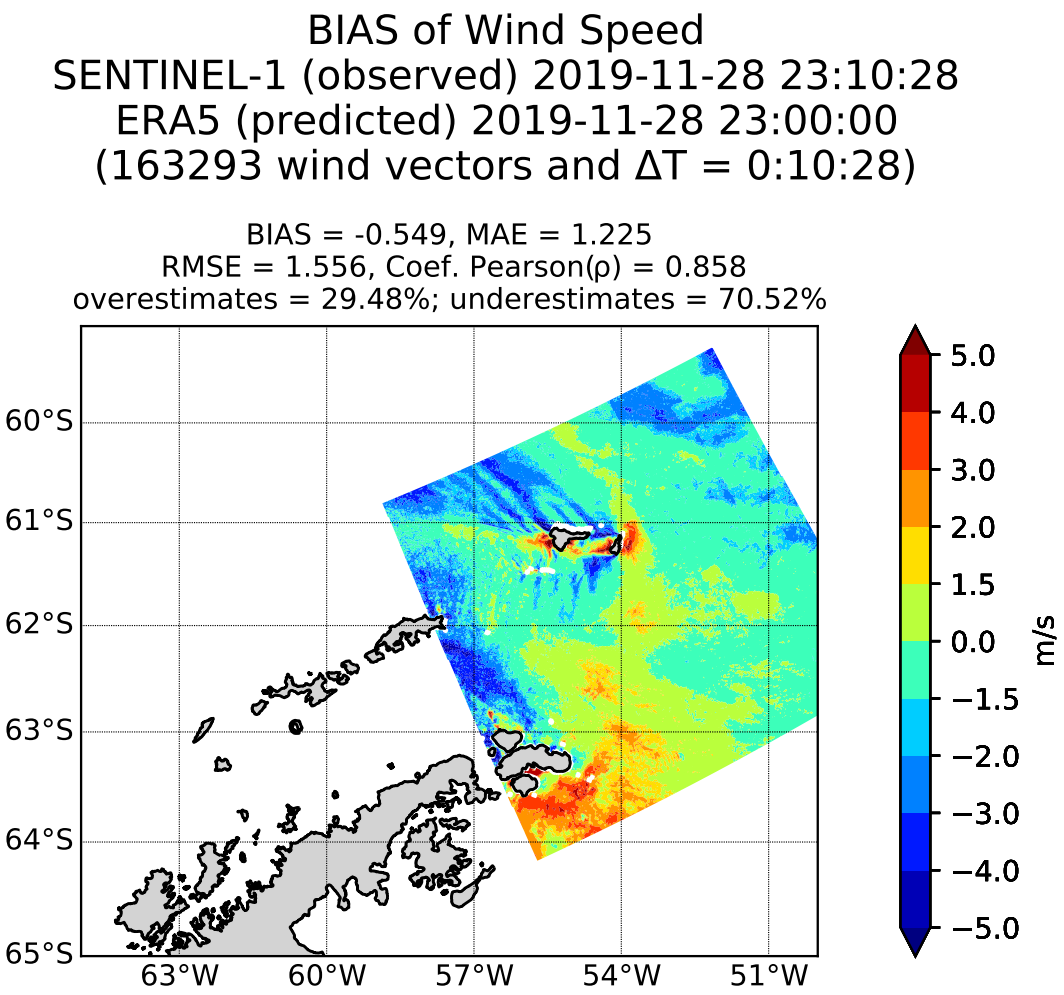

SOURCE: Author's production.

Figure 4.9 - BIAS ASCAT *versus* ERA5 wind field plotting - 2019-11-28.

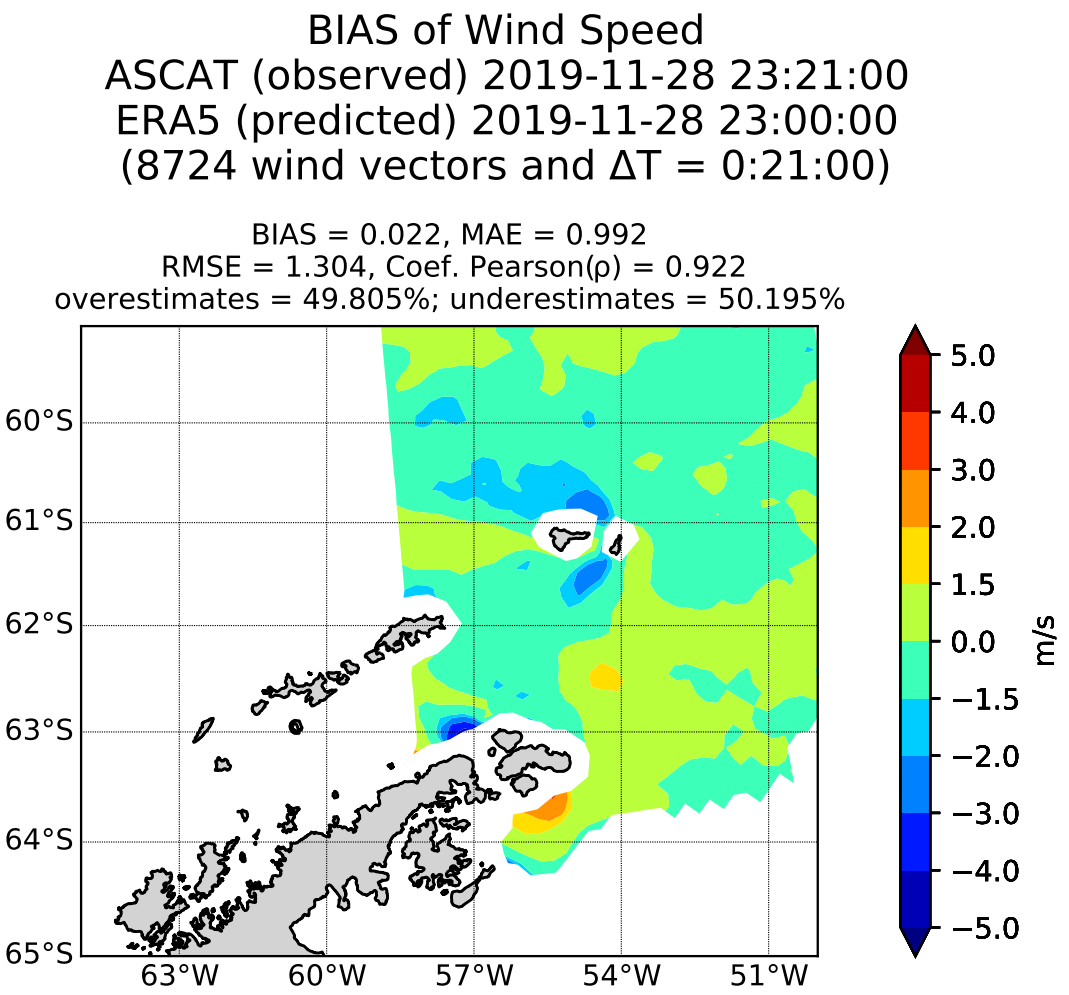

SOURCE: Author's production.

4.1.2 Example of "bad plotting"

Figure 4.10 - Sentinel-1 wind field plotting in level 2 - 2019-11-01.

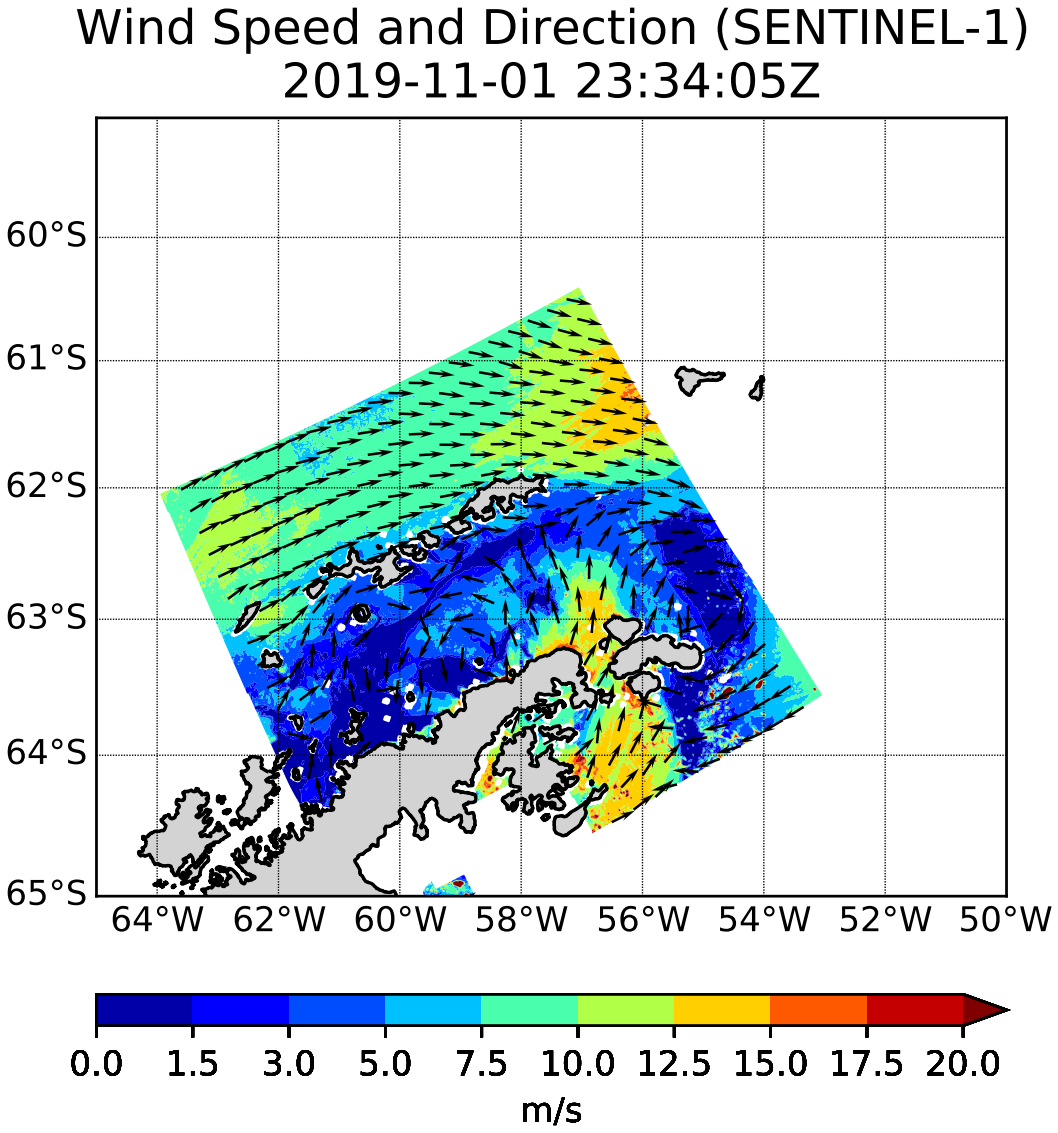

SOURCE: Author's production.

Figure 4.11 - ASCAT wind field plotting in level 2 - 2019-11-01.

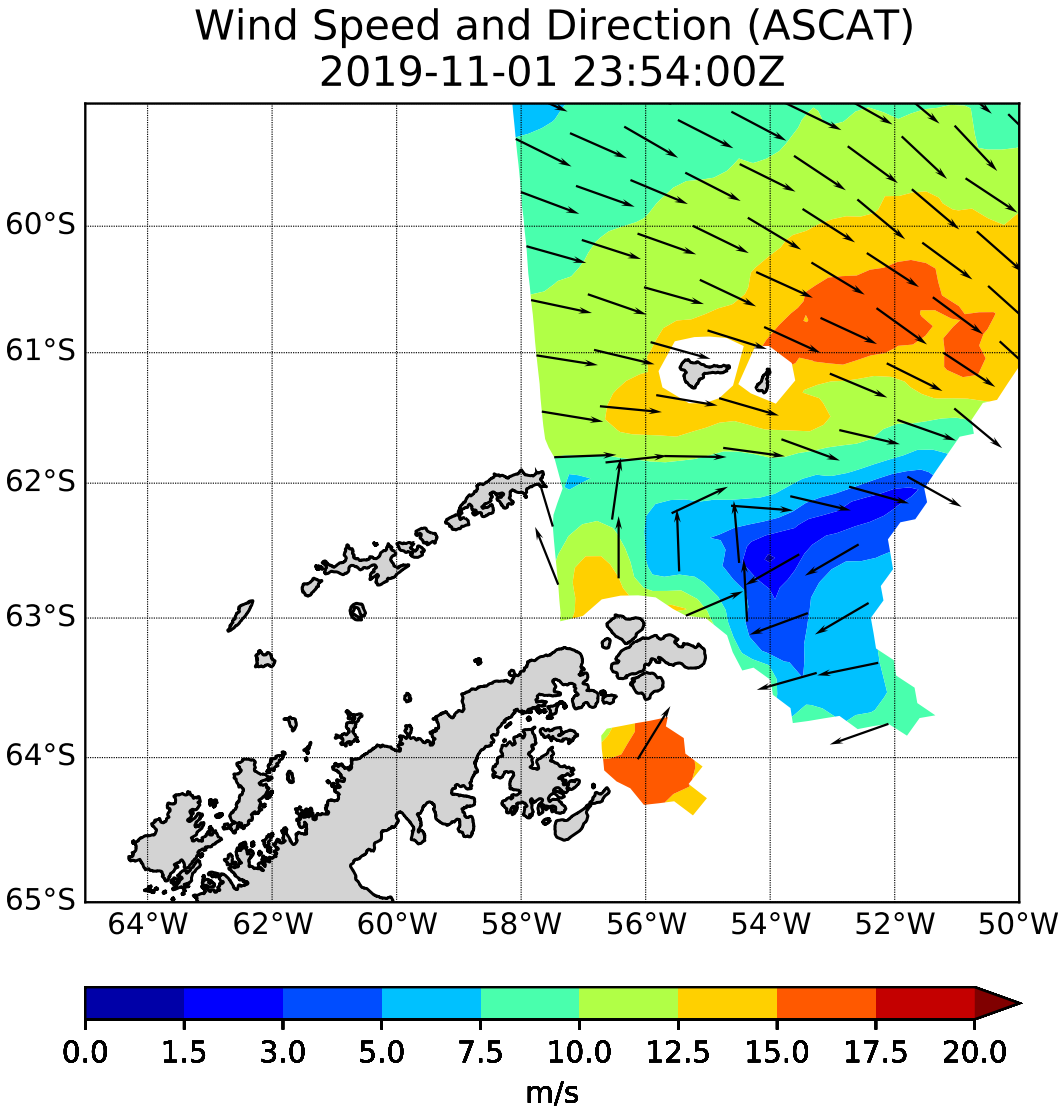

SOURCE: Author's production.

Figure 4.12 - ERA5 wind field plotting - 2019-11-01.

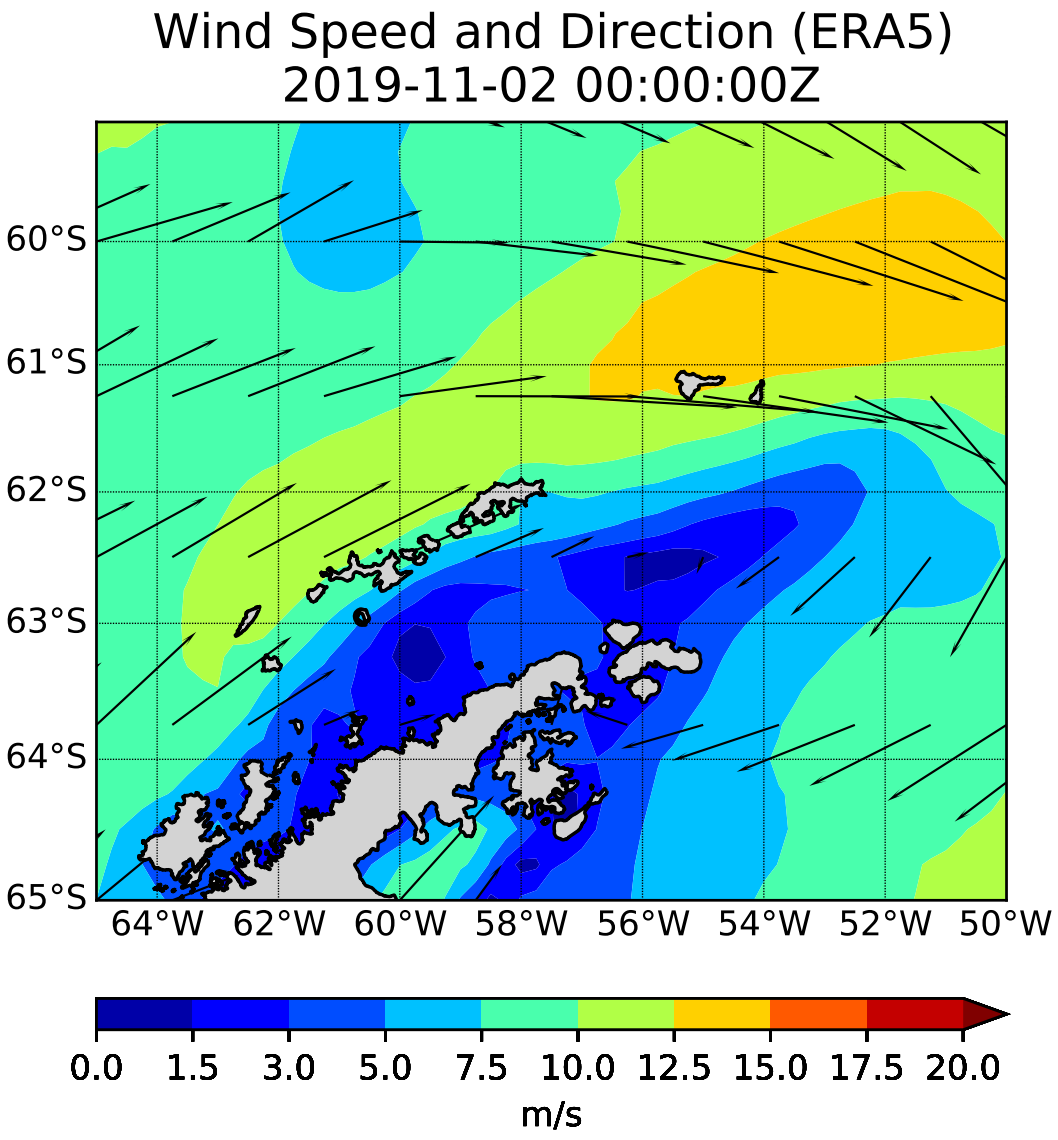

SOURCE: Author's production.

Figure 4.13 - RMSE Sentinel-1 *versus* ASCAT wind field plotting in level 2 - 2019-11-01.

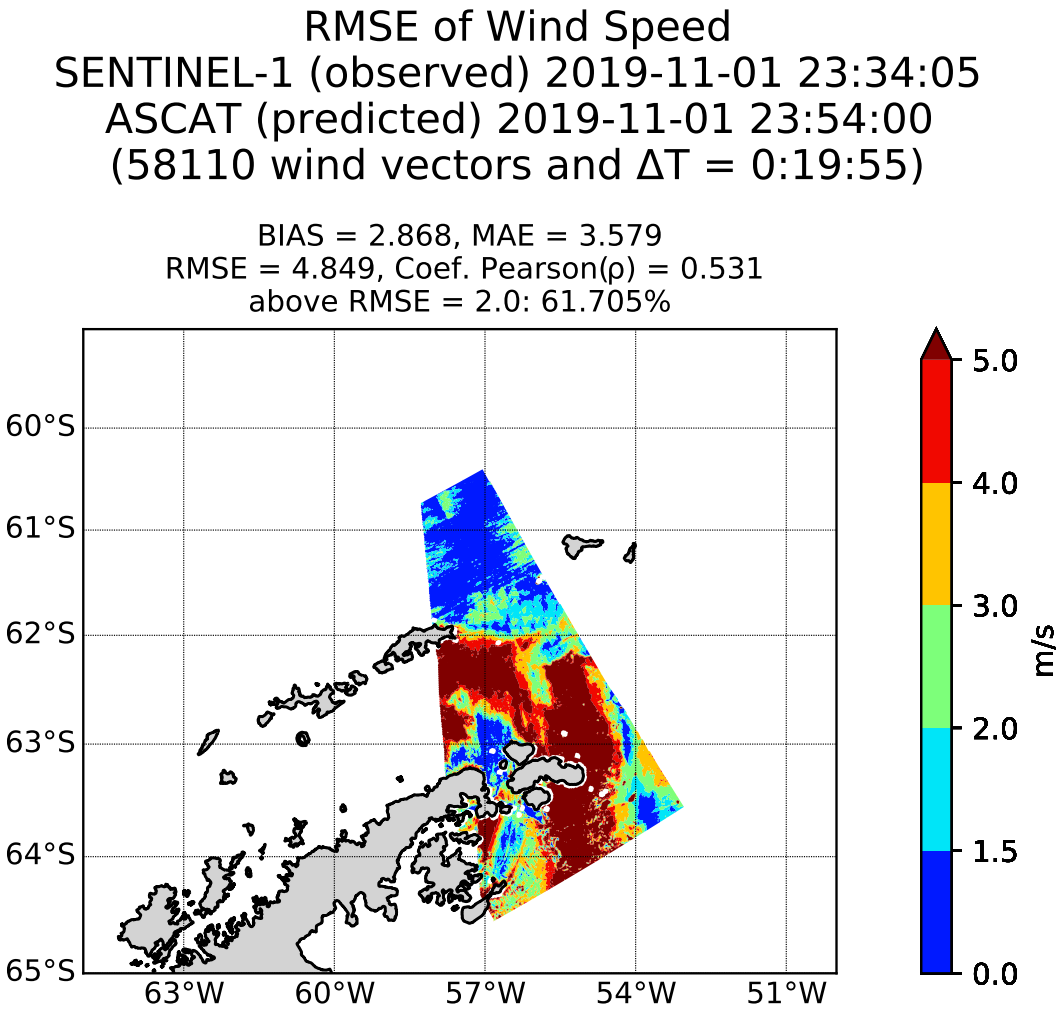

SOURCE: Author's production.

Figure 4.14 - RMSE Sentinel-1 *versus* ERA5 wind field plotting - 2019-11-01.

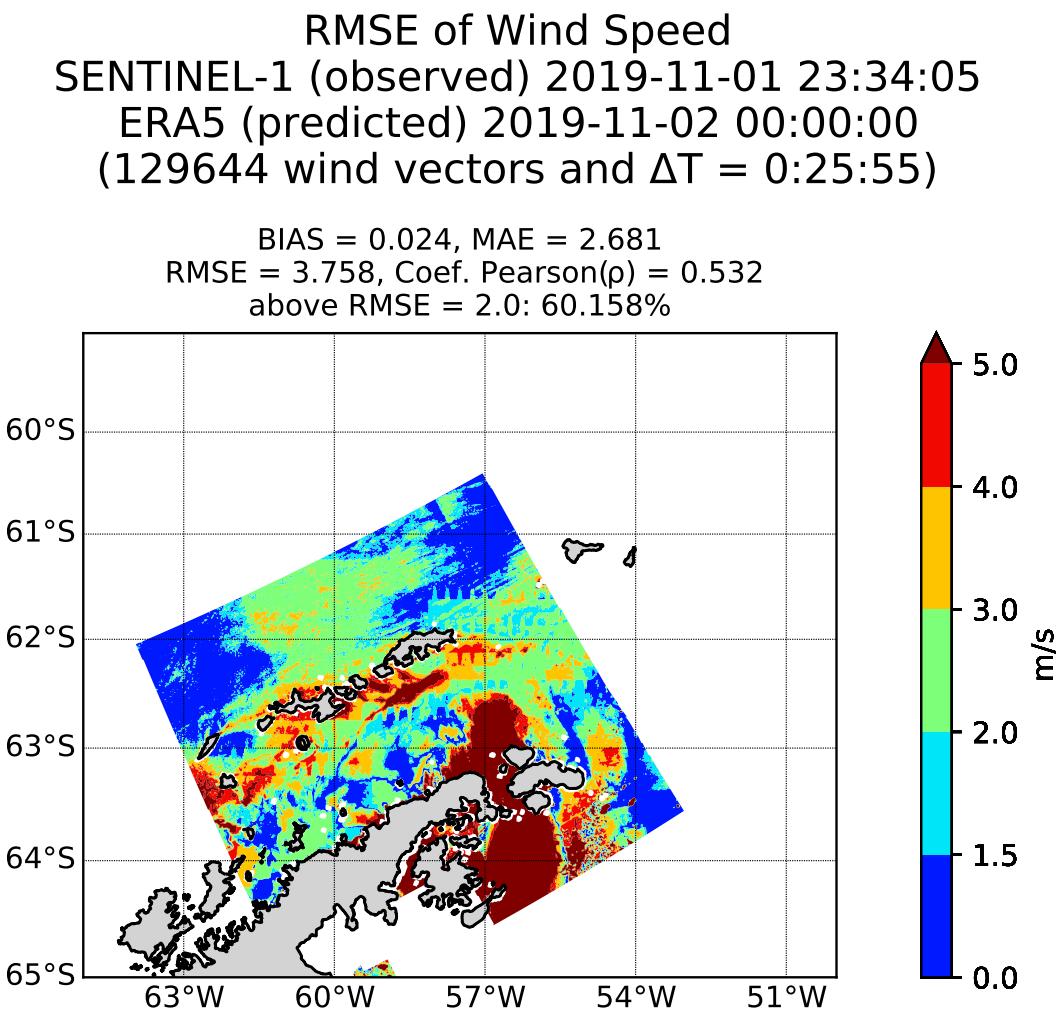

SOURCE: Author's production.

Figure 4.15 - RMSE ASCAT *versus* ERA5 wind field plotting - 2019-11-01.

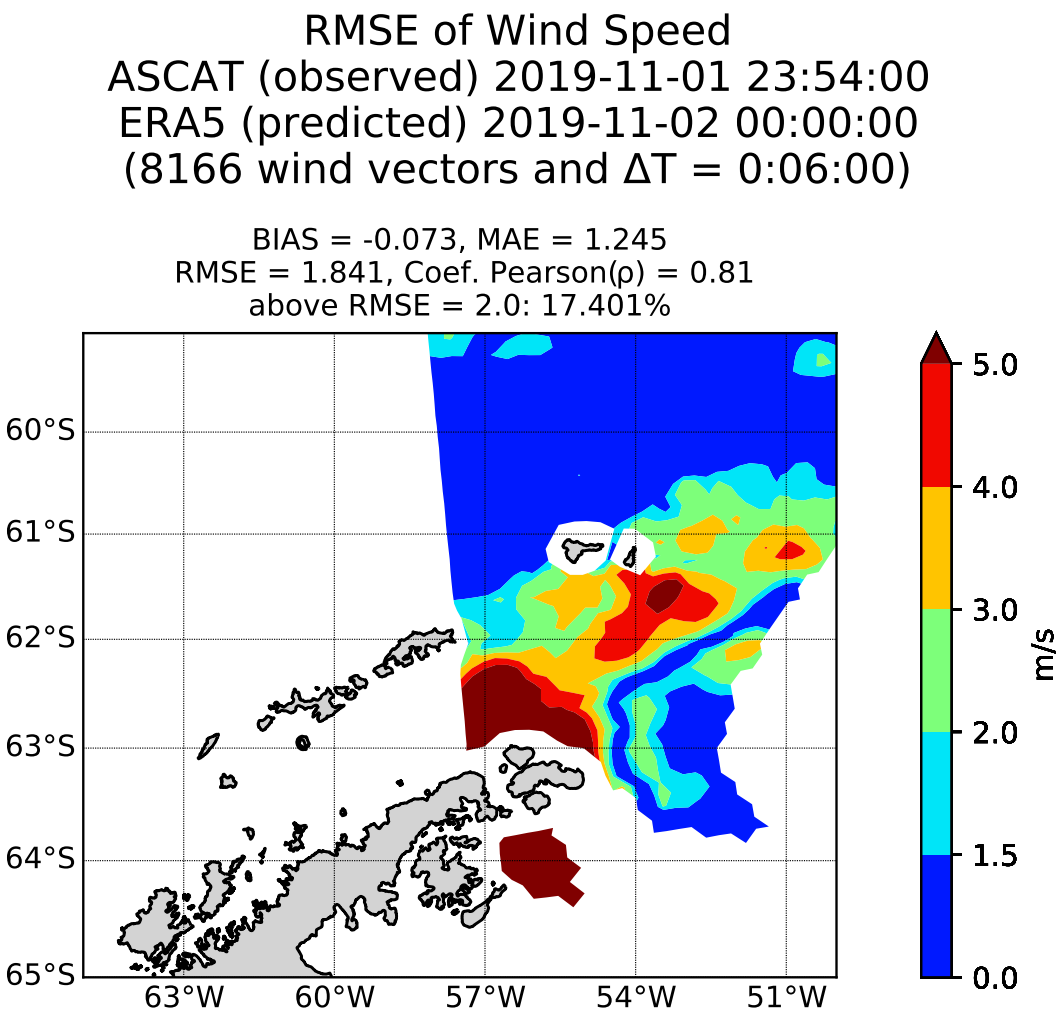

SOURCE: Author's production.

Figure 4.16 - BIAS Sentinel-1 *versus* ASCAT wind field plotting in level 2 - 2019-11-01.

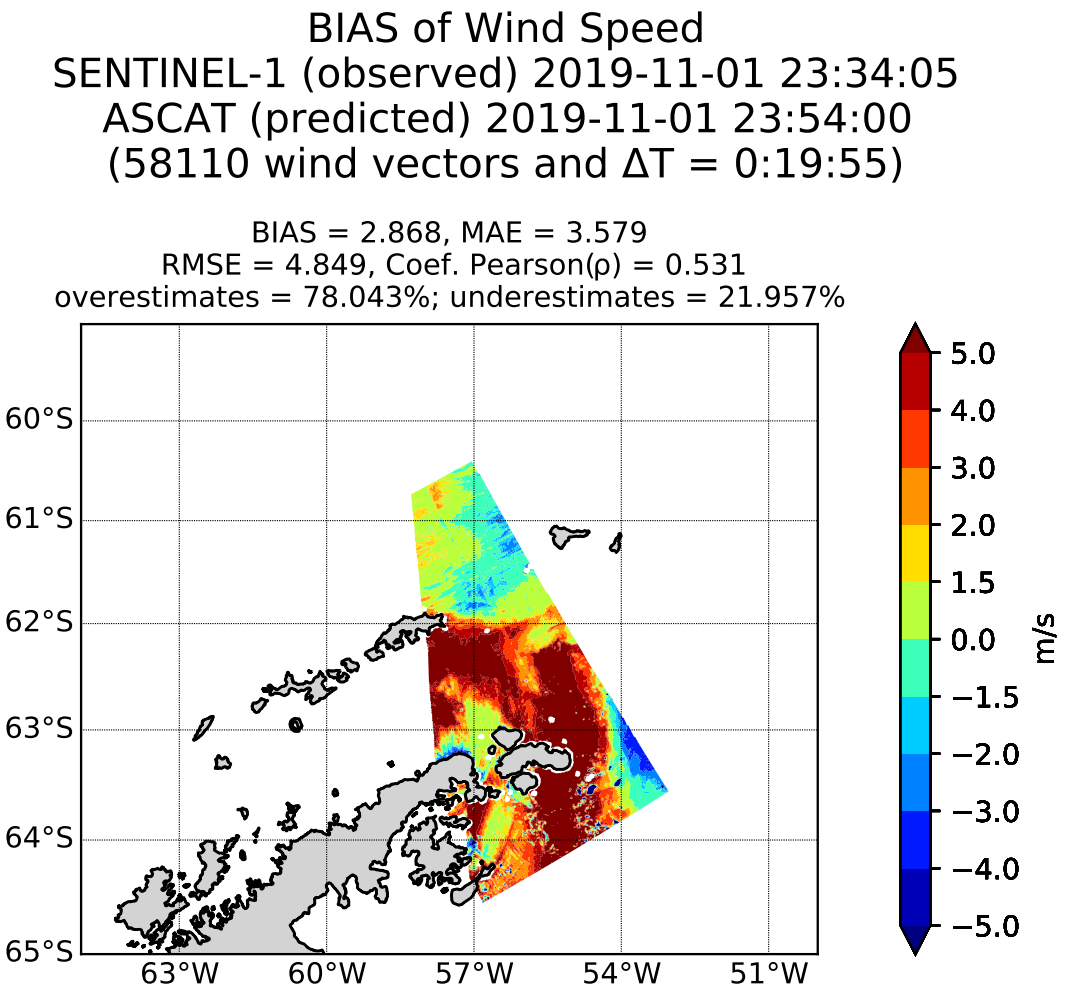

SOURCE: Author's production.

Figure 4.17 - BIAS Sentinel-1 *versus* ERA5 wind field plotting - 2019-11-01.

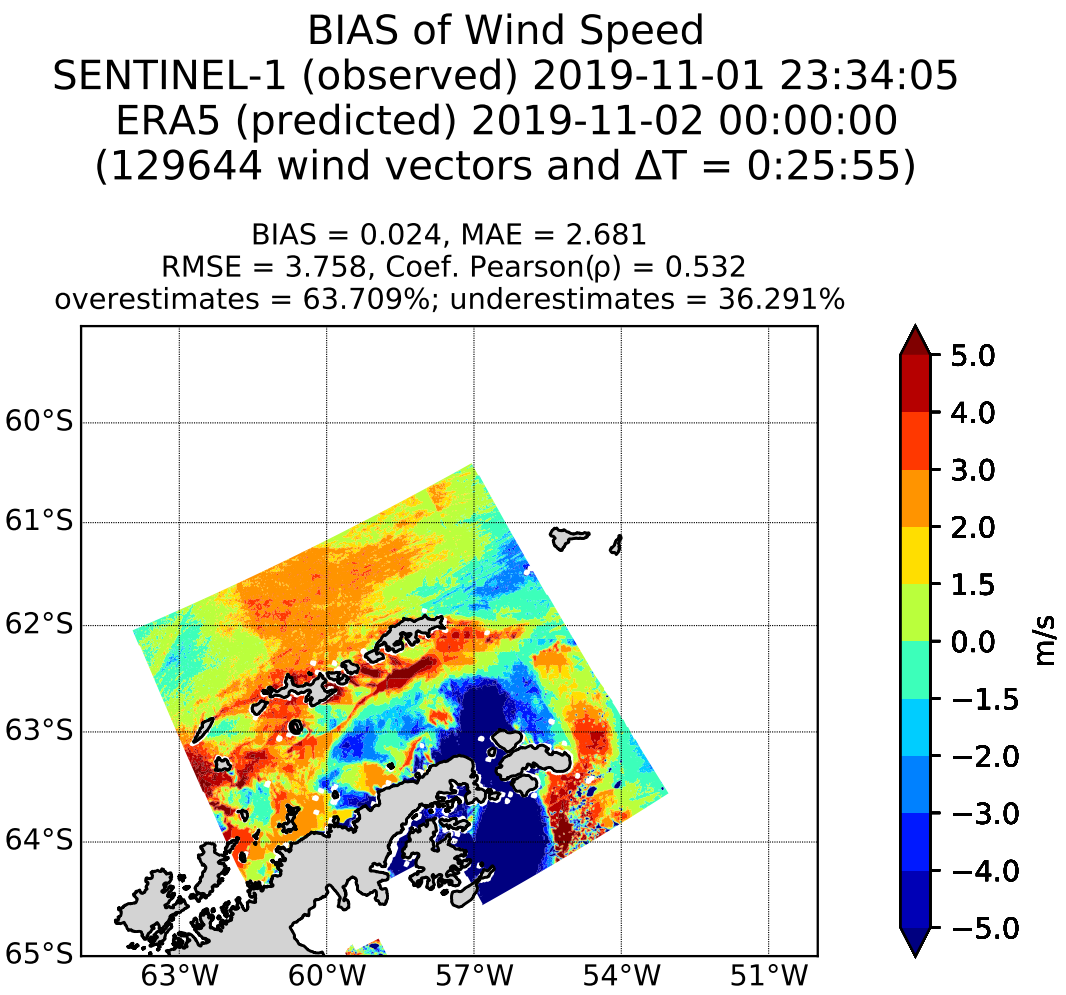

SOURCE: Author's production.

Figure 4.18 - BIAS ASCAT *versus* ERA5 wind field plotting - 2019-11-01.

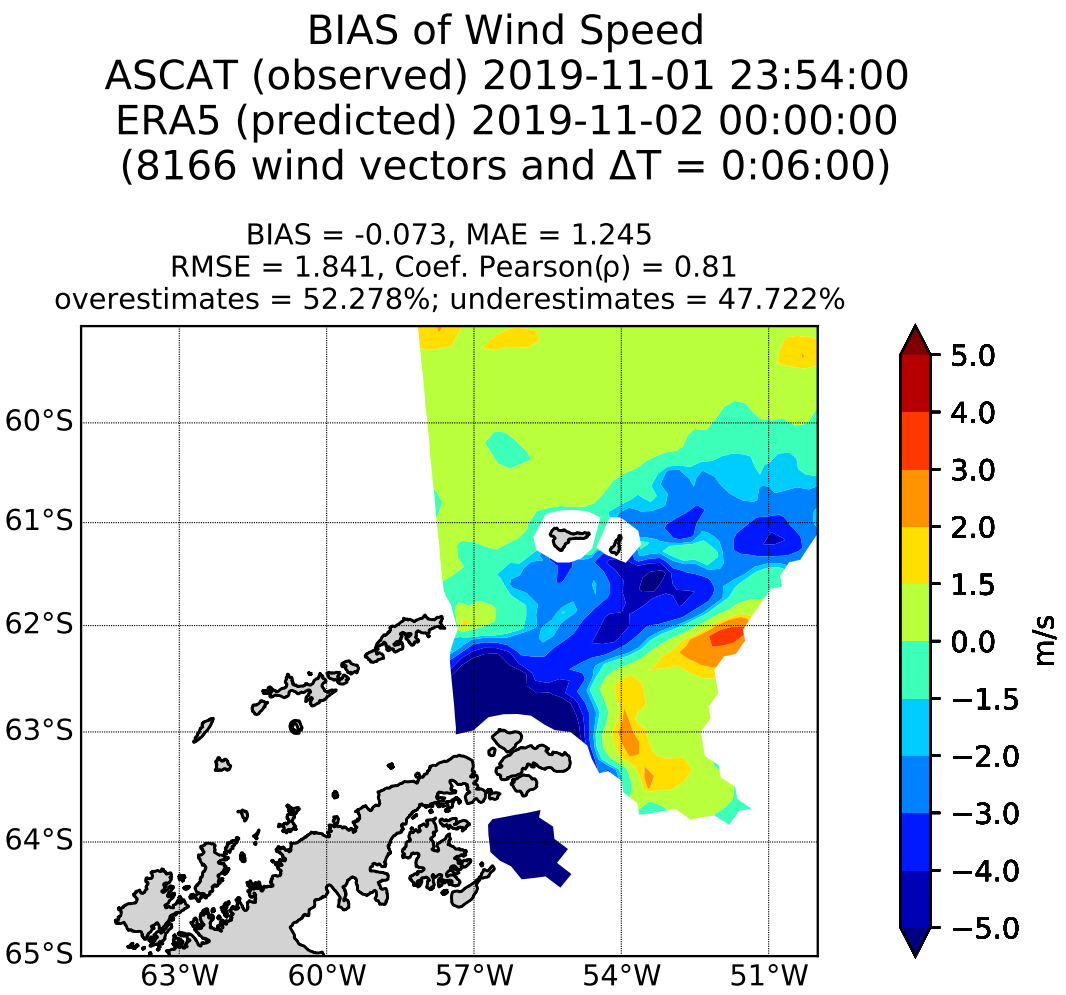

SOURCE: Author's production.

4.1.3 Compilation of plots from the two examples

The performance measures of the comparison of data sources that were taken in pairs are presented in Table 4.1. It can be seen that when comparing ERA5 with ASCAT, there was a better performance than when comparing ERA5 with Sentinel-1. Although ERA5 showed a bias of only 0.024 against Sentinel-1 scene for day 2019-11-01, it was observed that valid ERA5 wind vectors overestimate Sentinel-1 values. It should be noted that 63.709% of Sentinel-1 points with valid wind vectors measured a magnitude lower than that presented by the homologous ERA5 vectors for these same points, according to the correspondence criteria. Observing the RMSE value (4.849 and 3.758) and the Pearson coefficient (0.531 and 0.532) of Sentinel-1 in relation to the ASCAT and ERA5, respectively, combined with the observation of the RMSE values (1.841) and the Pearson's coefficient (ρ) = 0.81, we can suggest the occurrence of outliers in Sentinel-1 measurements, or the high temporal variability of the local wind field due to the time difference of approximately 20 minutes between Sentinel-1 and ASCAT and of approximately 26 minutes between Sentinel-1 and ERA5. Meanwhile, the difference between ASCAT and Sentinel-1 is only 6 minutes.

Table 4.1 - Values of statistical parameters for 2019-11-01 and 2019-11-28.

	Statistical parameters	**ASCAT**	**ERA5**
Sentinel-1 2019-11-28 "good"	BIAS	-0.354	-0.549
	MAE	0.956	1.225
	RMSE	1.258	1.556
	(ρ)	0.859	0.858
Sentinel-1 2019-11-01 "bad"	BIAS	2.868	0.024
	MAE	3.579	2.681
	RMSE	4.849	3.758
	(ρ)	0.531	0.532
ASCAT 2019-11-28 "good"	BIAS	–	0.022
	MAE	–	0.992
	RMSE	–	1.304
	(ρ)	–	0.922
ASCAT 2019-11-01 "bad"	BIAS	–	-0.073
	MAE	–	1.245
	RMSE	–	1.841
	(ρ)	–	0.81

On the other hand, for 2019-11-28 as described in Table 4.1, ASCAT had a much better performance against Sentinel-1. In addition, the time difference between the Sentinel-1 scene and the ASCAT scene as well as the difference for the ERA5 datetime was also approximately 10 minutes. Although the time difference between ASCAT and ERA5 had increased to 20 minutes, this did not affect the performance of comparison ASCAT versus ERA5. This allowed us to conclude that possibly a large part of the ERA5's data must have its origins in the ASCAT's data. And, it should also be noted that the greatest divergences between satellite-derived sources and the ERA5 occur in regions with winds of up to 3 m/s, followed by regions where winds are recorded with speeds above 12.5 m/s. In addition, the expected errors from temporal separation, spatial separation, sampling variability, satellite sensor and algorithm cannot be ignored.

4.2 Statiscal error analysis with *in situ* measurements

In this section we present our statistical error analysis to illustrate the calculation of performance measures for each data source against *in situ* observations. A total of 1247 measurements were made by the anchored buoy (buoy #1) at 10-minute intervals for a height of 2.5 meters, and then converted to a height of 10 meters, for the period between 10-18 November, 2019. Unfortunately, as mentioned in Section 3.2, due to logistic problems and electric failure, it was only possible to register the wind speed without direction data for the period between 10-18 November, 2019. On the other hand, the wave buoy was chained and tied to the anchoring system of buoy #1, and recorded 1579 measurements made at 2-hour intervals, between November 8, 2019 and March 1, 2020 with wind speed and direction data. Although there is a combination of low scene availability per day (134 Sentinel-1's scenes and 665 ASCAT's scenes) for the Bransfield Strait, the accuracy of wind data sets derived from satellites and ERA5 was calculated through the comparison with data sets obtained from *in situ* observations recorded by the meteorological anchored buoy and by the wave buoy installed in that region.

4.2.1 Comparison of satellite-derived wind fields with observations of the anchored buoy

The regression line was calculated for the distribution of wind speed obtained by Sentinel-1 and ASCAT for the position of the buoy within a maximum radius of 50 km inside of time interval of until 30 minutes for a given date-time, respectively, against wind speed recorded by buoy (Figure 4.19 and Figure 4.20). To assess

the performance of the accuracy, the buoy values were fixed as standard measures, and the measures of BIAS, MAE, and RMSE were calculated. Moreover, the Pearson coefficient was used to determine the linear correlation. The results in comparison of the wind speed from data Sentinel-1 and from buoy #1 show a low BIAS measurement whose value is -0.482 and a correlation coefficient whose value is $\rho = 0.767$ for the wind speed that representing a high positive degree of correlation. However, the results when in comparison with data of ASCAT and buoy #1, the results show a bigger BIAS measurement whose value is 2.335, and a correlation coefficient whose value is $\rho = 0.84$, representing a high positive degree of correlation for wind speed.

For Sentinel-1, 34922 wind vector matchups were obtained, while for ASCAT, only 404 matchup data were obtained. Although there is a low availability of level 2 scenes for both satellites, the superiority of the Sentinel-1's spatial resolution (1 km x 1 km) allowed the obtaining of a greater number of wind vectors. While for ASCAT which has a resolution of 12.5 km, it was possible to obtain only 404 matches. The results show that the accuracy of the Sentinel-1 data is superior to the precision of the ASCAT data, and that for this region within the observed period, the BIAS and RMSE values are outside the ASCAT mission requirements (0.5 and 2.0 m/s, respectively) (OSI SAF, 2019; KAKO et al., 2011) as well as the RMSE value of Sentinel-1 (2.0 m/s). In addition, Sentinel-1 underestimated the buoy measurements for winds with intensity below 10 m/s, and overestimated the buoy records for wind speeds above this value. While the ASCAT overestimated the wind speed during the buoy measurement period. The values of the correlation coefficients show a high consistency between the values recorded by the buoy and those obtained by both Sentinel-1 and ASCAT. Some reasons about the differences in buoy and satellite measurements were discussed in the Section 5.1.

Figure 4.19 - Scatter plot of wind speed between Sentinel-1 and Meteorological Buoy.

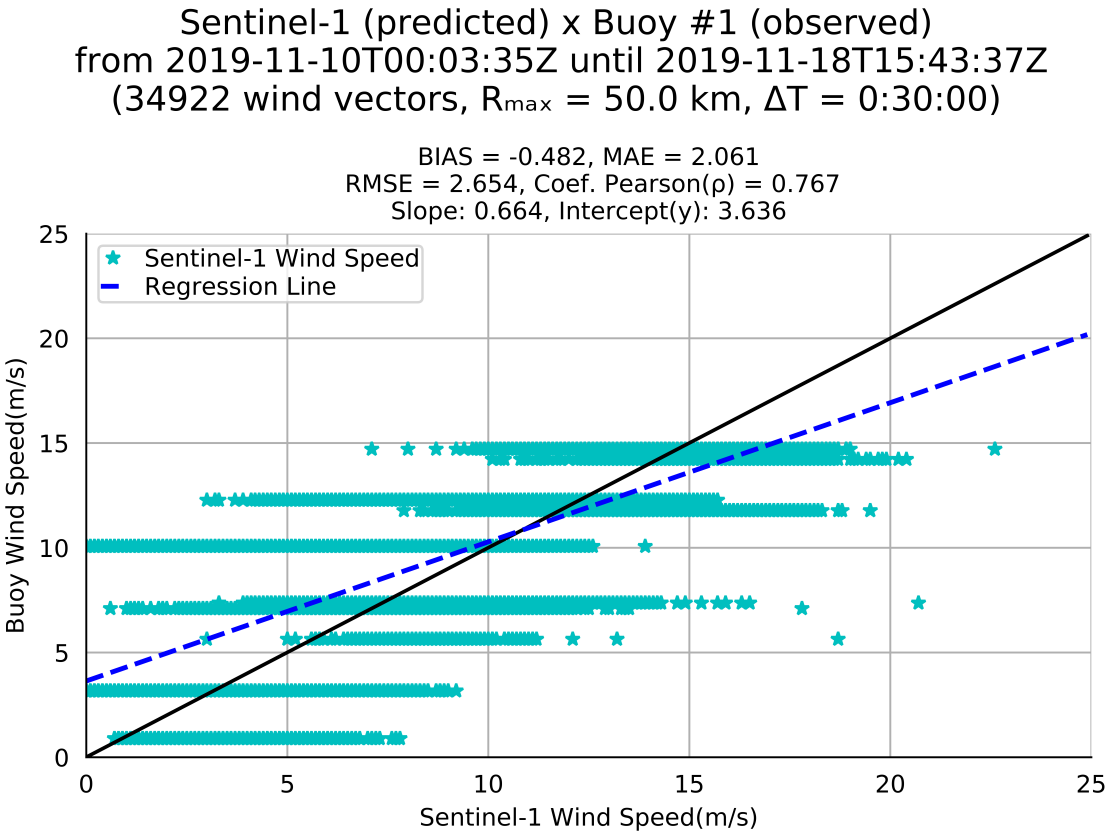

Scatter plot between Sentinel-1 and Meteorological Buoy for the period from 2019-11-10 00h03min35Z until 2019-11-18 15h43min37Z, with 34922 wind vectors, maximum radius of 50km and maximum time interval of 30min.

SOURCE: Author's production.

Figure 4.20 - Scatter plot of wind speed between ASCAT and Meteorological Buoy.

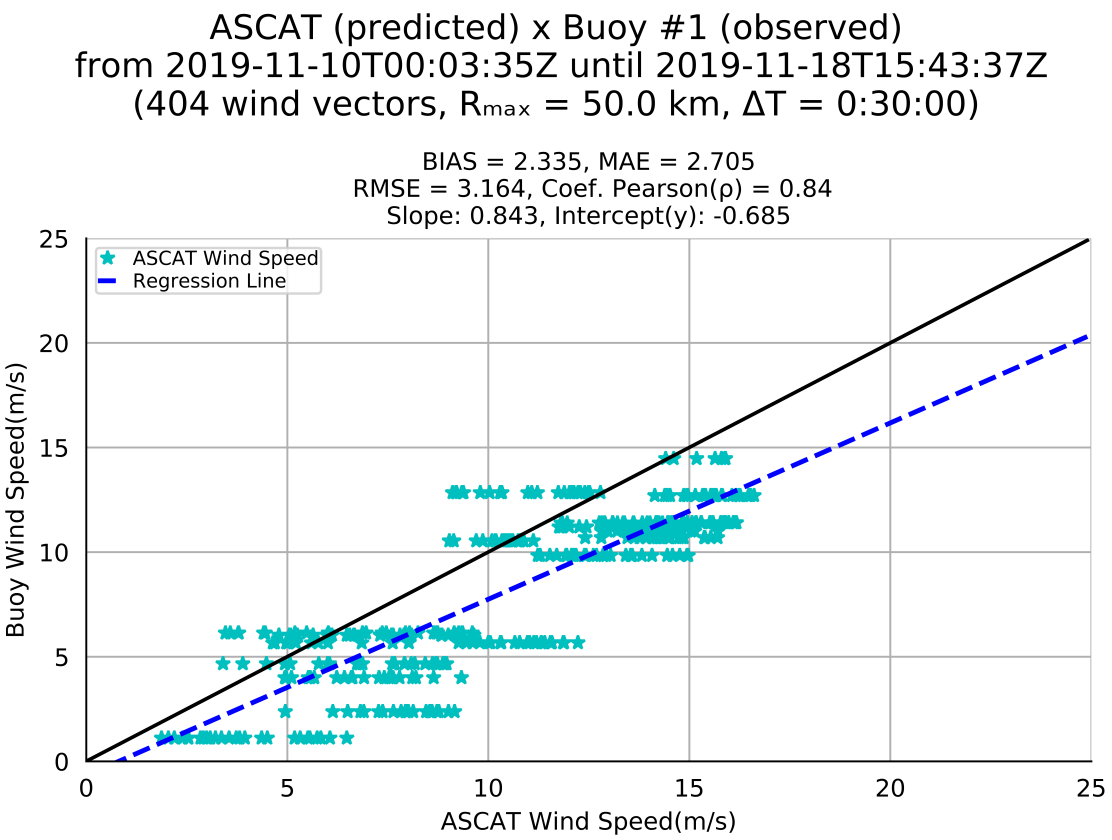

Scatter plot between ASCAT and Meteorological Buoy for the period from 2019-11-10 at 00h03min35Z until 2019-11-18 at 15h43min37Z, with 404 wind vectors, maximum radius of 50km and maximum time interval of 30min.

SOURCE: Author's production.

4.2.2 Comparison of ERA5 reanalysis-derived wind fields with observations of the anchored buoy

Likewise, the regression line was calculated for the distribution of wind speed obtained by ERA5 for the position of the buoy within a maximum radius of 50 km within the time interval of up to 30 minutes for a given date-time against buoy wind speed (Figure 4.21). In comparison with ERA5, 28681 the wind vectors were obtained, although the spatial resolution of ERA5 is 0.25°x 0.25°. The reason that allowed obtaining a greater number of wind vectors was hourly availability of ERA5 data combined with the number of data buoy records due to time interval of 10 minutes between the buoy measurements. The results show that ERA5's and Sentinel-1's RMSE are approximately equal, and also a better bias's per-

formance in relation to ASCAT. In addition, ERA5 overestimated the wind speed during the buoy measurement period. Finally, as in comparisons of previous subsection, the correlation coefficient also shows a high consistency between the values recorded by the buoy and those obtained by ERA5.

Figure 4.21 - Scatter plot of wind speed between ERA5 and Meteorological Buoy.

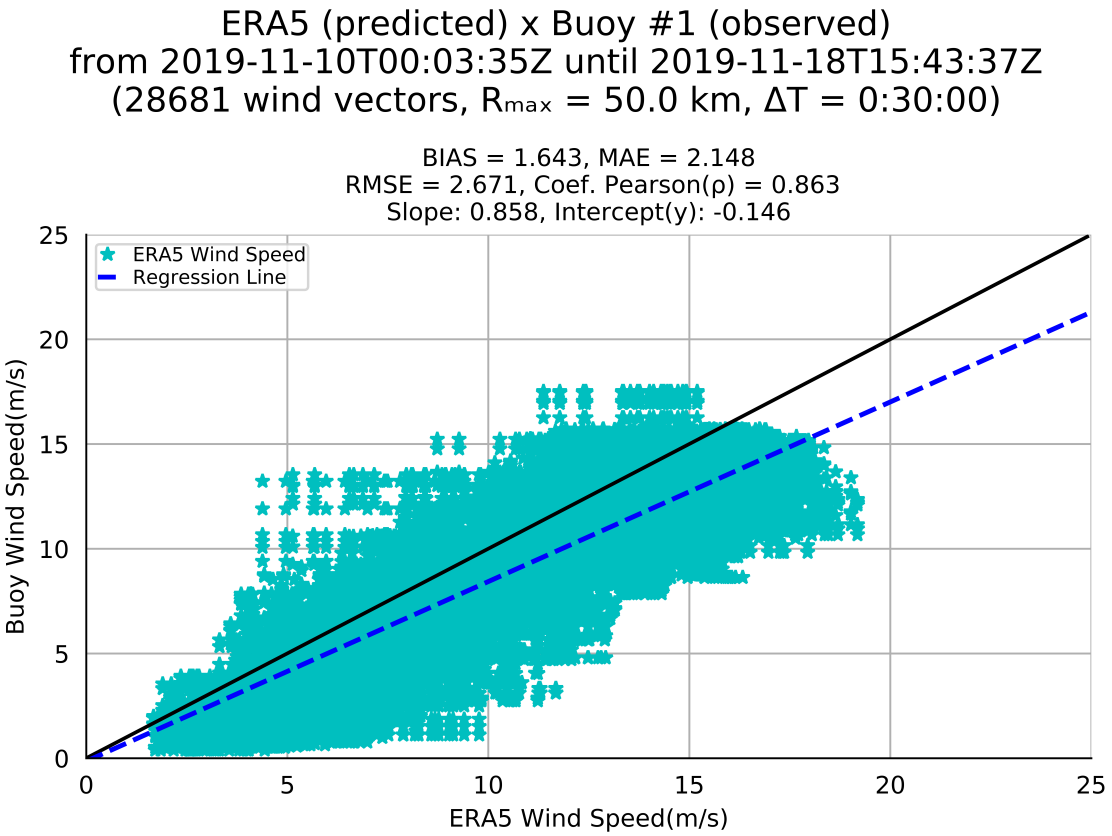

Scatter plot between ERA5 and Meteorological Buoy for the period from 2019-11-10 at 00h03min35Z until 2019-11-18 at 15h43min37Z with 28681 wind vectors, maximum radius of 50km and maximum time interval of 30min.

SOURCE: Author's production.

4.2.3 Comparison of satellite-derived wind fields with observations of the wave buoy

Due to the 4 months of measurements made by the wave buoy, 257073 matches of wind vectors were obtained by Sentinel-1, while for ASCAT, only 4573 matchup data were obtained. This longer period of observation allowed a considerable in-

crease in the availability of level 2 scenes for both satellites. Again, the superiority of the spatial resolution of Sentinel-1 (1 km x 1 km) when compared to that of ASCAT (12.5 km) allowed to obtain a greater number of correspondences for the wind vectors. However, the results show that the accuracy of the Sentinel-1 data is slightly superior to the accuracy of the ASCAT data only for wind magnitude measurements (Figure 4.22 and Figure 4.23).

Figure 4.22 - Scatter plot of wind speed between Sentinel-1 and Wave Buoy.

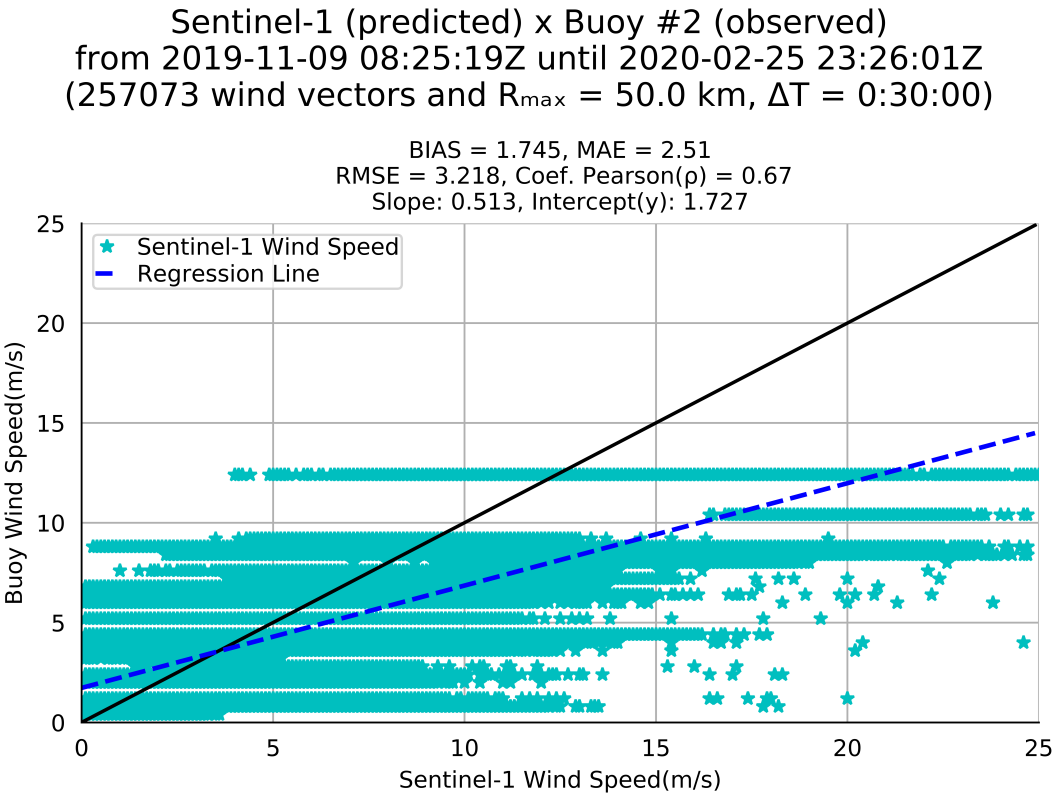

Scatter Plot of wind speed between Sentinel-1 and Wave Buoy for the period from 2019-11-09 at 08h25min19Z until 2020-02-25 at 23h26min01Z with 257073 wind vectors, maximum radius of 50km and maximum time interval of 30min.

SOURCE: Author's production.

Figure 4.23 - Scatter plot of wind speed between ASCAT and Wave Buoy.

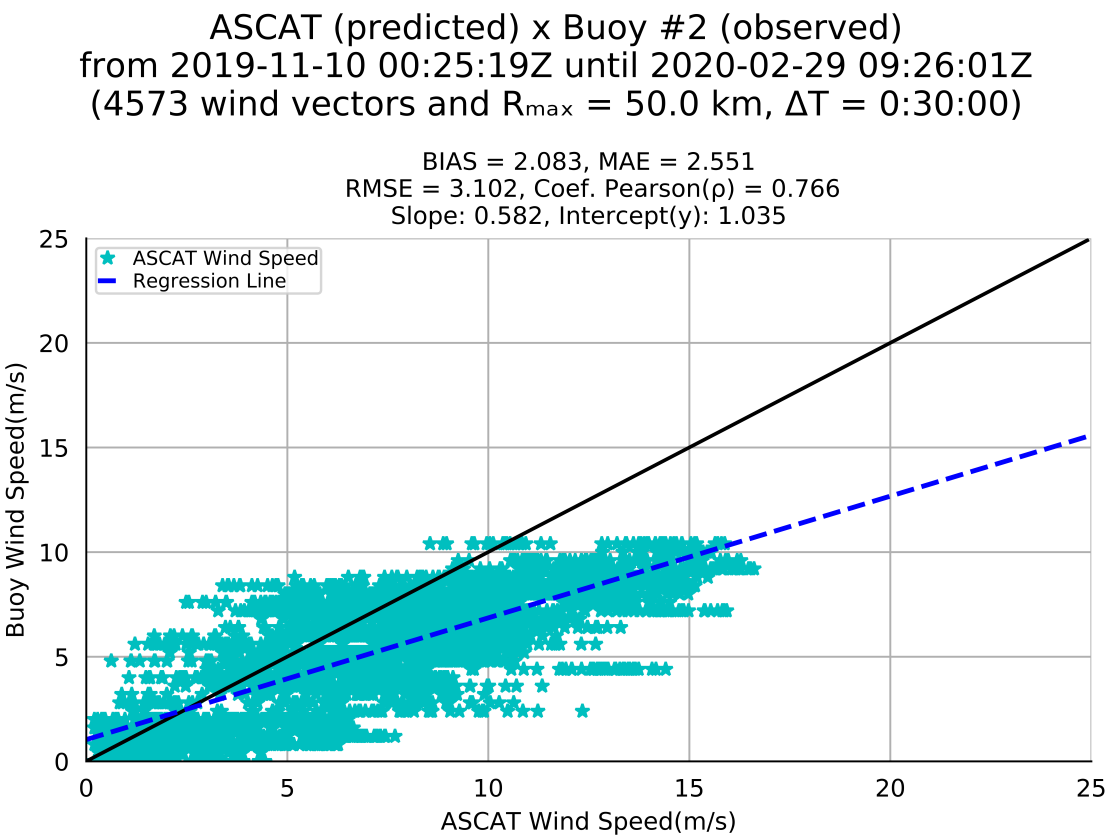

Scatter Plot of wind speed between ASCAT and Wave Buoy for the period from 2019-11-10 at 00h25min19Z until 2020-02-29 at 09h26min01Z with 4573 wind vectors, maximum radius of 50km and maximum time interval of 30min.

SOURCE: Author's production.

While in the comparison between the respective components U and V of the wind (Figure 4.24 and Figure 4.25), ASCAT shows a much better performance in relation to the bias, and a higher degree of correlation with the *in situ* data recorded by the wave buoy in comparison against Sentinel-1. The results also show that for this region within the observed period, the BIAS and RMSE values are outside the ASCAT mission requirements (0.5 and 2.0 m/s, respectively) (OSI SAF, 2019) as well as the RMSE value of Sentinel-1 (2.0 m/s) (ESA, 2019b). Nevertheless, the values of the correlation coefficients show a high consistency between the values recorded by the buoy and those obtained by both Sentinel-1 and ASCAT.

Figure 4.24 - Scatter plot of wind components between Sentinel-1 and Wave Buoy.

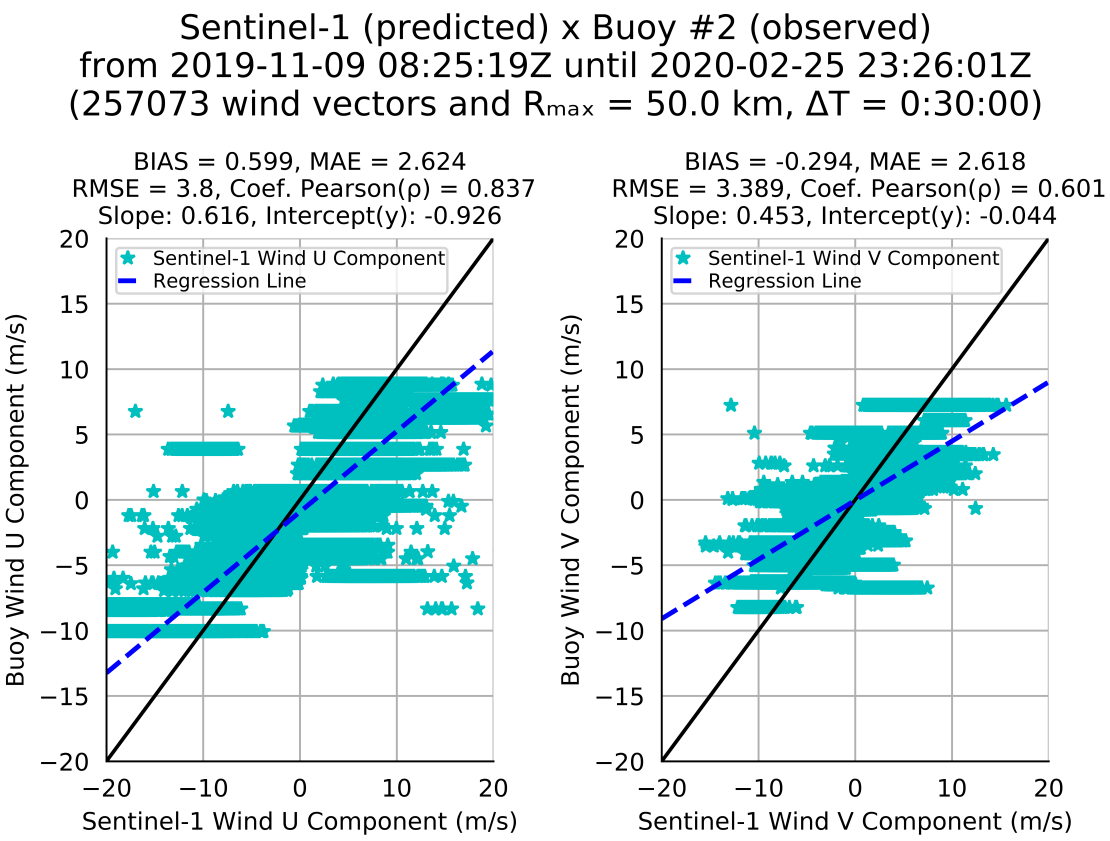

Scatter Plot of wind components between Sentinel-1 and Wave Buoy for the period from 2019-11-09 at 08h25min19Z until 2020-02-25 at 23h26min01Z with 257073 wind vectors, maximum radius of 50km and maximum time interval of 30min.

SOURCE: Author's production.

Figure 4.25 - Scatter plot of wind components between ASCAT and Wave Buoy.

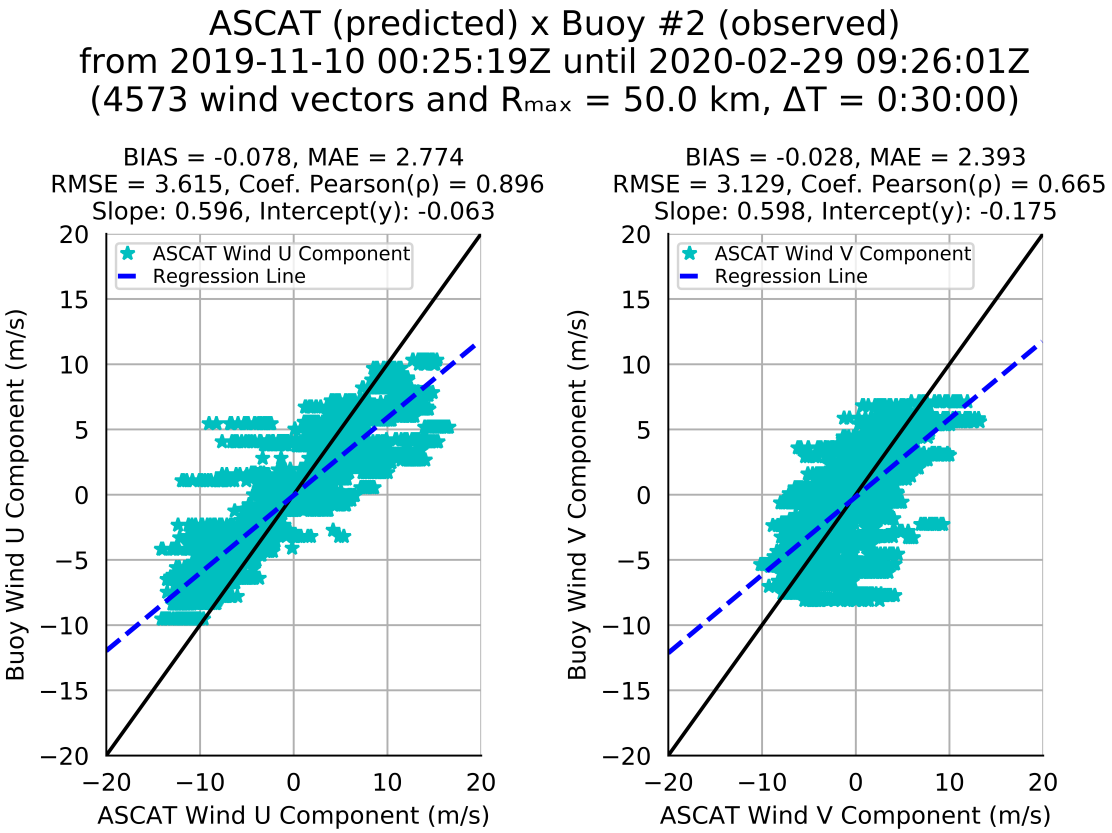

Scatter Plot of wind components between ASCAT and Wave Buoy for the period from 2019-11-10 at 00h25min19Z until 2020-02-29 at 09h26min01Z with 4573 wind vectors, maximum radius of 50km and maximum time interval of 30min.

SOURCE: Author's production.

4.2.4 Comparison of ERA5 reanalysis-derived wind fields with observations of the wave buoy

Similar to what happened with wind fields derived from satellites, in the comparison of ERA 5 with the wave buoy, a good number of wind vectors were obtained. A total of 34468 correspondences were obtained during these 4 months of observations according to the criteria used. In comparison with the wind magnitude values, ERA5 performed better than Sentinel-1 and ASCAT as seen in the BIAS, MAE and RMSE measurements, and a high degree of correlation, although the correlation coefficient has a value intermediate when compared to satellite wind magnitude assessments. However, for the U and V components,

the results showed that the bias values in the performance of the ERA5 were worse than those obtained by the satellites, although the ERA5 has values of correlation coefficient, MAE and RMSE close to the values obtained by the satellites (Figure 4.26 and Figure 4.27).

Figure 4.26 - Scatter plot of wind speed between ERA5 and Wave Buoy.

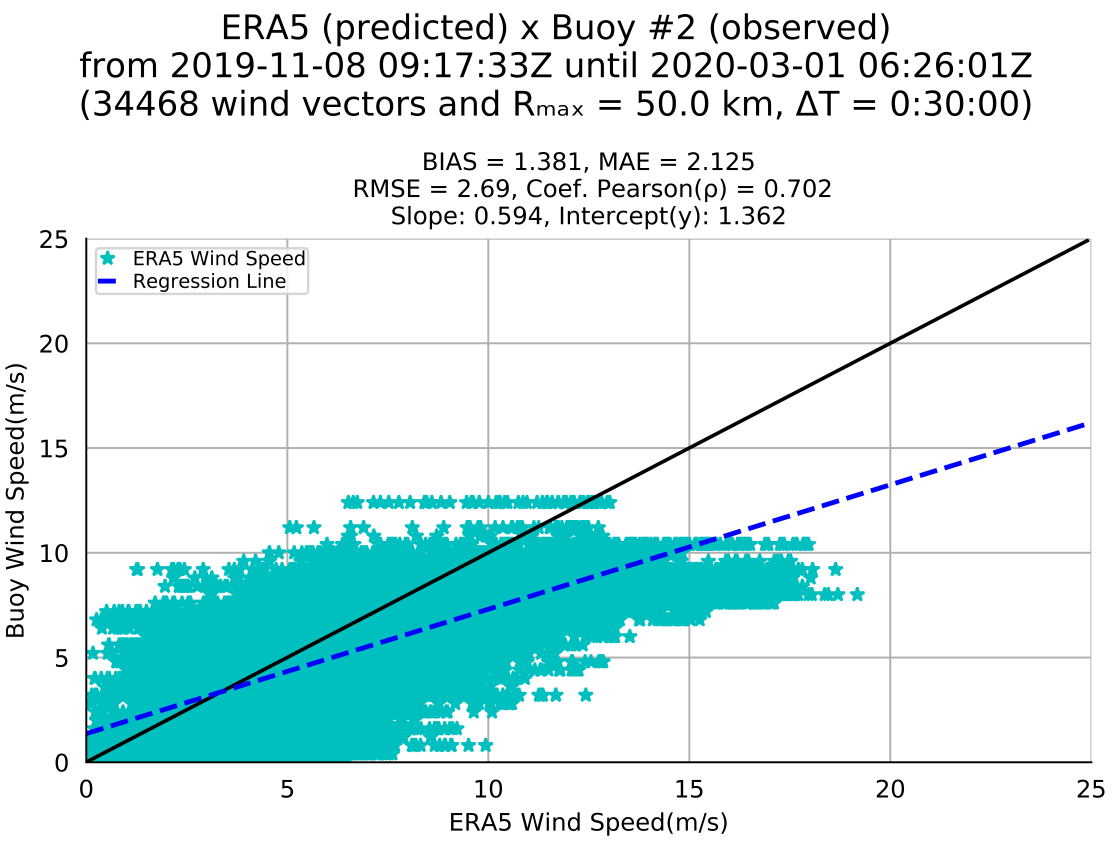

Scatter Plot of wind speed between ERA5 and Wave Buoy for the period from 2019-11-08 at 09h17min33Z until 2020-03-01 at 06h26min01Z with 34468 wind vectors, maximum radius of 50km and maximum time interval of 30min.

SOURCE: Author's production.

Figure 4.27 - Scatter plot of wind components between ERA5 and Wave Buoy.

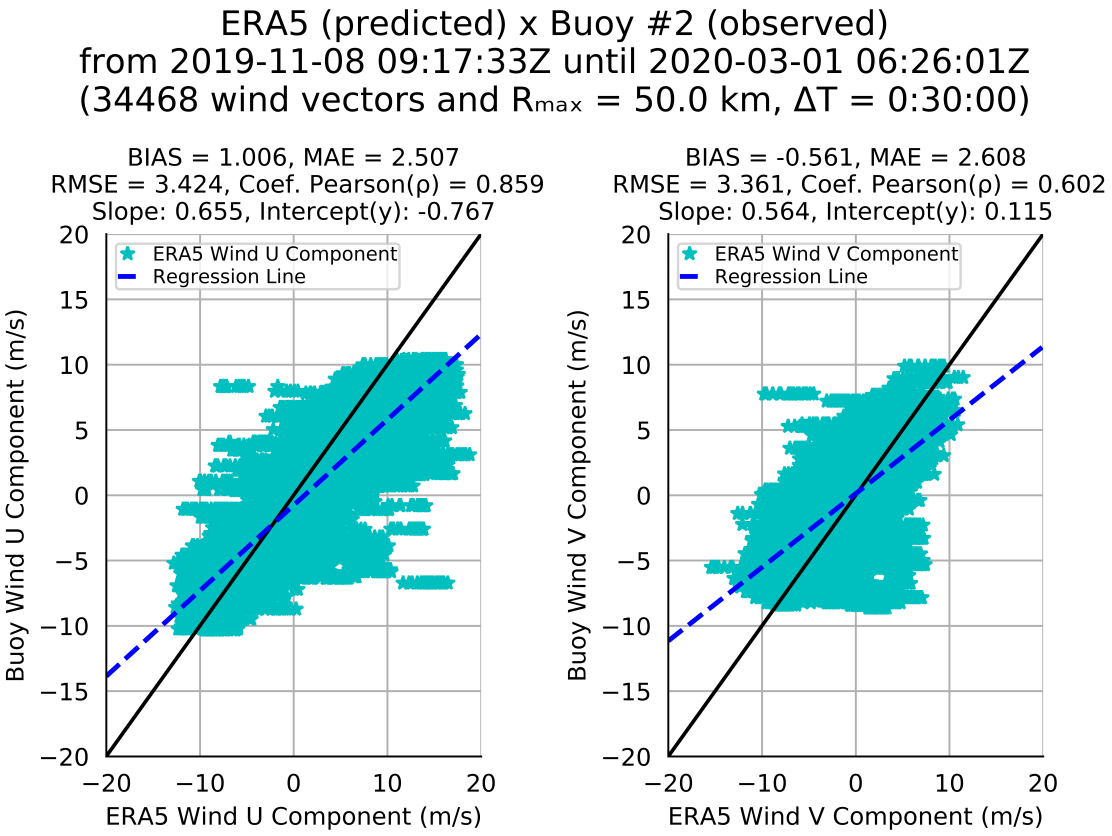

Scatter Plot of wind components between ERA5 and Wave Buoy for the period from 2019-11-08 at 09h17min33Z until 2020-03-01 at 06h26min01Z with 34468 wind vectors, maximum radius of 50km and maximum time interval of 30min.

SOURCE: Author's production.

5 DISCUSSION

5.1 Time series analysis

The time series of meteorological buoy (Figure 5.1 and Figure 5.2) and wave buoy (Figure 5.3) reaffirm the consistency of the data. Where the data from the meteorological buoy were resampled by arithmetic mean to 1-hour, for the wave buoy the time interval was 2-hours between measurements, and the plotting of satellite-derived data was according to availability for the region. In the time series of the anchored meteorological buoy, it was quite evident that the ERA5 overestimates the wind speed values most of the time.

Figure 5.1 - Time series of meteorological buoy resampled to 1-hour before 2019-11-14.

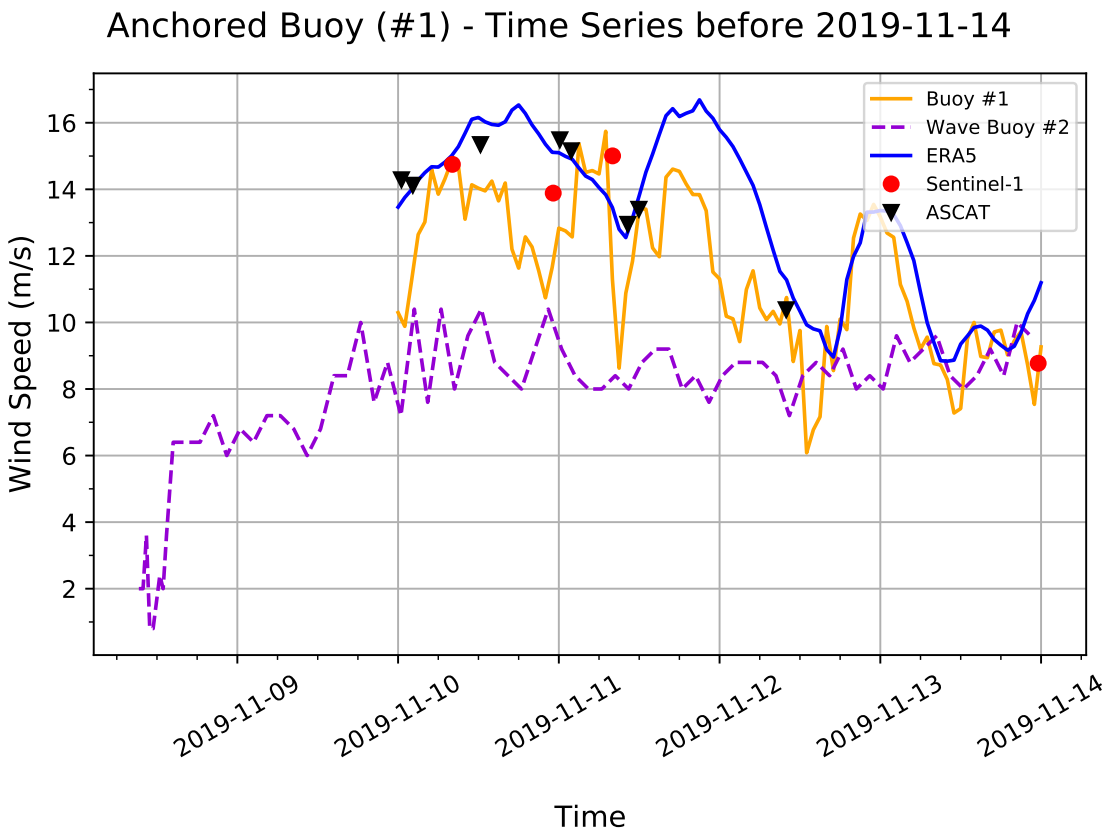

Time series of meteorological buoy resampled to 1-hour, wave buoy, ERA5, Sentinel-1 and ASCAT between 10 and 14 November, 2019.

SOURCE: Author's production.

Figure 5.2 - Time series of meteorological buoy resampled to 1-hour after 2019-11-14.

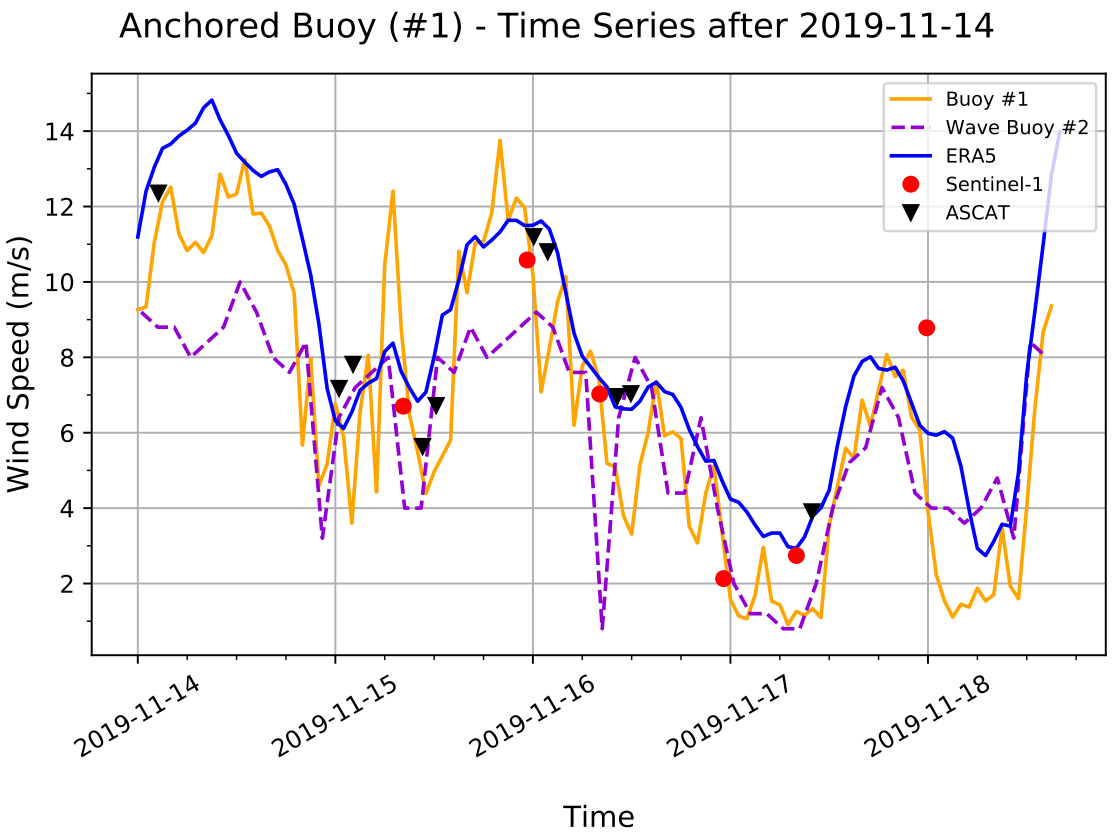

Time series of meteorological buoy resampled to 1-hour, wave buoy, ERA5, Sentinel-1 and ASCAT between 14 and 18 November, 2019.

SOURCE: Author's production.

The analysis work for the time series of the ERA5 data is much easier due to the hourly availability of the data. On the other hand, the wind data derived from Sentinel-1 and ASCAT do not have this abundance of records, not allowing the composition of a time series as robust as for ERA5. However, this difficulty was not prohibitive for the execution of the comparison with the observations *in situ*. This difficulty was overcome by the use of the wave buoy which provided measurements *in situ* for approximately 4 months, and consequently it was possible to obtain a satisfactory amount of scenes available for Sentinel-1 and ASCAT due to the longer time interval as showed in Figure 5.3. Therefore, for the days when scenes are available, the results show that Sentinel-1 recorded measurements very close to the wind speed values recorded by the anchored buoy, while ASCAT presented slightly overestimated measurements, and the measurements made by the wave buoy were underestimated in relation to the others data set.

As the results show in Section 4.2, RMSE are greater than 2.0 m/s for both zonal and meridional components at wave buoy's location. The reasons mentioned below and in the Section 3.2 are plausible for this relatively low accuracy (Figure 5.4 and Figure 5.5). First, due to an electrical failure caused by severe weather conditions, it only was possible to use meteo-oceanographic sensors for approximately 8 days and without records of wind direction data. Therefore, wind direction data was exclusively obtained by records from algorithm of wave buoy and not by GPS, compass or gyrocompass. In addition, land proximity can interfere in the backscatter observed by scatterometers (OSI SAF, 2019; OWEN; LONG, 2009) and by SAR instruments (WEI et al., 2020).

Second, according to manufacturer, fast and high wind variability around the region also lowers the accuracy of the wave buoy in the wind estimation. Thus, it can result in an underestimate of the wind speed estimate. The proximity to land does not allow the wind coming from that direction to have enough time to interact with the sea in order to cause any significant change or that this interaction is significantly reduced on the surface of the sea water, in such a way that the change in the sea wave is below or very close to the threshold to be detected by the sensitivity of the wave buoy, and thus, the calculation of the estimate of the wind vector can be done by the algorithm. Moreover, the Scatterometers convert the sea surface roughness into wind speed (ABDALLA; DE CHIARA, 2017), and so they can lose accuracy during changes in the wind speed due to atmospheric stratification.

Figure 5.3 - Wind Speed Time Series of Wave Buoy.

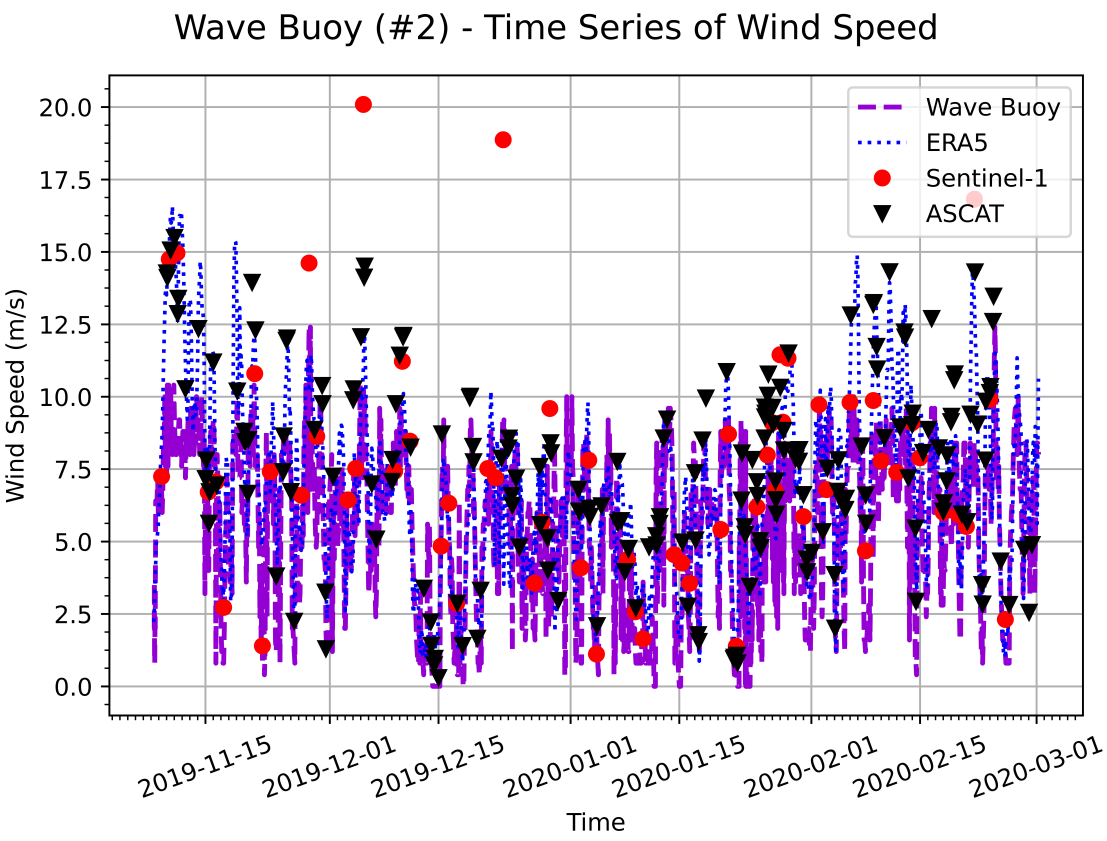

Wind Speed Time Series of Wave Buoy, Senitnel-1, ASCAT data, and ERA5 resampled to 2-hour from November 8, 2019 until March 1, 2020.

SOURCE: Author's production.

Figure 5.4 - Wind U Component Time Series of Wave Buoy.

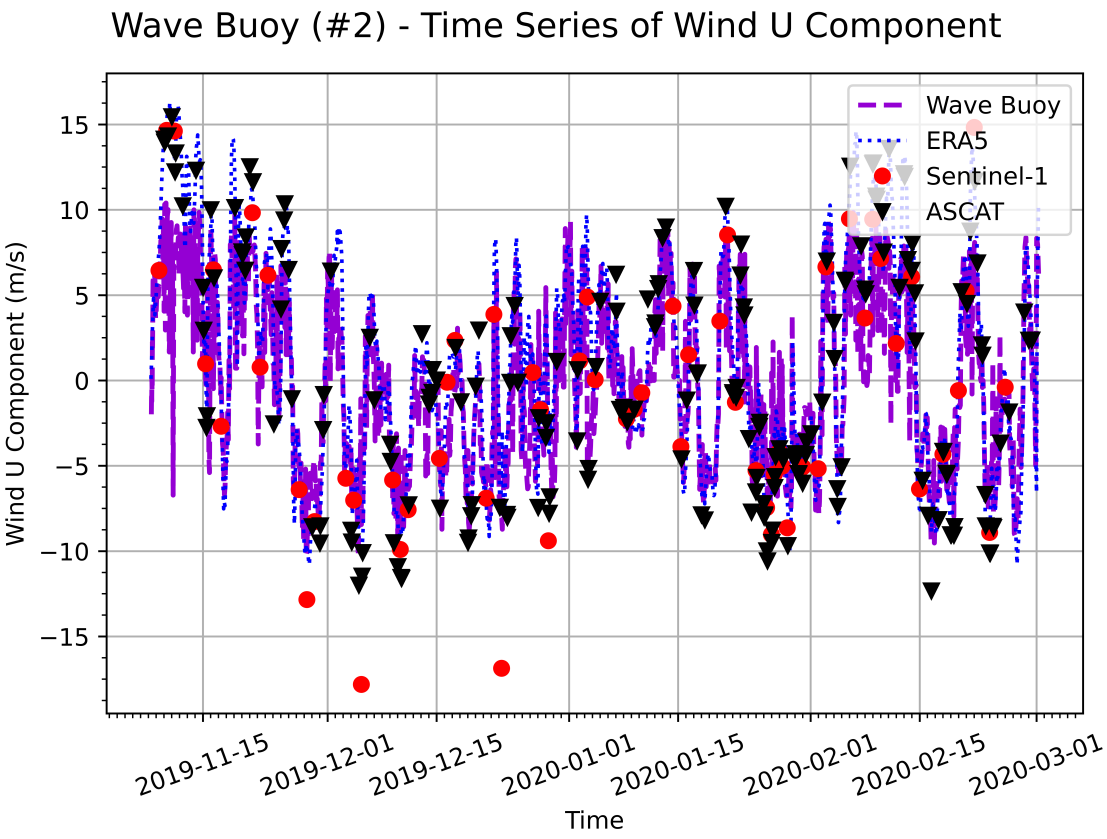

Wind U Component Time Series of Wave Buoy, Senitnel-1, ASCAT data, and ERA5 re-sampled to 2-hour from November 8, 2019 until March 1, 2020.

SOURCE: Author's production.

Figure 5.5 - Wind V Component Time Series of Wave Buoy.

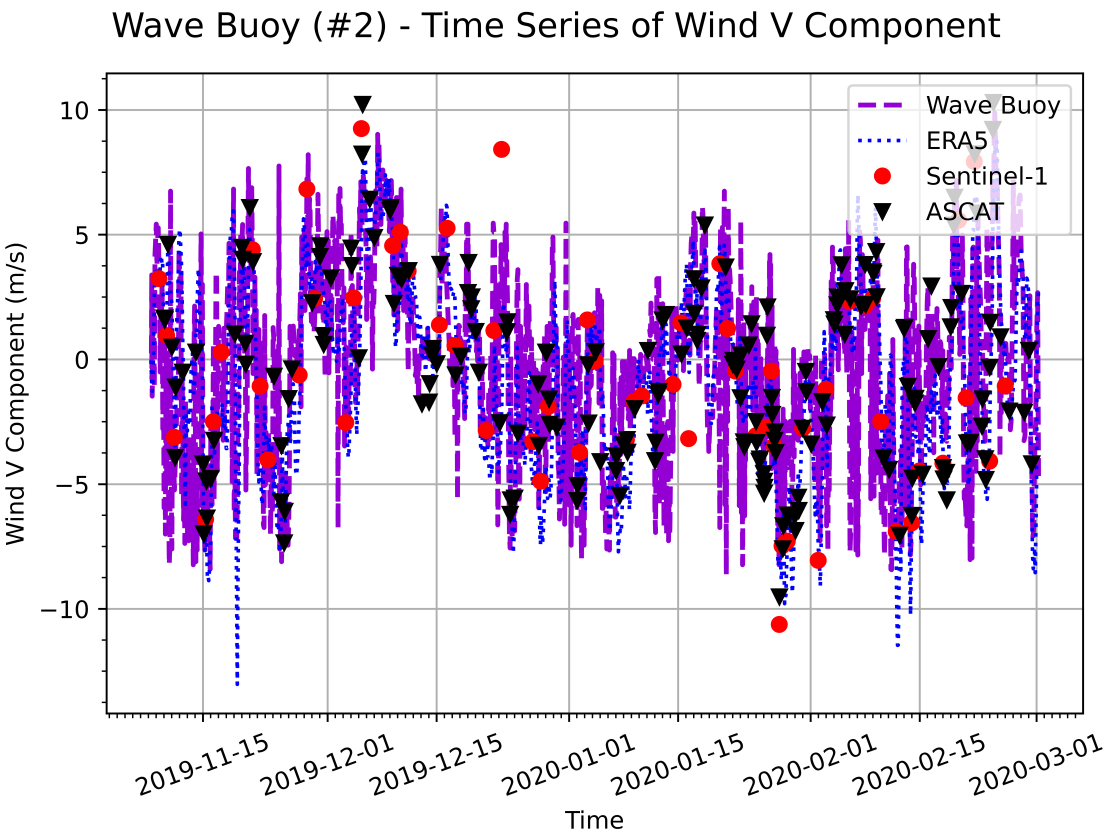

Wind V Component Time Series of Wave Buoy, Senitnel-1, ASCAT data, and ERA5 re-sampled to 2-hour from November 8, 2019 until March 1, 2020.

SOURCE: Author's production.

Finally, in regions where wind field has high temporal variations, the estimates become less reliable. In addition, a degradation of satellite-derived data is presumable due to a low temporal resolution (only once or twice a day). On the other hand, in mid latitudes, there is previous studies (TOMITA; KUBOTA, 2011) that have already demonstrated that daily wind speeds derived from a single satellite and those derived from hourly observations by surface moored buoys have an average of the RMSE and a difference between the maximum and minimum RMSE that are considerably large in the opinion of authors, that is, 0.93 m/s and 0.55 m/s, respectively. While to tropical Pacific is smaller, that is 0.65 m/s and 0.04 m/s, respectively. The results show that a simple method to avoid this sampling error is the use of sensors onboard of multiple satellites, preferably, freely access available. The values of the time series statistical parameters calculated in this section are compiled in the Table 5.1.

Table 5.1 - Values of the time series statistical parameters.

	Statistical parameters	Meteorological Buoy Wind speed	Wave Buoy		
			Wind speed	Wind Component U	Wind Component V
Sentinel-1	BIAS	-0.482	1.745	0.559	-0.294
	MAE	2.061	2.51	2.624	2.618
	RMSE	2.654	3.218	3.8	3.389
	(ρ)	0.767	0.67	0.837	0.601
ASCAT	BIAS	2.335	2.083	-0.078	-0.028
	MAE	2.705	2.551	2.774	2.393
	RMSE	3.164	3.102	3.615	3.129
	(ρ)	0.84	0.776	0.896	0.665
ERA5	BIAS	1.643	1.381	1.006	-0.561
	MAE	2.148	2.125	2.507	2.608
	RMSE	2.671	2.69	3.424	3.361
	(ρ)	0.863	0.702	0.859	0.602

6 CONCLUSIONS AND FINAL REMARKS

The lack and difficulties of obtaining *in situ* observations in the Antarctic Peninsula generate a great demand for data to attend the studies of ocean-atmosphere interaction in this region of great importance for the global climate. As the climate and the conditions of the sea make the region practically uninhabitable and hard to access, the remote sensing via satellite and reanalysis became valuable tools to fill this gap. Then, it is important to know and to determine the accuracy of satellite-derived (Sentinel-1 and ASCAT) wind field retrieved from the last level of processing and of reanalysis-derived wind field (ERA5) in the Bransfield Strait region at Antarctic Peninsula, for enhancing regional analyses.

The statistical error analysis showed availability and feasibility of satellite scenes and reanalysis data for comparison against *in situ* measurements, according to previously defined matchup criteria data (Section 3.3). To execute an spatial analysis, at least two sources of data was necessary. Considering the month of November, 2019, there were only nine days where all source of data fitted perfectly in all the comparison criteria (Section 4.1). The days 2019-11-01 and 2019-11-28 were taken as example of analysis, and the results compiled in Table 4.1 showed that when comparing ERA5 with ASCAT, there was a better performance than when comparing ERA5 with Sentinel-1.

Although ERA5 has showed a bias of only 0.024 against Sentinel-1 scene in the analysis of the day 2019-11-01, it was observed that valid ERA5 wind vectors overestimate Sentinel-1 values. On the other hand, in the analysis of the day 2019-11-28 (Subsection 4.1.3), ASCAT had a much better performance against Sentinel-1. Then, in due to expected errors (temporal separation, spatial separation, sampling variability, satellite sensor and algorithm) all sources should be studied with attention in both spatial analysis (made only with satellite-derived data) and *in situ* analysis (made with data from meteorological buoy and wave buoy).

Finally, the present work demonstrated the superior performance of ERA5 in wind speed measurements, and the superior performance of ASCAT for wind direction measurements when compared with meteorological buoy and wave buoy (Table 5.1). Moreover, the statistical measurements obtained for satellite-derived wind fields have showed slightly outside values from the requirements of each satellite mission, respectively, in comparison to *in situ* observations. However, this does not mean that the data is unreliable and should be ignored. Such differences

should be interpreted as an opportunity to reiterate that much more understanding of the regional system is required, as well as support the necessity of more measurements. Hence, when we have observed the performance of accuracy of these results, we also conclude that the data of wind field measurements, obtained by remote sensing via satellite and by ERA5 for Bransfield Strait region at Antarctic Peninsula, cannot be disregarded and have great scientific value, taking into account that accurate sea surface wind speed is an essential parameter for calculating the wind stress and the turbulent heat fluxes as well as mass fluxes (e.g., CO_2 and H_2O), highlighting the great importance of sea surface winds for budgeting energy, moisture and carbon, and for studies of ocean acidification and fish stocks (BOURASSA et al., 2019).

6.1 Contributions

The main contributions of this work are listed below:

a) The usage of state-of-the-art satellites to demonstrate that the remote sensing data and reanalysis data can be useful in cases of absence of data, as well as to overcome the difficulties imposed by the climate and by the conditions of the sea that rule the regions practically uninhabitable and hard to access;

b) To verify of the availability and feasibility of using Sentinel-1, ASCAT and ERA5 to obtain data from wind field measurements, as well as determine the regional and local accuracy of each source against *in situ* data, respectively; and

c) To demonstrate that there are practically no comparisons with buoys in the southern hemisphere, and that there are no regular comparisons with buoys deployed in the Antarctic Peninsula region, in due to the difficulties imposed by absence of a system of buoys.

d) To highlight that such differences between the observations should not be thought of as negative, in fact, such differences should be grabbed as an opportunity to reiterate that much more understanding of the regional system is required, as well as support the necessity of more measurements. Moreover, as explained by Bourassa et al. (2019), for reliable computations of air/sea heat fluxes (sensible and latent heat fluxes) as well as mass fluxes (e.g., CO_2 and H_2O), accurate wind speeds are

needed, resulting in importance of surface winds for budgeting energy, moisture and carbon, and for studies of ocean acidification and fish stocks. Thus, surface wind speed and direction were listed by WMO in the group of essential climate variables which is composed of physical, chemical or biological variables or a group of linked variables that critically contributes to the characterization of Earth' s climate.

6.2 Future works

a) Study of the use of Sentinel-1 data in studies of flux heat and momentum with application of algorithm Coupled Ocean–Atmosphere Response Experiment (COARE) described by Edson et al. (2013);

b) Study of a long term consistent comparison of data obtained by Sentinel-1, ASCAT and/or by another satellite in Future Antarctica Operations; and

c) Study of comparison of satellite-derived and reanalysis-derived wave field data with the same approach.

REFERENCES

ABDALLA, S.; DE CHIARA, G. Estimating random errors of scatterometer, altimeter, and model wind speed data. **IEEE Journal of Selected Topics in Applied Earth Observations and Remote Sensing**, v. 10, n. 5, 2017. ISSN 21511535. Available from: <https://doi.org/10.1109/jstars.2017.2659220>. Access in: 02 jun. 2021. 3, 67

ACEVEDO, O. C.; PEZZI, L. P.; SOUZA, R. B.; ANABOR, V.; DEGRAZIA, G. A. Atmospheric boundary layer adjustment to the synoptic cycle at the Brazil-Malvinas Confluence, South Atlantic Ocean. **Journal of Geophysical Research**, v. 115, n. D22, p. D22107, nov 2010. ISSN 0148-0227. Available from: <http://doi.wiley.com/10.1029/2009JD013785>. Access in: 02 jun. 2021. 1

ALVES, M.; Brito Silveira, R.; Boligon Minuzzi, R.; Elvino Franke, A. The Influence of the Antarctic Oscillation (AAO) on Cold Waves and Occurrence of Frosts in the State of Santa Catarina, Brazil. **Climate**, v. 5, n. 1, p. 17, mar 2017. ISSN 2225-1154. Available from: <http://www.mdpi.com/2225-1154/5/1/17>. Access in: 02 jun. 2021. 1

ARONSEN, M.; LANDMARK, K. **Density mapping of ship traffic**: FFI-RAPPORT 2016/02061. 2016. Available from: <http://hdl.handle.net/20.500.12242/1300>. Access in: 02 jun. 2021. 7

BELMONTE RIVAS, M.; STOFFELEN, A. Characterizing ERA-Interim and ERA5 surface wind biases using ASCAT. **Ocean Science**, v. 15, n. 3, p. 831–852, jun 2019. ISSN 1812-0792. Available from: <https://os.copernicus.org/articles/15/831/2019/>. Access in: 02 jun. 2021. 2

BOURASSA, M. A.; GILLE, S. T.; BITZ, C.; CARLSON, D.; CEROVECKI, I.; CLAYSON, C. A.; CRONIN, M. F.; DRENNAN, W. M.; FAIRALL, C. W.; HOFFMAN, R. N.; MAGNUSDOTTIR, G.; PINKER, R. T.; RENFREW, I. A.; SERREZE, M.; SPEER, K.; TALLEY, L. D.; WICK, G. A. High-Latitude Ocean and Sea Ice Surface Fluxes: Challenges for Climate Research. **Bulletin of the American Meteorological Society**, v. 94, n. 3, p. 403–423, mar 2013. ISSN 0003-0007. Available from: <https://doi.org/10.1175/BAMS-D-11-00244.1>. Access in: 02 jun. 2021. 1

BOURASSA, M. A.; GILLE, S. T.; JACKSON, D. L.; ROBERTS, J. B.; WICK, G. A. Ocean winds and turbulent air-sea fluxes inferred from remote sensing. **Oceanography**, v. 23, n. 4, 2010. ISSN 10428275. Available from: <https://doi.org/10.5670/oceanog.2010.04>. Access in: 02 jun. 2021. 1

BOURASSA, M. A.; HUGHES, P. J. Turbulent Heat Fluxes and Wind Remote Sensing. In: CHASSIGNET, E. P.; PASCUAL, A.; TINTORÉ, J.; VERRON, J. (Ed.). **New Frontiers in Operational Oceanography**. Tallahassee: GODAE OceanView, 2018. p. 245–270. ISBN 1720549974. Available from: <https://dx.doi.org/10.17125/gov2018.ch10>. Access in: 02 jun. 2021. 1

BOURASSA, M. A.; MEISSNER, T.; CEROVECKI, I.; CHANG, P. S.; DONG, X.; De Chiara, G.; DONLON, C.; DUKHOVSKOY, D. S.; ELYA, J.; FORE, A.; FEWINGS, M. R.; FOSTER, R. C.; GILLE, S. T.; HAUS, B. K.; HRISTOVA-VELEVA, S.; HOLBACH, H. M.; JELENAK, Z.; KNAFF, J. A.; KRANZ, S. A.; MANASTER, A.; MAZLOFF, M.; MEARS, C.; MOUCHE, A.; PORTABELLA, M.; REUL, N.; RICCIARDULLI, L.; RODRIGUEZ, E.; SAMPSON, C.; SOLIS, D.; STOFFELEN, A.; STUKEL, M. R.; STILES, B.; WEISSMAN, D.; WENTZ, F. Remotely Sensed Winds and Wind Stresses for Marine Forecasting and Ocean Modeling. **Frontiers in Marine Science**, v. 6, p. 443, aug 2019. ISSN 2296-7745. Available from: <https://doi.org/10.3389/fmars.2019.00443>. Access in: 02 jun. 2021. 1, 4, 74

CAMARGO, R.; TODESCO, E.; PEZZI, L. P.; SOUZA, R. B. de. Modulation mechanisms of marine atmospheric boundary layer at the Brazil-Malvinas Confluence region. **Journal of Geophysical Research: Atmospheres**, v. 118, n. 12, p. 6266–6280, jun 2013. ISSN 2169897X. Available from: <http://doi.wiley.com/10.1002/jgrd.50492>. Access in: 02 jun. 2021. 1

CHELTON, D. B.; RIES, J. C.; HAINES, B. J.; FU, L.-L.; CALLAHAN, P. S. Chapter 1 satellite altimetry. In: FU, L.-L.; CAZENAVE, A. (Ed.). **Satellite altimetry and Earth sciences**. San Diego: Academic Press, 2001, (International Geophysics, v. 69). p. 1–131. ISBN 9780122695452. Available from: <https://www.sciencedirect.com/science/article/pii/S0074614201801467>. Access in: 02 jun. 2021. 17

COHEN, I.; HUANG, Y.; CHEN, J.; BENESTY, J. **Noise reduction in speech processing**. Berlin, Heidelberg: Springer Berlin Heidelberg, 2009. 37 p. (Springer Topics in Signal Processing, v. 2). ISBN 978-3-642-00295-3. Available

from: <http://link.springer.com/10.1007/978-3-642-00296-0>. Access in: 02 jun. 2021. 32

COMBES, V.; MATANO, R. P. Trends in the Brazil/Malvinas Confluence region. **Geophysical Research Letters**, v. 41, n. 24, p. 8971–8977, dec 2014. ISSN 00948276. Available from: <http://doi.wiley.com/10.1002/2014GL062523>. Access in: 02 jun. 2021. 1

CONVEY, P.; BINDSCHADLER, R.; PRISCO, G. di; FAHRBACH, E.; GUTT, J.; HODGSON, D.; MAYEWSKI, P.; SUMMERHAYES, C.; TURNER, J. Antarctic climate change and the environment. **Antarctic Science**, v. 21, n. 6, p. 541–563, dec 2009. ISSN 0954-1020. Available from: <https://www.cambridge.org/core/product/identifier/S0954102009990642/type/journal_article>. Access in: 02 jun. 2021. 2

CURRY, J. A.; BENTAMY, A.; BOURASSA, M. A.; BOURRAS, D.; BRADLEY, E. F.; BRUNKE, M.; CASTRO, S.; CHOU, S. H.; CLAYSON, C. A.; EMERY, W. J.; EYMARD, L.; FAIRALL, C. W.; KUBOTA, M.; LIN, B.; PERRIE, W.; REEDER, R. A.; RENFREW, I. A.; ROSSOW, W. B.; SCHULZ, J.; SMITH, S. R.; WEBSTER, P. J.; WICK, G. A.; ZENG, X. SEAFLUX. **Bulletin of the American Meteorological Society**, v. 85, n. 3, p. 409–424, mar 2004. ISSN 0003-0007. Available from: <https://doi.org/10.1175/BAMS-85-3-409>. Access in: 02 jun. 2021. 1

DOBSON, E.; MONALDO, F.; GOLDHIRSH, J.; WILKERSON, J. Validation of Geosat altimeter-derived wind speeds and significant wave heights using buoy data. **Journal of Geophysical Research**, v. 92, n. C10, p. 10719, 1987. ISSN 0148-0227. Available from: <http://doi.wiley.com/10.1029/JC092iC10p10719>. Access in: 02 jun. 2021. 30

DONG, X.; WANG, Y.; HOU, S.; DING, M.; YIN, B.; ZHANG, Y. Robustness of the Recent Global Atmospheric Reanalyses for Antarctic Near-Surface Wind Speed Climatology. **Journal of Climate**, v. 33, n. 10, p. 4027–4043, may 2020. ISSN 0894-8755. Available from: <https://doi.org/10.1175/JCLI-D-19-0648.1>. Access in: 02 jun. 2021. 2, 3

EDSON, J. B.; JAMPANA, V.; WELLER, R. A.; BIGORRE, S. P.; PLUEDDEMANN, A. J.; FAIRALL, C. W.; MILLER, S. D.; MAHRT, L.; VICKERS, D.; HERSBACH, H. On the Exchange of Momentum over the Open Ocean.

Journal of Physical Oceanography, v. 43, n. 8, p. 1589–1610, aug 2013. ISSN 0022-3670. Available from: <https://doi.org/10.1175/JPO-D-12-0173.1>. Access in: 02 jun. 2021. 75

ELACHI, C.; ZYL, J. van. **Introduction to the physics and techniques of remote sensing**. 3. ed. Hoboken: Wiley, 2021. 534 p. ISBN 9781119523048. Available from: <https://onlinelibrary.wiley.com/doi/book/10.1002/9781119523048>. Access in: 02 jun. 2021. 7, 9

EMERY, W.; CAMPS, A. **Introduction to satellite remote sensing: atmosphere, ocean, cryosphere and land applications**. Amsterdam: Elsevier, 2017. 860 p. ISBN 9780128092545. Available from: <https://doi.org/10.1016/C2015-0-04517-8>. Access in: 02 jun. 2021. 9, 17

EUROPEAN ORGANISATION FOR THE EXPLOITATION OF METEOROLOGICAL SATELLITES (EUMETSAT). **ASCAT user guide**. jan. 2017. 164 p. Available from: <https://www.eumetsat.int/media/45987>. Access in: 02 jun. 2021. 23, 24

EUROPEAN SPACE AGENCY (ESA). **Copernicus: Sentinel-1 - Satellite Missions - eoPortal Directory**. 2019. Available from: <https://earth.esa.int/web/eoportal/satellite-missions/c-missions/copernicus-sentinel-1>. Access in: 02 jun. 2021. 19, 20

____. **Ocean wind field component - Sentinel-1 SAR technical guide**. 2019. Available from: <https://sentinels.copernicus.eu/web/sentinel/ocean-wind-field-component>. Access in: 02 jun. 2021. 21, 59

____. **Sentinel-1 - data products - Sentinel Online**. 2019. Available from: <https://sentinel.esa.int/web/sentinel/missions/sentinel-1/data-products>. Access in: 02 jun. 2021. 21, 22

____. **Sentinel-1- observation scenario - planned acquisitions - ESA**. 2019. Available from: <https://sentinel.esa.int/web/sentinel/missions/sentinel-1/observation-scenario>. Access in: 02 jun. 2021. 21, 22

____. **User guides - Sentinel-1 SAR - acquisition modes - Sentinel Online**. 2019. Available from: <https://sentinel.esa.int/web/sentinel/

user-guides/sentinel-1-sar/acquisition-modes>. Access in: 02 jun. 2021. 20

____. **User guides - Sentinel-1 SAR - mapping of applications to Sentinel-1 Modes - Sentinel Online**. 2019. Available from: <https://sentinel.esa.int/web/sentinel/user-guides/sentinel-1-sar/applications/mapping-applications-s1-modes>. Access in: 02 jun. 2021. 19

____. **CMEMS buoy-based in-situ wave coverage**. 2020. Available from: <https://sentinels.copernicus.eu/web/success-stories/-/cmems-buoy-based-in-situ-wave-coverage>. Access in: 02 jun. 2021. 5

____. **Validation - Sentinel-1 SAR technical guide**. 2020. Available from: <https://sentinels.copernicus.eu/web/sentinel/technical-guides/sentinel-1-sar/cal-val-activities/validation>. Access in: 02 jun. 2021. 4

FUREVIK, B.; KORSBAKKEN, E. Comparison of derived wind speed from synthetic aperture radar and scatterometer during the ERS tandem phase. **IEEE Transactions on Geoscience and Remote Sensing**, v. 38, n. 2, p. 1113–1121, mar 2000. ISSN 01962892. Available from: <https://doi.org/10.1109/36.841990>. Access in: 02 jun. 2021. 3

GILHOUSEN, D. B. The Value of NDBC Observations during March 1993's "Storm of the Century". **Weather and Forecasting**, v. 9, n. 2, p. 255–264, jun 1994. ISSN 0882-8156. Available from: <http://journals.ametsoc.org/doi/10.1175/1520-0434(1994)009%3C0255:TVONOD%3E2.0.CO;2>. Access in: 02 jun. 2021. 2

GOWER, J. F. R. Intercalibration of wave and wind data from TOPEX/POSEIDON and moored buoys off the west coast of Canada. **Journal of Geophysical Research: Oceans**, v. 101, n. C2, p. 3817–3829, feb 1996. ISSN 01480227. Available from: <http://doi.wiley.com/10.1029/95JC03281>. Access in: 02 jun. 2021. 30

GRIECO, A. G.; PORTABELLA, M.; VOGELZANG, J.; VERHOEF, A.; STOFFELEN, A. **Initial development of pencil-beam scatterometer coastal processing**: visiting scientisc activity, technical report OSI_VS20_01. oct 2020. Available from: <https://osi-saf.eumetsat.int/sites/osi-saf.eumetsat.int/files/inline-files/OSI_VSA20_01_report_PenWP_coastal.pdf>. Access in: 02 jun. 2021. 29

HACKEROTT, J. A.; PEZZI, L. P.; BAKHODAY PASKYABI, M.; OLIVEIRA, A. P.; REUDER, J.; SOUZA, R. B. de; CAMARGO, R. de. The role of roughness and stability on the momentum flux in the marine atmospheric surface layer: a study on the southwestern Atlantic Ocean. **Journal of Geophysical Research: Atmospheres**, v. 123, n. 8, p. 3914–3932, apr 2018. ISSN 2169897X. Available from: <http://doi.wiley.com/10.1002/2017JD027994>. Access in: 02 jun. 2021. 1

HANSOM, J. D.; GORDON, J. E. **Antarctic Environments and Resources**. London: Routledge, 2014. 416 p. ISBN 9781315845166. Available from: <https://doi.org/10.4324/9781315845166>. Access in: 02 jun. 2021. 2

HASAGER, C. B.; HAHMANN, A. N.; AHSBAHS, T.; KARAGALI, I.; SILE, T.; BADGER, M.; MANN, J. Europe's offshore winds assessed with synthetic aperture radar, ASCAT and WRF. **Wind Energy Science**, v. 5, n. 1, p. 375–390, mar 2020. ISSN 2366-7451. Available from: <https://wes.copernicus.org/articles/5/375/2020/>. Access in: 02 jun. 2021. 30

HERSBACH, H. **CMOD5.N: A C-band geophysical model function for equivalent neutral wind.** ECMWF, 2008. 20 p. Available from: <https://www.ecmwf.int/node/9873>. Access in: 02 jun. 2021. 18

HOLTHUIJSEN, L. H. **Waves in oceanic and coastal waters**. Cambridge: Cambridge University Press, 2007. 387 p. ISBN 9780511618536. Available from: <http://ebooks.cambridge.org/ref/id/CBO9780511618536>. Access in: 02 jun. 2021. 17

HSU, S. A.; MEINDL, E. A.; GILHOUSEN, D. B. Determining the power-law wind-profile exponent under near-neutral stability conditions at sea. **Journal of Applied Meteorology**, v. 33, n. 6, p. 757–765, jun 1994. ISSN 0894-8763. Available from: <http://journals.ametsoc.org/doi/10.1175/1520-0450(1994)033%3C0757:DTPLWP%3E2.0.CO;2>. Access in: 02 jun. 2021. 29

HUTCHINGS, N.; KILPATRICK, T.; LONG, D. G. Ultrahigh resolution scatterometer winds near Hawaii. **Remote Sensing**, v. 12, n. 3, p. 564, feb 2020. ISSN 2072-4292. Available from: <https://www.mdpi.com/2072-4292/12/3/564>. Access in: 02 jun. 2021. 3, 29

JANG, J.-C.; PARK, K.-A.; MOUCHE, A. A.; CHAPRON, B.; LEE, J.-H. Validation of Sea Surface Wind From Sentinel-1A/B SAR Data in the Coastal Regions of the Korean Peninsula. **IEEE Journal of Selected Topics in Applied Earth Observations and Remote Sensing**, v. 12, n. 7, p. 2513–2529, jul 2019. ISSN 1939-1404. Available from: <https://doi.org/10.1109/JSTARS.2019.2911127>. Access in: 02 jun. 2021. 3

JONES, R. W.; RENFREW, I. A.; ORR, A.; WEBBER, B. G. M.; HOLLAND, D. M.; LAZZARA, M. A. Evaluation of four global reanalysis products using in situ observations in the Amundsen Sea Embayment, Antarctica. **Journal of Geophysical Research: Atmospheres**, v. 121, n. 11, p. 6240–6257, jun 2016. ISSN 2169897X. Available from: <http://doi.wiley.com/10.1002/2015JD024680>. Access in: 02 jun. 2021. 2

KAKO, S.; ISOBE, A.; KUBOTA, M. High-resolution ASCAT wind vector data set gridded by applying an optimum interpolation method to the global ocean. **Journal of Geophysical Research Atmospheres**, v. 116, n. 23, 2011. ISSN 01480227. Available from: <https://doi.org/10.1029/2010JD015484>. Access in: 02 jun. 2021. 54

KILPATRICK, T.; XIE, S.; TOKINAGA, H.; LONG, D.; HUTCHINGS, N. Systematic scatterometer wind errors near coastal mountains. **Earth and Space Science**, v. 6, n. 10, p. 1900–1914, oct 2019. ISSN 2333-5084. Available from: <https://onlinelibrary.wiley.com/doi/abs/10.1029/2019EA000757>. Access in: 02 jun. 2021. 29

KIRCHHOFF, V.; SCHUCH, N.; PINHEIRO, D.; HARRIS, J. M. Evidence for an ozone hole perturbation at 30° South. **Atmospheric Environment**, v. 30, n. 9, p. 1481–1488, jan 1996. ISSN 13522310. Available from: <https://linkinghub.elsevier.com/retrieve/pii/1352231095003622>. Access in: 02 jun. 2021. 1

KNOTT, E. F.; SHAEFFER, J. F.; TULEY, M. T. **Radar Cross Section**. 2. ed. Raleigh: SciTech Publishing, 2004. 626 p. ISBN 9781891121258. Available from: <https://doi.org/10.1049/SBRA026E>. Access in: 02 jun. 2021. 11, 12, 13

KORSBAKKEN, E.; JOHANNESSEN, J. A.; JOHANNESSEN, O. M. Coastal wind field retrievals from ERS synthetic aperture radar images. **Journal of Geophysical Research: Oceans**, v. 103, n. C4, p. 7857–7874, apr 1998. ISSN 01480227. Available from: <https://doi.org/10.1029/97JC02580>. Access in: 02 jun. 2021. 3

LABORATORY OF OCEAN AND ATMOSPHERE STUDIES (LOA) OF BRAZILIAN NATIONAL INSTITUTE FOR SPACE RESEARCH (INPE). **Antarctic Modeling Observation System (ATMOS)**. 2021. Available from: <https://loa-inpe.github.io/atmos.html>. Access in: 02 jun. 2021. 28

LANDWEHR, S.; THURNHERR, I.; CASSAR, N.; GYSEL-BEER, M.; SCHMALE, J. Using global reanalysis data to quantify and correct airflow distortion bias in shipborne wind speed measurements. **Atmospheric Measurement Techniques**, v. 13, n. 6, p. 3487–3506, jun 2020. ISSN 1867-8548. Available from: <https://amt.copernicus.org/articles/13/3487/2020/>. Access in: 02 jun. 2021. 2

LI, M.; LIU, J.; WANG, Z.; WANG, H.; ZHANG, Z.; ZHANG, L.; YANG, Q. Assessment of sea surface wind from NWP reanalyses and satellites in the Southern Ocean. **Journal of Atmospheric and Oceanic Technology**, v. 30, n. 8, p. 1842–1853, 2013. ISSN 07390572. Available from: <https://doi.org/10.1175/JTECH-D-12-00240.1>. Access in: 02 jun. 2021. 1, 2

LINDSLEY, R. D.; BLODGETT, J. R.; LONG, D. G. Analysis and validation of high-resolution wind from ASCAT. **IEEE Transactions on Geoscience and Remote Sensing**, v. 54, n. 10, p. 5699–5711, 2016. ISSN 01962892. Available from: <https://ieeexplore.ieee.org/document/7486106>. Access in: 02 jun. 2021. 29

LORENZZETTI, J. A. **Princípios físicos de sensoriamento remoto**. São Paulo: Blucher, 2015. 292 p. ISBN 978-85-212-0835-8. Available from: <https://www.blucher.com.br/livro/detalhes/principios-fisicos-de-sensoriamento-remoto-1053>. Access in: 02 jun. 2021. 7, 9

LYGRE, A.; KROGSTAD, H. E. Maximum Entropy Estimation of the Directional Distribution in Ocean Wave Spectra. **Journal of Physical Oceanography**, American Meteorological Society, v. 16, n. 12, p. 2052–2060, dec 1986. ISSN 0022-3670. Available from: <https://doi.org/10.1175/1520-0485(1986)016%3C2052:MEEOTD%3E2.0.CO;2>. Access in: 02 jun. 2021. 25

MARINHA DO BRASIL (MB). **AIS - Automatic Identification System | CISMAR**. 2021. Available from: <https://www.marinha.mil.br/cismar/?q=ais>. Access in: 02 jun. 2021. 7

____. **Programa Antártico Brasileiro | SECIRM**. 2021. Available from: <https://www.marinha.mil.br/secirm/proantar/sobre>. Access in: 02 jun. 2021. 1

MAYEWSKI, P. A.; MEREDITH, M. P.; SUMMERHAYES, C. P.; TURNER, J.; WORBY, A.; BARRETT, P. J.; CASASSA, G.; BERTLER, N. A. N.; BRACEGIRDLE, T.; Naveira Garabato, A. C.; BROMWICH, D.; CAMPBELL, H.; HAMILTON, G. S.; LYONS, W. B.; MAASCH, K. A.; AOKI, S.; XIAO, C.; OMMEN, T. van. State of the Antarctic and Southern Ocean climate system. **Reviews of Geophysics**, v. 47, n. 1, p. RG1003, jan 2009. ISSN 8755-1209. Available from: <http://doi.wiley.com/10.1029/2007RG000231>. Access in: 02 jun. 2021. 2

MEINDL, A. **Guide to moored buoys and other ocean data acquisition systems**: DBCP technical document no. 8. Geneva: WMO & IOC Data Buoy Cooperation Panel, 1996. 40 p. ISBN OCLC:1016991866. Available from: <https://library.wmo.int/doc_num.php?explnum_id=7053>. Access in: 02 jun. 2021. 28

MEISSNER, T.; WENTZ, F. J. Wind-vector retrievals under rain with passive satellite microwave radiometers. **IEEE Transactions on Geoscience and Remote Sensing**, v. 47, n. 9, p. 3065–3083, sep 2009. ISSN 0196-2892. Available from: <http://ieeexplore.ieee.org/document/5196732/>. 17

____. The emissivity of the ocean surface between 6 and 90 GHz over a large range of wind speeds and Earth incidence angles. **IEEE Transactions on Geoscience and Remote Sensing**, v. 50, n. 8, p. 3004–3026, aug 2012. ISSN 0196-2892. Available from: <http://ieeexplore.ieee.org/document/6145646/>. Access in: 02 jun. 2021. 17

MONALDO, F. Expected differences between buoy and radar altimeter estimates of wind speed and significant wave height and their implications on buoy-altimeter comparisons. **Journal of Geophysical Research**, v. 93, n. C3, p. 2285, 1988. ISSN 0148-0227. Available from: <http://doi.wiley.com/10.1029/JC093iC03p02285>. Access in: 02 jun. 2021. 30

OCEAN AND SEA ICE SATELLITE APPLICATION FACILITY (OSI SAF). **ASCAT L2 winds data record validation report**. jul. 2016. 20 p. Available from: <https:

//scatterometer.knmi.nl/publications/pdf/ascat_a_cdr_validation.pdf>. Access in: 02 jun. 2021. 5

____. **Algorithm theoretical basis document for the OSI SAF wind products**. may 2018. 22 p. Available from: <https://scatterometer.knmi.nl/old_manuals/osisaf_cdop2_ss3_atbd_1.6.pdf>. Access in: 02 jun. 2021. 24

____. **ASCAT wind validation report**. may 2018. 12 p. Available from: <https://scatterometer.knmi.nl/publications/pdf/ascat_validation.pdf>. Access in: 02 jun. 2021. 5, 6, 24

____. **EUMETSAT advanced retransmission service ASCAT wind product user manual**. oct. 2019. 13 p. Available from: <https://scatterometer.knmi.nl/publications/pdf/ASCAT_Product_Manual.pdf>. Access in: 02 jun. 2021. 23, 24, 54, 59, 67

OWEN, M.; LONG, D. Land-contamination compensation for QuikSCAT near-coastal wind retrieval. **IEEE Transactions on Geoscience and Remote Sensing**, v. 47, n. 3, p. 839–850, mar 2009. ISSN 0196-2892. Available from: <http://ieeexplore.ieee.org/document/4785190/>. Access in: 02 jun. 2021. 29, 67

PEARMAN, D.; HERBERS, T.; JANSSEN, T.; ETTINGER, H. van; MCINTYRE, S.; JESSEN, P. Drifter observations of the effects of shoals and tidal-currents on wave evolution in San Francisco Bight. **Continental Shelf Research**, Elsevier Ltd, v. 91, p. 109–119, dec 2014. ISSN 02784343. Available from: <https://linkinghub.elsevier.com/retrieve/pii/S0278434314002738>. Access in: 02 jun. 2021. 26

PECK, R.; DEVORE, J. **Statistics: the exploration & analysis of data**. 7. ed. Boston: Cengage Learning, 2011. 213 p. ISBN 978-0-8400-5801-0. 32

PEZZI, L. P.; SOUZA, R. B.; DOURADO, M. S.; GARCIA, C. A. E.; MATA, M. M.; SILVA-DIAS, M. A. F. Ocean-atmosphere in situ observations at the Brazil-Malvinas Confluence region. **Geophysical Research Letters**, v. 32, n. 22, nov 2005. ISSN 00948276. Available from: <http://doi.wiley.com/10.1029/2005GL023866>. Access in: 02 jun. 2021. 1

PEZZI, L. P.; SOUZA, R. B. de; ACEVEDO, O.; WAINER, I.; MATA, M. M.; GARCIA, C. A. E.; CAMARGO, R. de. Multiyear measurements of the oceanic

and atmospheric boundary layers at the Brazil-Malvinas confluence region. **Journal of Geophysical Research**, v. 114, n. D19, p. D19103, oct 2009. ISSN 0148-0227. Available from: <http://doi.wiley.com/10.1029/2008JD011379>. Access in: 02 jun. 2021. 1

PEZZI, L. P.; SOUZA, R. B. de; SANTINI, M. F.; MILLER, A. J.; CARVALHO, J. T.; PARISE, C. K.; QUADRO, M. F.; ROSA, E. B.; JUSTINO, F.; SUTIL, U. A.; CABRERA, M. J.; BABANIN, A. V.; VOERMANS, J.; NASCIMENTO, E. L.; ALVES, R. C. M.; MUNCHOW, G. B.; RUBERT, J. Oceanic eddy-induced modifications to air–sea heat and CO2 fluxes in the Brazil-Malvinas Confluence. **Scientific Reports**, v. 11, n. 1, p. 10648, dec 2021. ISSN 2045-2322. Available from: <http://www.nature.com/articles/s41598-021-89985-9>. Access in: 02 jun. 2021. 1

PHILLIPS, O. M. Spectral and statistical properties of the equilibrium range in wind-generated gravity waves. **Journal of Fluid Mechanics**, v. 156, n. -1, p. 505, jul 1985. ISSN 0022-1120. Available from: <https://doi.org/10.1017/S0022112085002221>. Access in: 02 jun. 2021. 25

PINHEIRO, D. K.; LEME, N. P.; PERES, L. V.; KALL, E. Influence of the Antarctic Ozone Hole over the South of Brazil in 2008 and 2009. **INCT-APA Annual Activity Report**, p. 33–37, 2010. ISSN 2177-918X. Available from: <http://dx.doi.org/10.4322/apa.2014.020>. Access in: 02 jun. 2021. 1

QUEFFEULOU, P. Validation of ENVISAT RA-2 and JASON-1 altimeter wind and wave measurements. In: 2003 IEEE INTERNATIONAL GEOSCIENCE AND REMOTE SENSING SYMPOSIUM (IGARSS), IEEE Cat. No.03CH37477., 2003, Toulouse, France. **Proceedings...** Piscataway, New Jersey: IEEE, 2003. v. 5, p. 2987–2989. ISBN 0-7803-7929-2. Available from: <http://ieeexplore.ieee.org/document/1294656/>. Access in: 02 jun. 2021. 29

_____. Long-term validation of wave height measurements from altimeters. **Marine Geodesy**, v. 27, n. 3-4, p. 495–510, jul 2004. ISSN 0149-0419. Available from: <http://www.tandfonline.com/doi/abs/10.1080/01490410490883478>. Access in: 02 jun. 2021. 17, 30

QUEFFEULOU, P.; BENTAMY, A.; GUYADER, J. Satellite wave height validation over the Mediterranean Sea. **European Space Agency, (Special Publication) ESA SP**, v. 2004, n. 572, p. 1247–1251, 2005. ISSN 03796566. Available from:

<http://citeseerx.ist.psu.edu/viewdoc/download?doi=10.1.1.380.6467&rep=rep1&type=pdf>. Access in: 02 jun. 2021. 25

RAGHUKUMAR, K.; CHANG, G.; SPADA, F.; JONES, C.; JANSSEN, T.; GANS, A. Performance characteristics of "Spotter," a newly developed real-time wave measurement buoy. **Journal of Atmospheric and Oceanic Technology**, v. 36, n. 6, p. 1127–1141, jun 2019. ISSN 0739-0572. Available from: <https://journals.ametsoc.org/view/journals/atot/36/6/jtech-d-18-0151.1.xml>. Access in: 02 jun. 2021. 29

RANA, F. M.; ADAMO, M.; LUCAS, R.; BLONDA, P. Sea surface wind retrieval in coastal areas by means of Sentinel-1 and numerical weather prediction model data. **Remote Sensing of Environment**, v. 225, p. 379–391, may 2019. ISSN 00344257. Available from: <https://doi.org/10.1016/j.rse.2019.03.019>. Access in: 02 jun. 2021. 3

RIBAL, A.; YOUNG, I. R. 33 years of globally calibrated wave height and wind speed data based on altimeter observations. **Scientific Data**, v. 6, n. 1, 2019. ISSN 20524463. Available from: <https://www.nature.com/articles/s41597-019-0083-9/>. Access in: 02 jun. 2021. 25, 29, 30, 31, 32

RICHARDS, M. A.; SCHEER, J. A.; HOLM, W. A. **Principles of modern radar: basic principles**. Edison: SciTech Publishing, 2010. 962 p. ISBN 9781891121524. Available from: <https://doi.org/10.1049/SBRA021E>. Access in: 02 jun. 2021. 7, 9, 10, 11, 12, 14, 15, 16

SANTINI, M. F.; SOUZA, R. B.; PEZZI, L. P.; SWART, S. Observations of air–sea heat fluxes in the southwestern Atlantic under high-frequency ocean and atmospheric perturbations. **Quarterly Journal of the Royal Meteorological Society**, v. 146, n. 733, p. 4226–4251, sep 2020. ISSN 1477870X. Available from: <https://doi.org/10.1002/qj.3905>. Access in: 02 jun. 2021. 1

SCHMIDT, K. M.; SWART, S.; REASON, C.; NICHOLSON, S.-A. Evaluation of satellite and reanalysis wind products with in situ wave glider wind observations in the Southern Ocean. **Journal of Atmospheric and Oceanic Technology**, v. 34, n. 12, p. 2551–2568, dec 2017. ISSN 0739-0572. Available from: <https://journals.ametsoc.org/view/journals/atot/34/12/jtech-d-17-0079.1.xml>. Access in: 02 jun. 2021. 2

SREELAKSHMI, S.; BHASKARAN, P. K. Spatio-temporal distribution and variability of high threshold wind speed and significant wave height for the Indian Ocean. **Pure and Applied Geophysics**, v. 177, n. 9, p. 4559–4575, sep 2020. ISSN 0033-4553. Available from: <http://link.springer.com/10.1007/s00024-020-02462-8>. Access in: 02 jun. 2021. 29

STOPA, J. E.; CHEUNG, K. F. Intercomparison of wind and wave data from the ECMWF Reanalysis Interim and the NCEP Climate Forecast System Reanalysis. **Ocean Modelling**, v. 75, p. 65–83, mar 2014. ISSN 14635003. Available from: <https://linkinghub.elsevier.com/retrieve/pii/S1463500313002205>. Access in: 02 jun. 2021. 2

THOMPSON, D. W. J.; SOLOMON, S.; KUSHNER, P. J.; ENGLAND, M. H.; GRISE, K. M.; KAROLY, D. J. Signatures of the Antarctic ozone hole in Southern Hemisphere surface climate change. **Nature Geoscience**, v. 4, n. 11, p. 741–749, nov 2011. ISSN 1752-0894. Available from: <http://www.nature.com/articles/ngeo1296>. Access in: 02 jun. 2021. 2

THOMSON, J.; D'ASARO, E. A.; CRONIN, M. F.; ROGERS, W. E.; HARCOURT, R. R.; SHCHERBINA, A. Waves and the equilibrium range at Ocean Weather Station P. **Journal of Geophysical Research: Oceans**, v. 118, n. 11, p. 5951–5962, nov 2013. ISSN 21699275. Available from: <http://doi.wiley.com/10.1002/2013JC008837>. Access in: 02 jun. 2021. 26

TOMITA, H.; KUBOTA, M. Sampling error of daily mean surface wind speed and air specific humidity due to Sun-synchronous satellite sampling and its reduction by multi-satellite sampling. **International Journal of Remote Sensing**, v. 32, n. 12, p. 3389–3404, jun 2011. ISSN 0143-1161. Available from: <https://www.tandfonline.com/doi/full/10.1080/01431161003749428>. Access in: 02 jun. 2021. 3, 29, 71

ULABY, F.; LONG, D. **Microwave radar and radiometric remote sensing**. Ann Arbor: University of Michigan Press, 2014. 1013 p. ISBN 9780472119356. Available from: <http://mrs.eecs.umich.edu/>. Access in: 02 jun. 2021. 8, 9, 11, 12, 13, 14, 15, 17, 18

VENKATESAN, R.; RAMESH, K.; KISHOR, A.; VEDACHALAM, N.; ATMANAND, M. A. Best practices for the ocean moored observatories. **Frontiers in Marine**

Science, v. 5, dec 2018. ISSN 2296-7745. Available from: <https://www.frontiersin.org/article/10.3389/fmars.2018.00469/full>. Access in: 02 jun. 2021. 2, 28

VOERMANS, J. J.; BABANIN, A. V.; KIREZCI, C.; CARVALHO, J. T.; SANTINI, M. F.; PAVANI, B. F.; PEZZI, L. P. Wave anomaly detection in wave measurements. **Journal of Atmospheric and Oceanic Technology**, v. 38, n. 3, p. 525–536, mar 2021. ISSN 0739-0572. Available from: <https://journals.ametsoc.org/view/journals/atot/38/3/JTECH-D-20-0090.1.xml>. Access in: 02 jun. 2021. 1, 2, 25, 28

VOERMANS, J. J.; SMIT, P. B.; JANSSEN, T. T.; BABANIN, A. V. Estimating wind speed and direction using wave spectra. **Journal of Geophysical Research: Oceans**, v. 125, n. 2, feb 2020. ISSN 2169-9275. Available from: <https://onlinelibrary.wiley.com/doi/10.1029/2019JC015717>. Access in: 02 jun. 2021. 29

WALTHER, B. A.; MOORE, J. L. The concepts of bias, precision and accuracy, and their use in testing the performance of species richness estimators, with a literature review of estimator performance. **Ecography**, v. 28, n. 6, p. 815–829, 2005. ISSN 09067590. Available from: <https://onlinelibrary.wiley.com/doi/epdf/10.1111/j.2005.0906-7590.04112.x>. Access in: 02 jun. 2021. 31, 32

WEI, S.; YANG, S.; XU, D. On accuracy of SAR wind speed retrieval in coastal area. **Applied Ocean Research**, v. 95, p. 102012, feb 2020. ISSN 01411187. Available from: <https://linkinghub.elsevier.com/retrieve/pii/S0141118719302469>. Access in: 02 jun. 2021. 29, 67

WHITE, W. B.; PETERSON, R. G. An Antarctic circumpolar wave in surface pressure, wind, temperature and sea-ice extent. **Nature**, v. 380, n. 6576, p. 699–702, apr 1996. ISSN 0028-0836. Available from: <http://www.nature.com/articles/380699a0>. Access in: 02 jun. 2021. 2

WILKS, D. S. **Statistical methods in the atmospheric sciences**. 4. ed. Amsterdam: Elsevier, 2019. 818 p. ISBN 9780128158234. Available from: <https://linkinghub.elsevier.com/retrieve/pii/C20170039216>. Access in: 02 jun. 2021. 32

WOODHOUSE, I. H. **Introduction to microwave remote sensing**. Boca Raton: CRC Press, 2017. 400 p. ISBN 9781315272573. Available from: <https://www.taylorfrancis.com/books/9781351989015>. Access in: 02 jun. 2021. 9, 13, 17

WU, L.; XU, Y.; WANG, Q.; WANG, F.; XU, Z. Mapping global shipping density from AIS data. **Journal of Navigation**, v. 70, n. 1, p. 67–81, jan 2017. ISSN 14697785. Available from: <https://doi.org/10.1017/S0373463316000345>. Access in: 02 jun. 2021. 7

YANG, X.; LI, X.; ZHENG, Q.; GU, X.; PICHEL, W. G.; LI, Z. Comparison of Ocean-Surface Winds Retrieved From QuikSCAT Scatterometer and Radarsat-1 SAR in Offshore Waters of the U.S. West Coast. **IEEE Geoscience and Remote Sensing Letters**, v. 8, n. 1, p. 163–167, jan 2011. ISSN 1545-598X. Available from: <https://doi.org/10.1109/LGRS.2010.2053345>. Access in: 02 jun. 2021. 3

YOUNG, I.; DONELAN, M. On the determination of global ocean wind and wave climate from satellite observations. **Remote Sensing of Environment**, v. 215, p. 228–241, sep 2018. ISSN 00344257. Available from: <https://linkinghub.elsevier.com/retrieve/pii/S0034425718302840>. Access in: 02 jun. 2021. 2

YOUNG, I. R.; SANINA, E.; BABANIN, A. V. Calibration and cross validation of a global wind and wave database of altimeter, radiometer, and scatterometer measurements. **Journal of Atmospheric and Oceanic Technology**, v. 34, n. 6, p. 1285–1306, 2017. ISSN 15200426. Available from: <https://doi.org/10.1175/JTECH-D-16-0145.1>. Access in: 02 jun. 2021. 16, 17, 18, 25, 29, 30

ZHANG, L.; SHI, H.; WANG, Z.; YU, H.; YIN, X.; LIAO, Q. Comparison of wind speeds from spaceborne microwave radiometers with in situ observations and ECMWF data over the global ocean. **Remote Sensing**, v. 10, n. 3, p. 425, mar 2018. ISSN 2072-4292. Available from: <http://www.mdpi.com/2072-4292/10/3/425>. Access in: 02 jun. 2021. 2

ZIEGER, S.; BABANIN, A.; YOUNG, I. Changes in ocean surface wind with a focus on trends in regional and monthly mean values. **Deep Sea Research Part I: Oceanographic Research Papers**, v. 86, p. 56–67, apr 2014. ISSN 09670637. Available from:

<https://linkinghub.elsevier.com/retrieve/pii/S0967063714000089>. Access in: 02 jun. 2021. 17

ZIEGER, S.; VINOTH, J.; YOUNG, I. R. Joint calibration of multiplatform altimeter measurements of wind speed and wave height over the past 20 years. **Journal of Atmospheric and Oceanic Technology**, v. 26, n. 12, p. 2549–2564, dec 2009. ISSN 1520-0426. Available from: <http://journals.ametsoc.org/doi/10.1175/2009JTECHA1303.1>. Access in: 02 jun. 2021. 17, 30

APPENDIX A - GRAPHICS OF SPATIAL ANALYSIS

Figure A.1 - Plotting of wind field from date 2019-11-05 23:51:01Z.

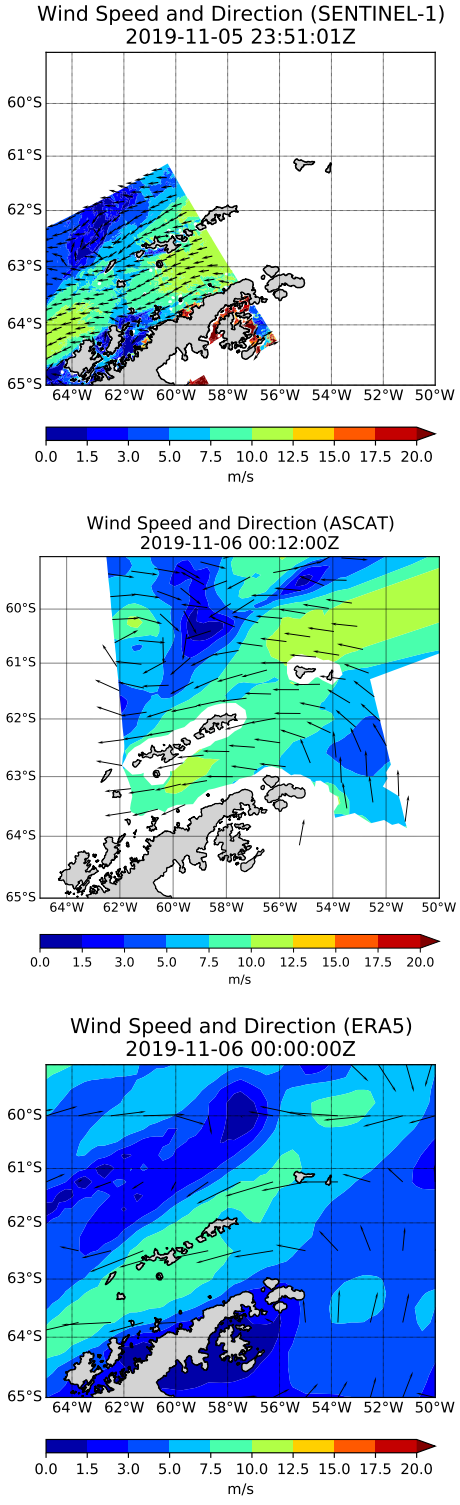

SOURCE: Author's production.

Figure A.2 - Plotting of statistical parameters from date 2019-11-05 23:51:01Z.

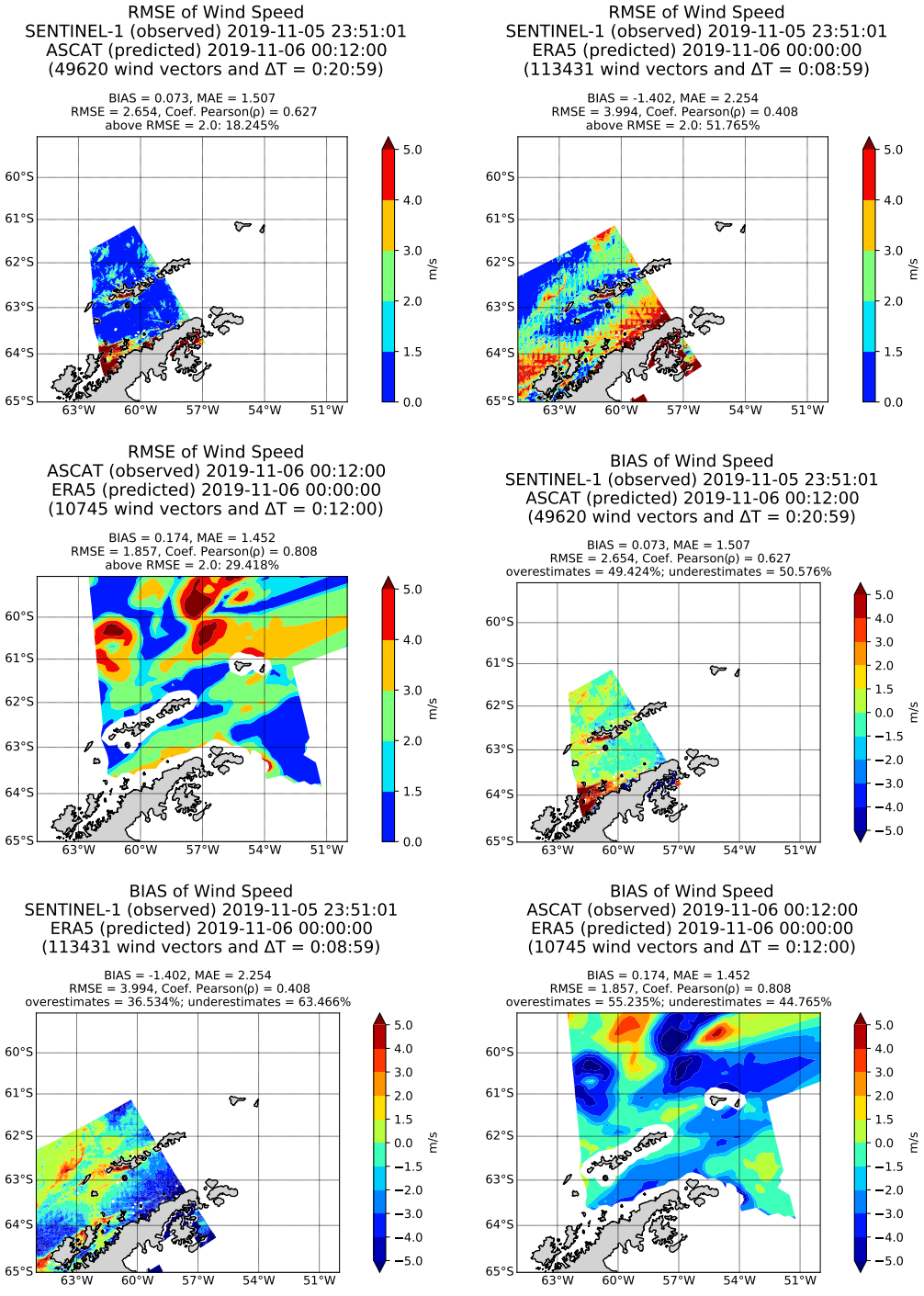

SOURCE: Author's production.

Figure A.3 - Plotting of wind field from date 2019-11-16 23:10:28Z.

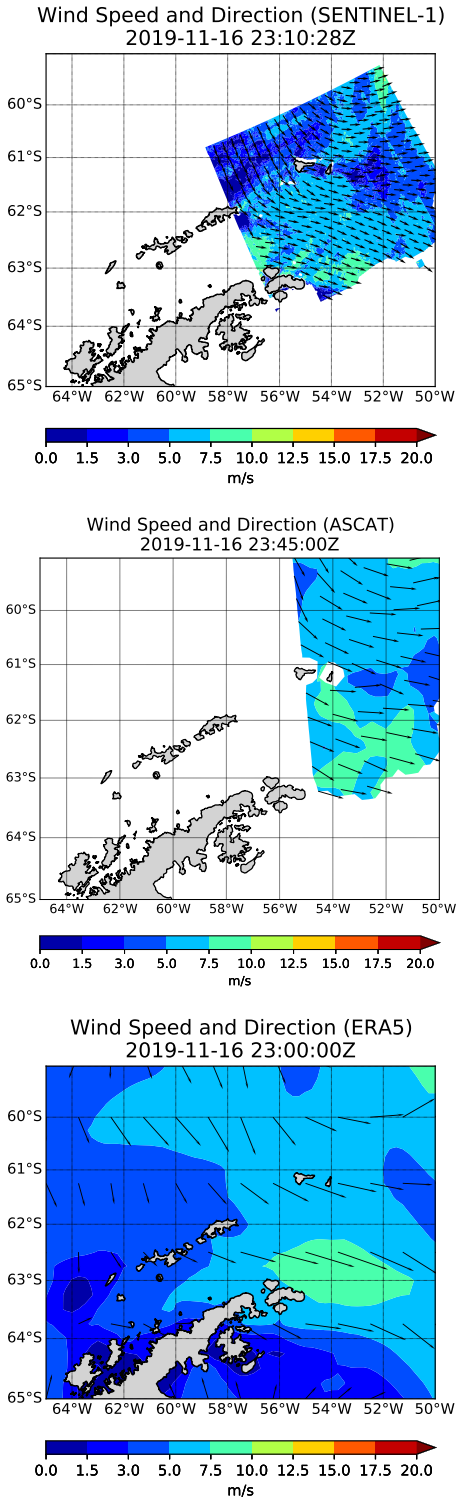

SOURCE: Author's production.

Figure A.4 - Plotting of statistical parameters from date 2019-11-16 23:10:28Z.

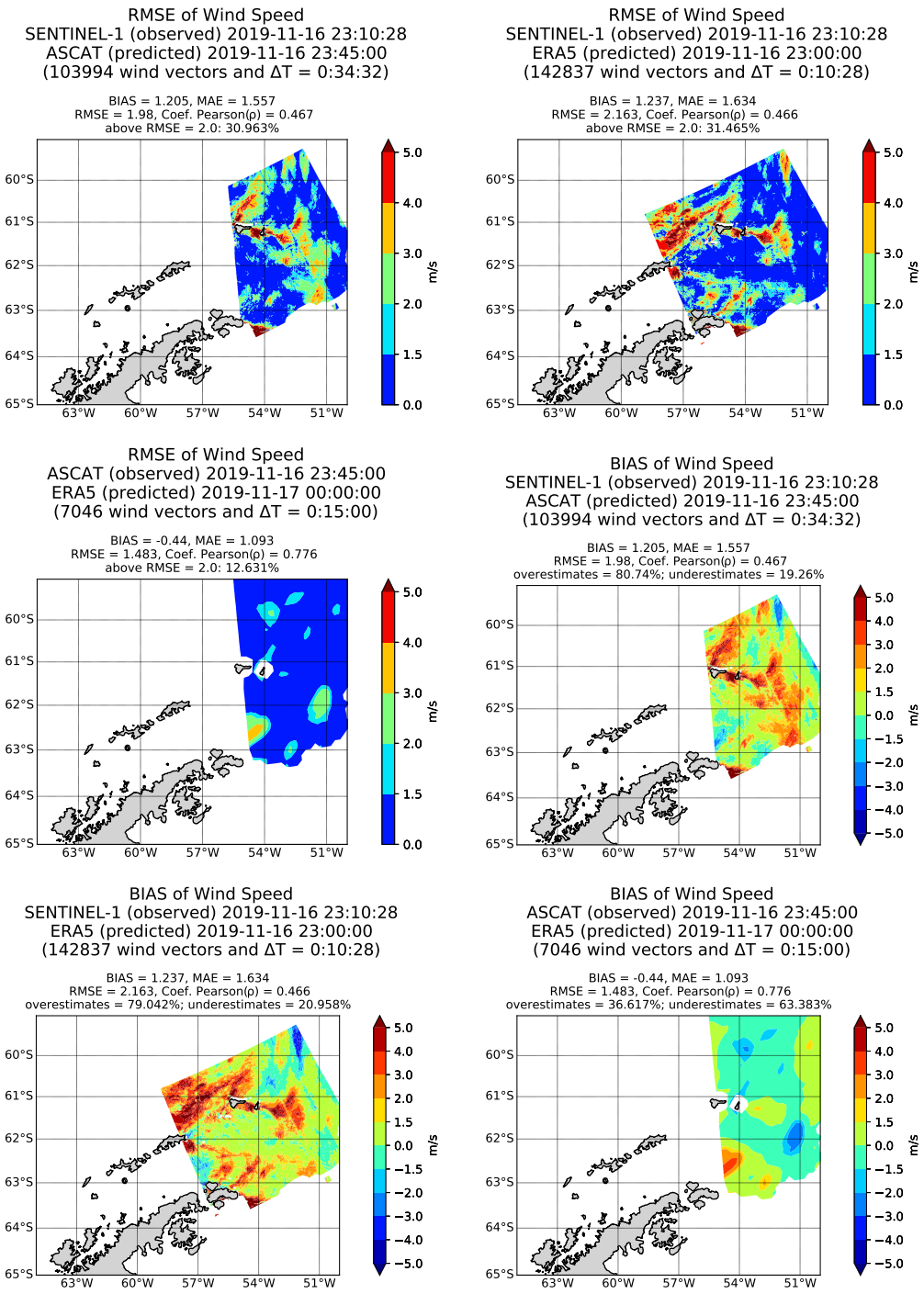

SOURCE: Author's production.

Figure A.5 - Plotting of wind field from date 2019-11-19 23:34:47Z.

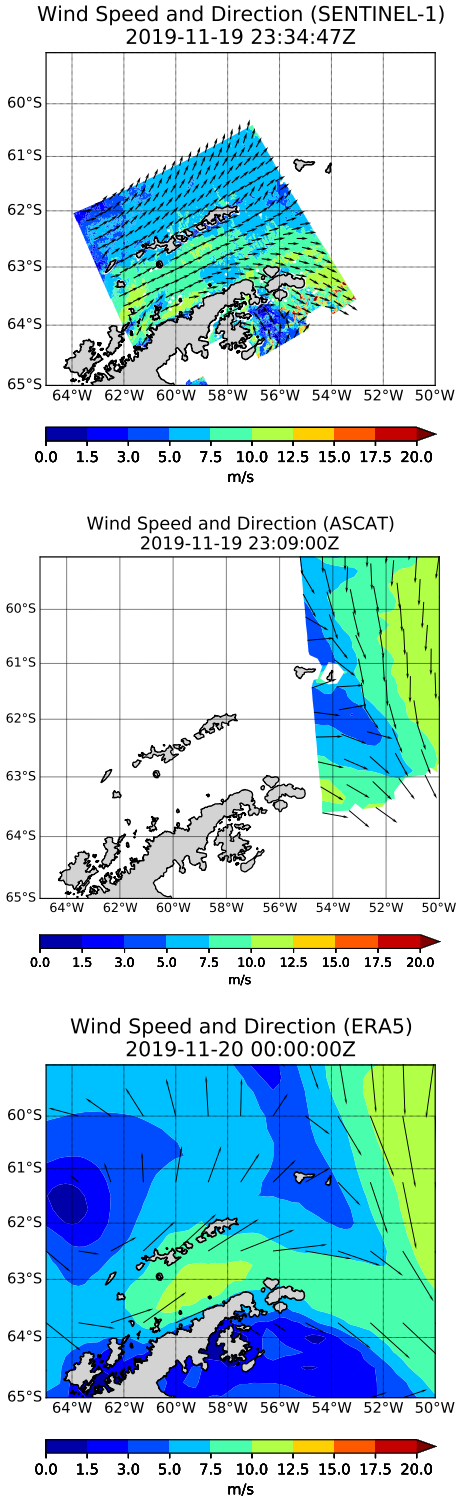

SOURCE: Author's production.

Figure A.6 - Plotting of statistical parameters from date 2019-11-19 23:34:47Z.

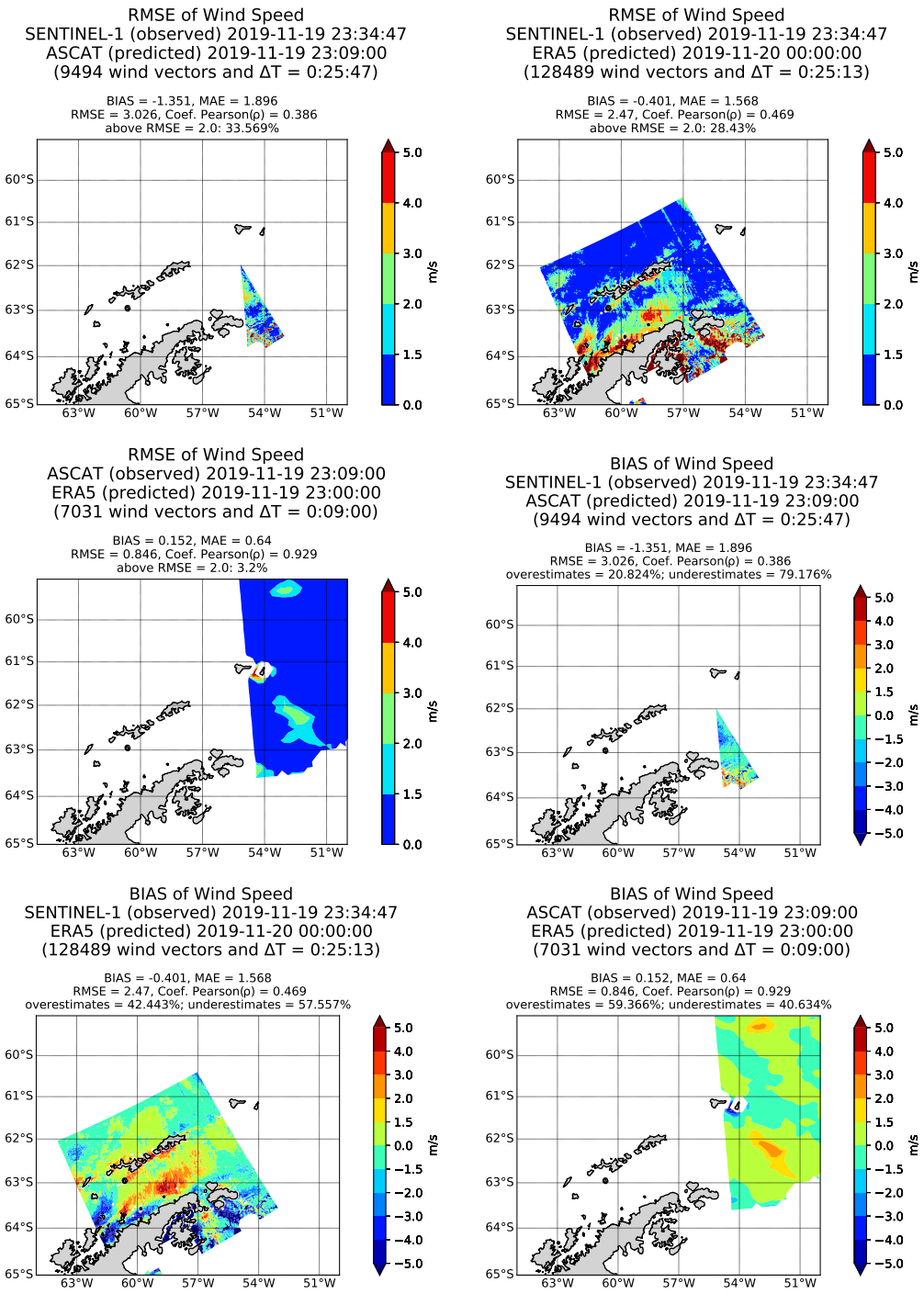

SOURCE: Author's production.

Figure A.7 - Plotting of wind field from date 2019-11-22 23:09:46Z.

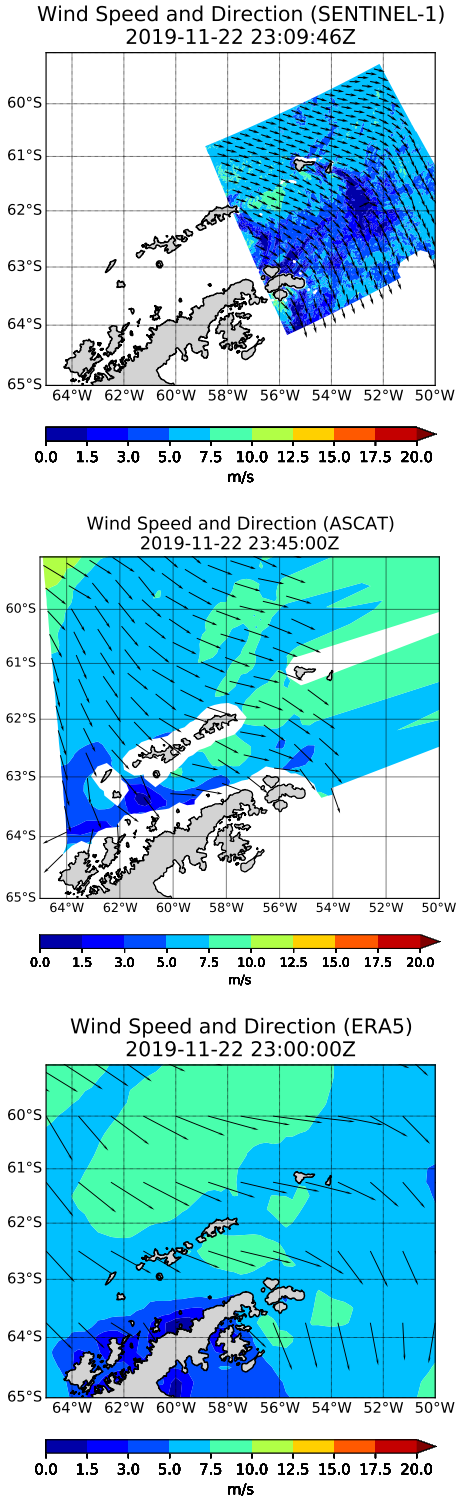

SOURCE: Author's production.

Figure A.8 - Plotting of statistical parameters from date 2019-11-22 23:09:46Z.

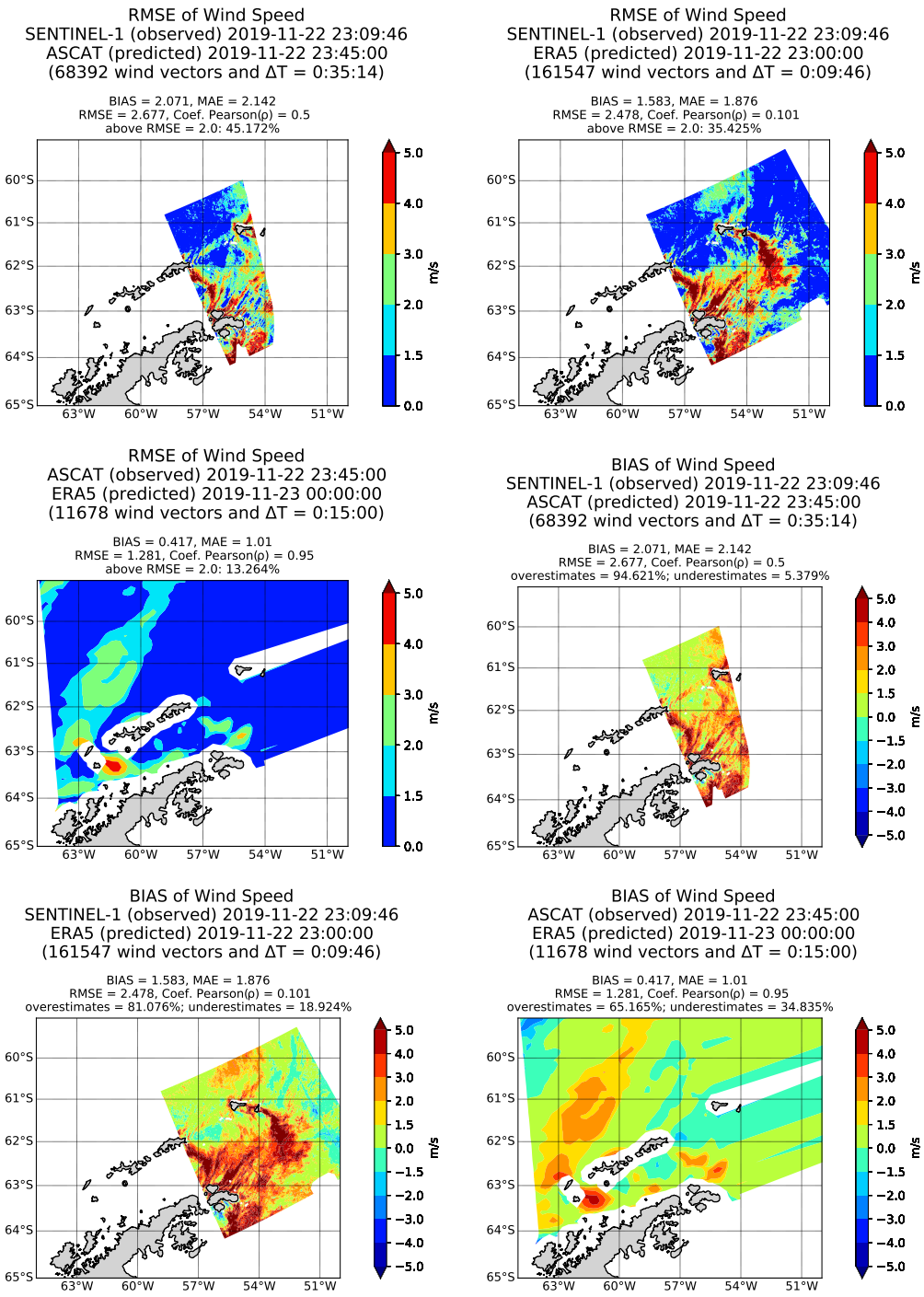

SOURCE: Author's production.

Figure A.9 - Plotting of wind field from date 2019-11-25 23:34:05Z.

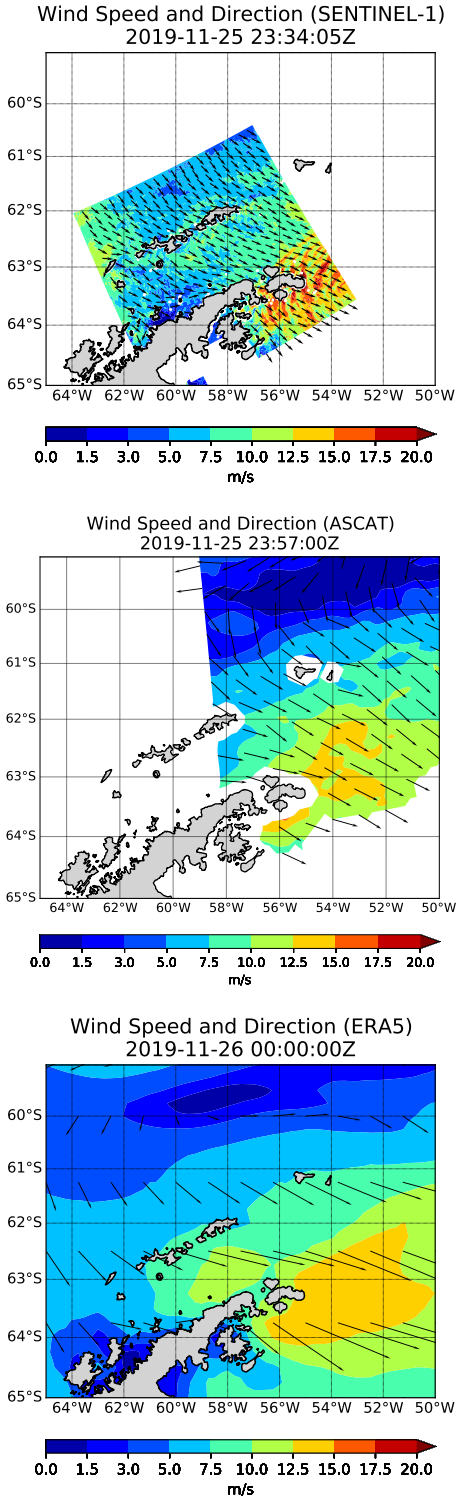

SOURCE: Author's production.

Figure A.10 - Plotting of statistical parameters from date 2019-11-25 23:34:05Z.

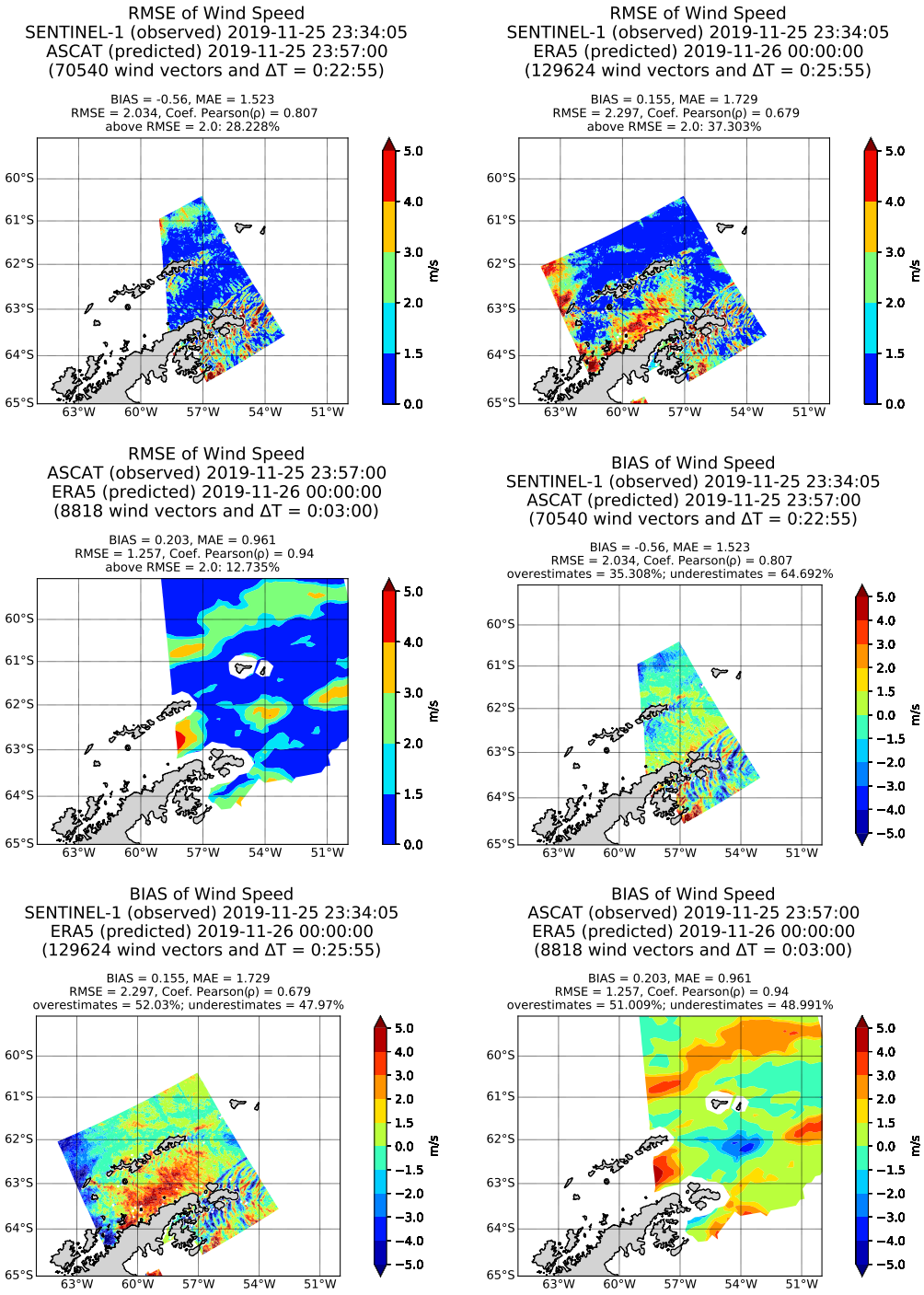

SOURCE: Author's production.

Figure A.11 - Plotting of wind field from date 2019-11-27 23:17:54Z.

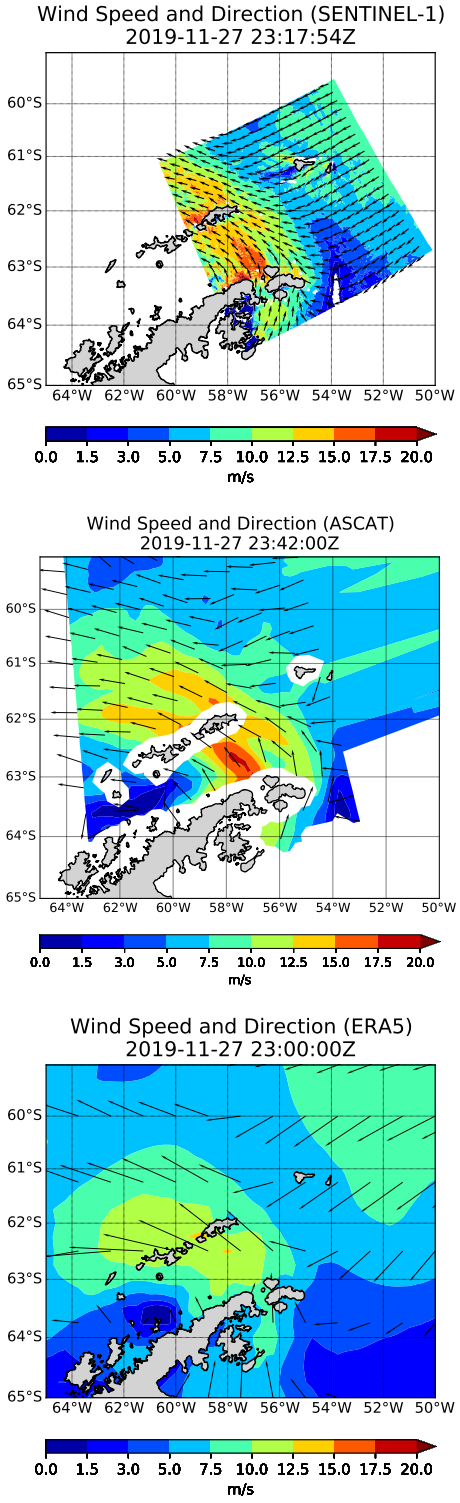

SOURCE: Author's production.

Figure A.12 - Plotting of statistical parameters from date 2019-11-27 23:17:54Z.

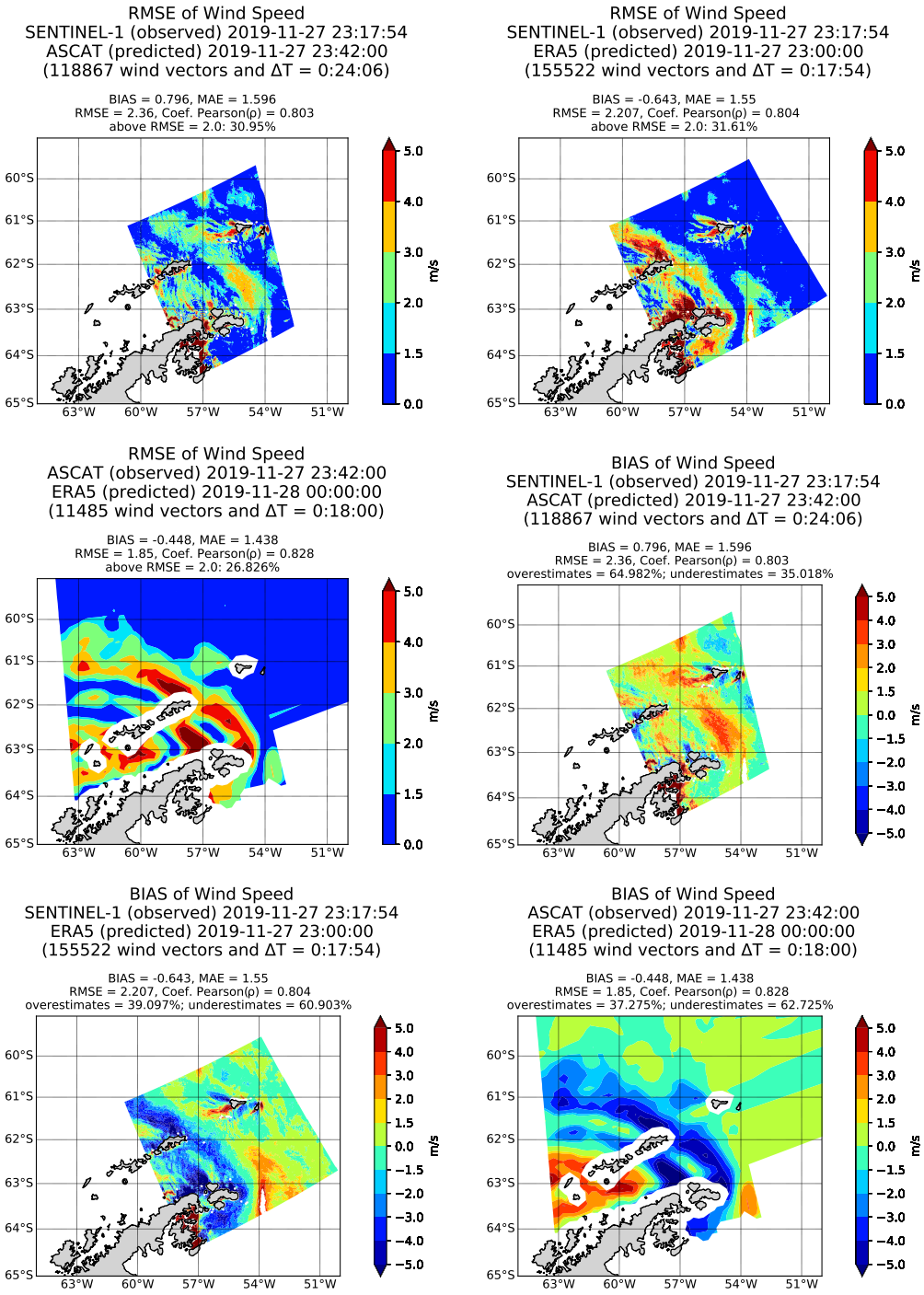

SOURCE: Author's production.

Figure A.13 - Plotting of wind field from date 2019-11-29 23:51:01Z.

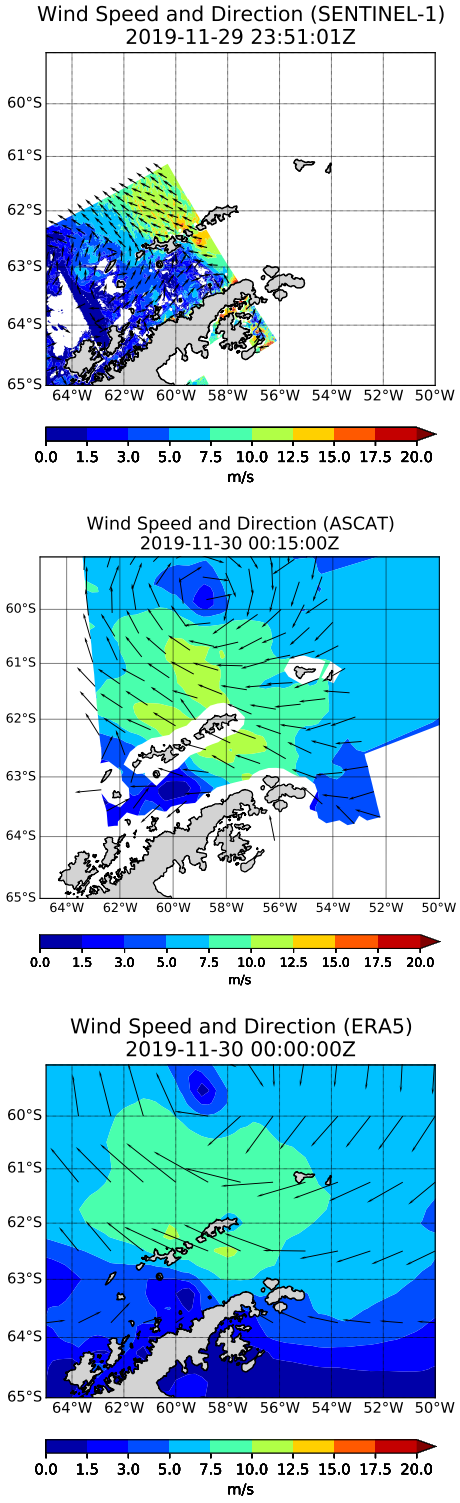

SOURCE: Author's production.

Figure A.14 - Plotting of statistical parameters from date 2019-11-29 23:51:01Z.

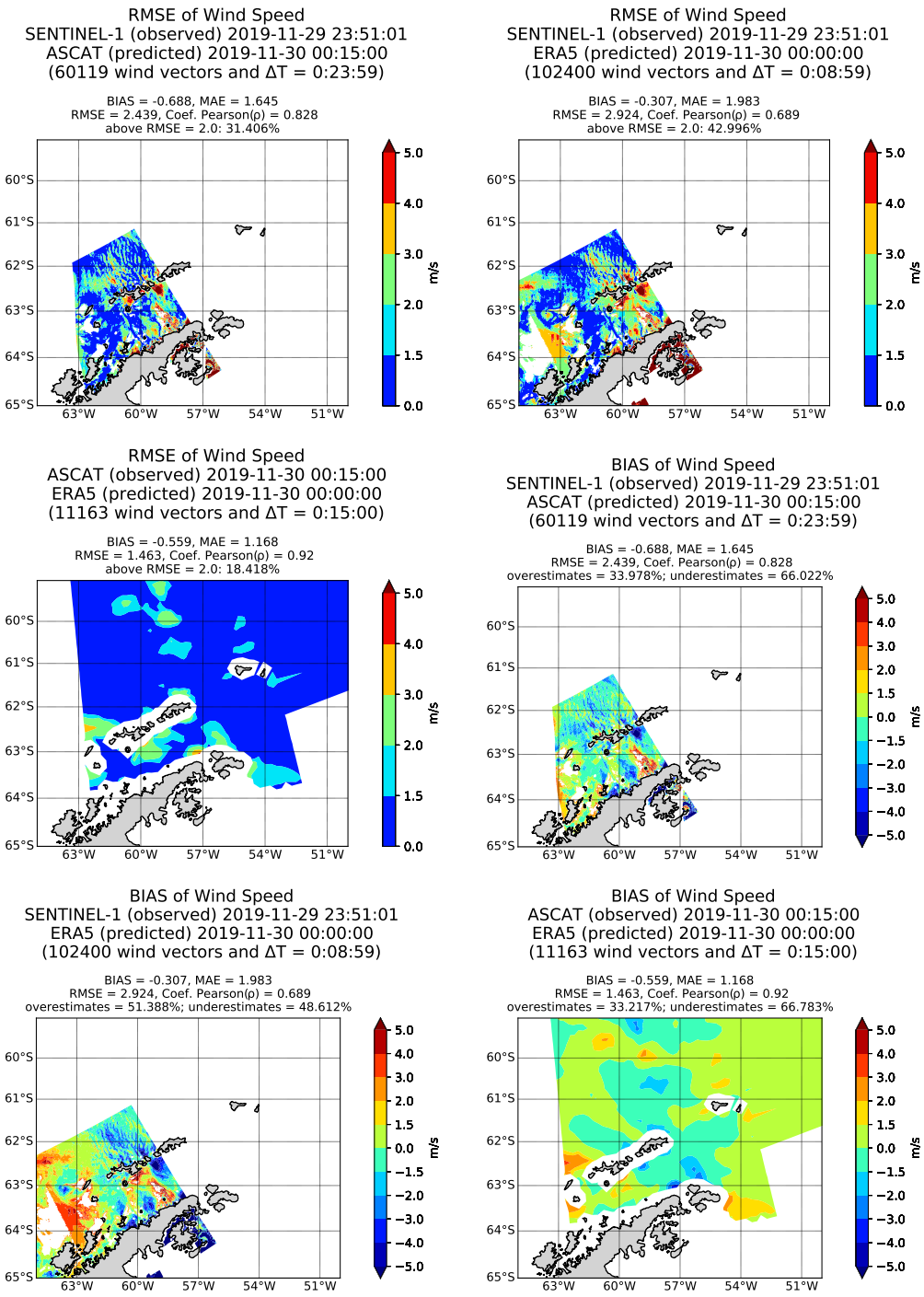

SOURCE: Author's production.

PUBLICAÇÕES TÉCNICO-CIENTÍFICAS EDITADAS PELO INPE

Teses e Dissertações (TDI)

Teses e Dissertações apresentadas nos Cursos de Pós-Graduação do INPE.

Notas Técnico-Científicas (NTC)

Incluem resultados preliminares de pesquisa, descrição de equipamentos, descrição e ou documentação de programas de computador, descrição de sistemas e experimentos, apresentação de testes, dados, atlas, e documentação de projetos de engenharia.

Propostas e Relatórios de Projetos (PRP)

São propostas de projetos técnico-científicos e relatórios de acompanhamento de projetos, atividades e convênios.

Publicações Seriadas

São os seriados técnico-científicos: boletins, periódicos, anuários e anais de eventos (simpósios e congressos). Constam destas publicações o Internacional Standard Serial Number (ISSN), que é um código único e definitivo para identificação de títulos de seriados.

Pré-publicações (PRE)

Todos os artigos publicados em periódicos, anais e como capítulos de livros.

Manuais Técnicos (MAN)

São publicações de caráter técnico que incluem normas, procedimentos, instruções e orientações.

Relatórios de Pesquisa (RPQ)

Reportam resultados ou progressos de pesquisas tanto de natureza técnica quanto científica, cujo nível seja compatível com o de uma publicação em periódico nacional ou internacional.

Publicações Didáticas (PUD)

Incluem apostilas, notas de aula e manuais didáticos.

Programas de Computador (PDC)

São a seqüência de instruções ou códigos, expressos em uma linguagem de programação compilada ou interpretada, a ser executada por um computador para alcançar um determinado objetivo. Aceitam-se tanto programas fonte quanto os executáveis.